Important Notice

UNIVERSITY OF CALGARY

Reservoir property prediction from well-logs, VSP and multicomponent seismic data: Pikes Peak heavy oilfield, Saskatchewan

by

Natalia Soubotcheva

A THESIS

SUBMITTED TO THE FACULTY OF GRADUATE STUDIES

IN PARTIAL FULFILMENT OF THE REQUIREMENTS FOR THE

DEGREE OF MASTER OF SCIENCE

DEPARTMENT OF GEOLOGY AND GEOPHYSICS

CALGARY, ALBERTA
January, 2006

UNIVERSITY OF CALGARY

FACULTY OF GRADUATE STUDIES

The undersigned certify that they have read, and recommend to the Faculty of Graduate Studies for acceptance, a thesis entitled "Reservoir property prediction from well-logs, VSP and multicomponent seismic data: Pikes Peak heavy oilfield, Saskatchewan" submitted by Natalia Soubotcheva in partial fulfilment of the requirements of the degree of Master of Science.

Supervisor, Dr. Robert Stewart, Department of Geology and Geophysics

Dr. Larry Lines, Department of Geology and Geophysics

Dr. Mehran Pooladi-Darvish, Department of Petroleum Engineering

Date

Abstract

Reservoir property estimation plays an important role in the exploitation and successful development of oil and gas fields. In this thesis, well log data, VSP and 2D multicomponent seismic data are combined to predict reservoir properties.

PP and PS synthetic seismograms generated from well logs correlate convincingly with the surface seismic data. The productive formation has a Vp/Vs value noticeably lower (1.7) than the overlying formations (which are around 4.4). The top of the productive interval is interpreted as a PP impedance drop (5010 m/s*g/cc) and PS increase (3066 m/s*g/cc). Inversion and other seismic attributes were used to predict the density and porosity along the seismic line. The Waseca oil sands are characterized as a low-density (2170 kg/m^3) and high-porosity (22%) zone. Angle and spectral maps were generated from the PP seismic data to show the dipping angle of the geological structure and the frequency content of the seismic data respectively. A low-frequency anomaly is found below the reservoir and might be used as another indicator of the productive zone.

As a whole, combining different types of data provides a more confident geophysical interpretation.

Acknowledgements

I would like to thank my supervisor Dr. Robert Stewart for his guidance and great patience. Thanks to Dr. Larry Lines for his helpful advice and discussions. My acknowledgements to Brian Russell for help with Hampson-Russell software. I acknowledge Husky Energy for providing the seismic and well log data. My special thanks to Calgary Scientific Inc. for permission to use their software, for collaboration and support.

I would like to show my appreciation to Kim Munro, Amber Kelter and Kevin Hall for their time and sharing of knowledge.

Thanks to CREWES (Consortium for Research in Elastic Wave Exploration Seismology) for financial and technical support.

Table of contents

List of tables

List of figures

Chapter 1

Introduction

1.1 Introduction

The Pikes Peak oilfield is located 40 km east of Lloydminister, Saskatchewan (Figure 1.1) and produces heavy oil from the Waseca sands of the Lower Cretaceous Mannville Group. Over 42 million barrels of heavy oil have been produced at this site over the last 22 years. Presently, it is one of the largest oil fields in Canada with a daily production of about 8000 barrels (Husky Energy reports, 2004).

Considerable effort has been expended to research the effect of steam injection in this area. Hulten (1984) provided a comprehensive geologic description for the Waseca formation in and around the Pikes Peak field. Downton (2001) performed an AVO study to map the steam chamber. Xu et al. (2001) reported on the acquisition and processing of VSP data. Newrick et al. (2001) presented an investigation of seismic velocity anisotropy at Pikes Peak using VSP data. Zou at al. (2002) conducted time-lapse seismic modelling at Pikes Peak. Watson (2004) investigated acoustic impedance inversion and showed the stratigraphy of the reservoir.

It was shown by the above researchers that steam injection significantly changes the elastic parameters of the reservoir. For example, they indicated that acoustic impedance is lowered where steam has been injected into the reservoir formation. The significant time delay caused by fluid substitution was observed on the time-lapse seismic data. VSP data were used to generate the velocity model that allowed successful migration of the seismic data.

The main producing zone within the Waseca formation is a homogeneous sand unit. The coal and sideritic shale of the McLaren and the shale at the top of the Waseca form an excellent seal for the hydrocarbon (Hulten, 1984). Wells 1A15-6, D15-6, 3C8-6, B16-1 and D2-6 were used to create P-P synthetic seismograms. Wells 1A15-6 and B16-1 were also used to tie to the converted-wave seismic data, because they had S-wave sonic logs.

The primary objective for this research was to integrate different types of geological and geophysical information to conduct the reservoir analysis. It implies the estimation of elastic properties, lithology, acoustic impedance and porosity. As a continuation, the Vp/Vs coloured section was created using multi-component data, gathered at Pikes Peak. To estimate the PP and PS acoustic impedance, three post-stack seismic inversion methods were used: model-based, recursive and sparse-spike.

Finally, a cokriging method was applied to integrate the sparse well measurements and the dense seismic data to estimate the desired rock properties.

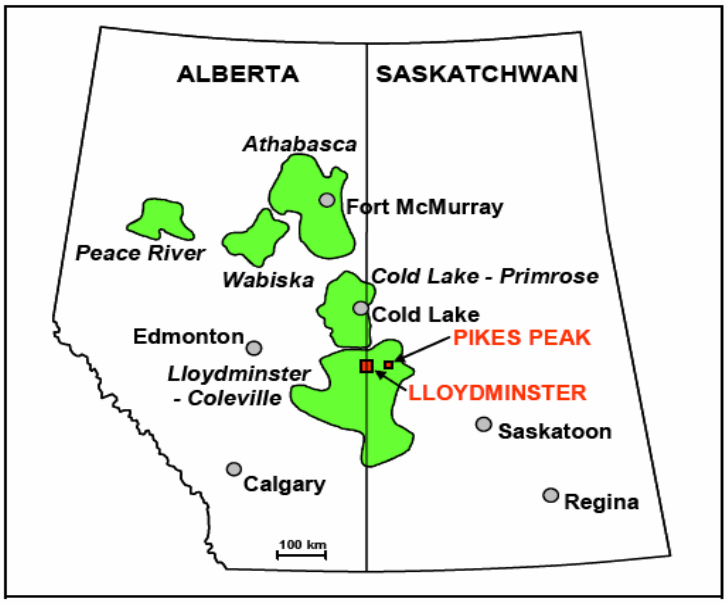

Figure 1.1. Map of major heavy-oil deposits of Alberta and Saskatchewan, and location of the study area (after Watson, 2004).

1.2 Geology

The Pikes Peak heavy oilfield is situated in the east-central part of the Western Canada sedimentary basin. The productive Waseca formation is located about 500 m below the surface and its thickness varies from 5 to 30 m (Figure 1.2).

The top of the Precambrian basement lies at a depth of approximately 1600 m. There are essentially Devonian and Cretaceous age formations above the basement. The dominant lithologies of the Devonian formation are limestone and dolomite, with the exception of the Prairie Evaporate, which consists largely of salt. The dissolution of this Devonian salt played an important role in the forming of the hydrocarbon trap at Pikes Peak.

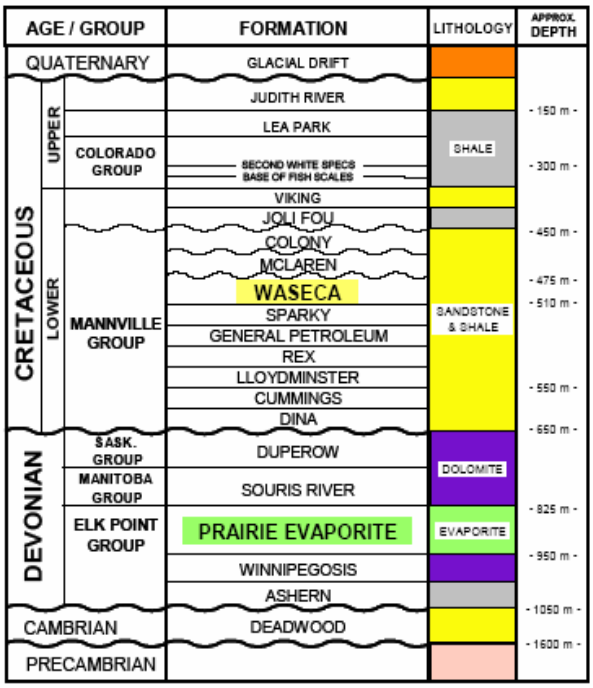

Figure 1.2. Pikes Peak stratigraphy (after Core laboratories-Stratigraphic Chart for Saskatchewan).

There is a 250 million year gap between the Devonian and Cretaceous formations. This boundary is also known as PreCretaceous Unconformity. A mixture of sand and shale

cycles were deposited above this Unconformity, and it formed the Lower Cretaceous Mannville group. The Cretaceous strata are dipping largely to the southwest (Hulten, 1984). In this chapter, only the Waseca formation is discussed in detail, since it is the focus for exploration.

The productive Waseca formation consists of three main facies (Hulten, 1984). From top to bottom they are:

1. sideritic silty shale unit;
2. interbedded sand and shale unit;
3. homogeneous sand unit.

The homogeneous sand, which is saturated with heavy oil, is the main target for development. This unit has the greatest thickness and continuity across the reservoir. The sands are well sorted, fine- to medium-grained. The typical sedimentary structure in the lower part of this unit is planar crossbeds. Parallel laminations are more common for the upper part. The sands are locally cemented by siderite and calcium carbonates, which deteriorate the porosity in the areas of cementation. The Sparky coal layer identifies the low limit of this unit. In general, the homogeneous sand unit has excellent reservoir quality. The interbedded unit is characterized with lamination of sand and shale, which makes well log data “highly variable” in this part of a section. No carbonate cement has been observed. Compared to the homogeneous sand, the interbedded unit has lower oil saturation. The upper shale unit plays the role of a cap in the hydrocarbon trap. It has low porosity and permeability, and creates a seal over the oil- or water-saturated sand. The ironstone, due to its high cementation, forms a well defined boundary between the McLaren and the upper Waseca.

The trapping mechanism at Pikes Peak is considered to be both structural and stratigraphic: its stratigraphic component comes from the sealing shale unit, and the structural component is determined by the dissolution of the Prairie evaporite.

Available log suites for most wells include P-wave sonic, density, gamma ray, resistivity and SP logs. A simple way to differentiate the lithologies is to crossplot the Vp/Vs ratio versus gamma ray log (Figure 1.3).

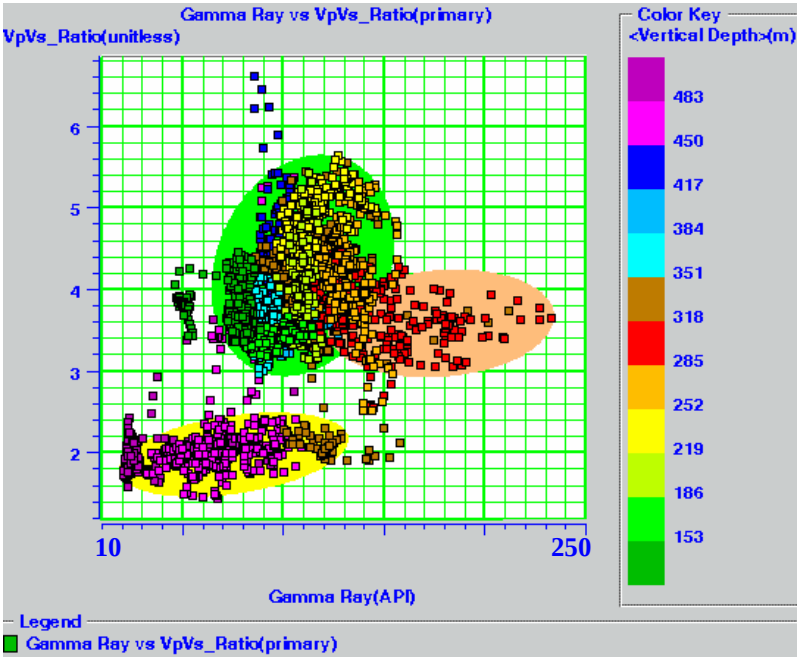

Figure 1.3. (a) Vp/Vs versus gamma ray for the well 1A15-6.

This cross-plot was created for the well 1A15-6 which of all the wells is the closest to the seismic line. Different coloured points represent different depths. In our case, three major types of lithology were selected. Applying this result to the cross-section (Figure 1.4), we can observe the shale zone (brown), the mixture of sand and shale cycles (green), and the homogeneous or oil sands (yellow) for this well. This result slightly varies from well to well at Pikes Peak; however the same sequence is observed along the whole section from north to south.

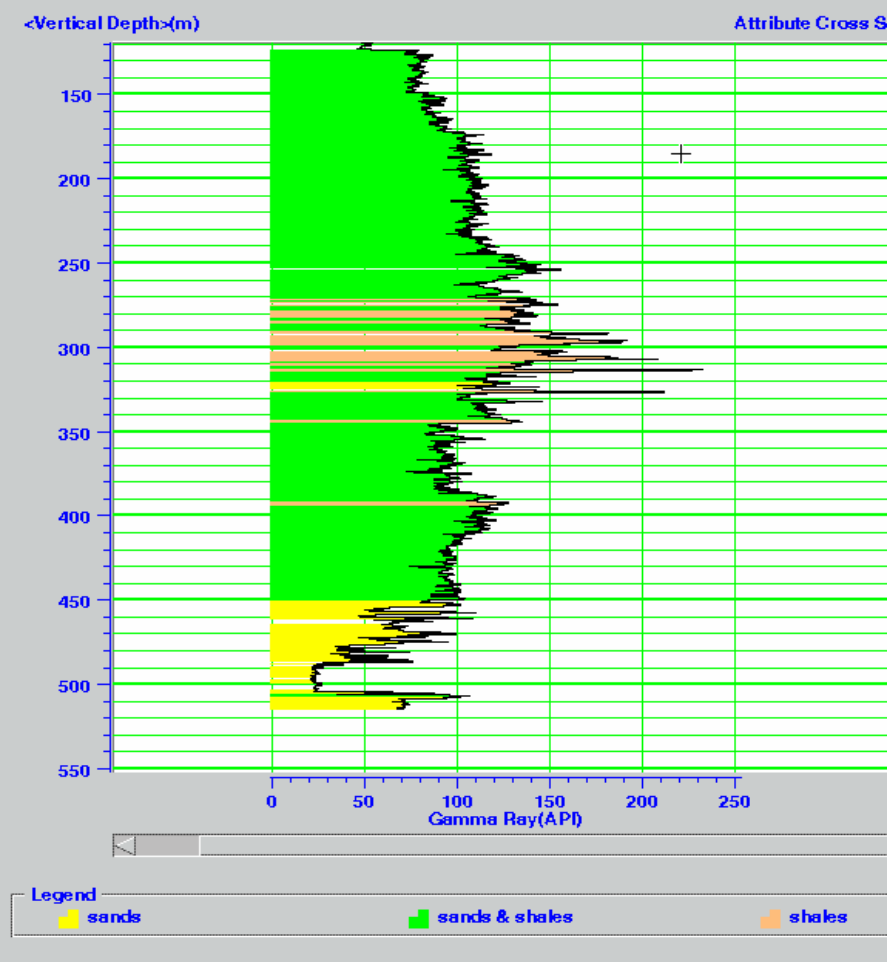

Figure 1.4. Cross-section for well 1A15-6 delineating zones with different lithology: shales, mixture of sand and shale cycles and oil sand.

The mineralogy of the Waseca (from Hulten, 1984) is dominated by quartz (92%) and also contains the small amount of feldspar (3%), kaolinite (3%) and other minerals (2%). Oil saturation is relatively high at 80-90%. The porosity in the homogeneous sand is also high at 32%; permeability ranges from 5 to 10 Darcies.

Cyclic Steam Stimulation (CSS) has been used at Pikes Peak to increase the mobility of oil and facilitate its production. The steam is injected into the reservoir over a period of several months. During this time, the well is shut in to let the heat propagate through the reservoir. As the oil near the injector well warms, its viscosity is greatly reduced. Then the oil is

produced from the injector well. This process is repeated several times. Another method of oil recovery is Steam Assisted Gravity drainage (SAGD). This method uses two horizontal well vertically offset a few metres. Steam is injected into the upper wellbore, melted oil drains down through the rock to the lower wellbore and is produced.

Presently, Pikes Peak is one of the largest fields in Canada with daily production 1,200-1,300 m^3 which is equivalent to 7,600-8,300 bbl (from Husky production report). Since many wells in the area are produced using cyclic steam stimulation, the production number changes depending on the phases of a cycle, and may exceed this range.

1.3 Review of acquisition and processing

A three-component seismic line, shot with a Vibroseis source, was collected in March 2000 by the CREWES Project and Husky Energy (Figure 1.5). This line was about 3.8 km long with a receiver interval of 10 m and a source interval of 20 m (Hoffe, 2000). This source was swept for 16 seconds over 8-150 Hz. The main difference for the processed PP and PS data was in the bandwidth: for the PP data – 14-150 Hz, and for PS data – 8-40 Hz (Appendix 1). The seismic data were acquired by Veritas DGC (Land) and processed by Matrix Geoservices Ltd in May 2000.

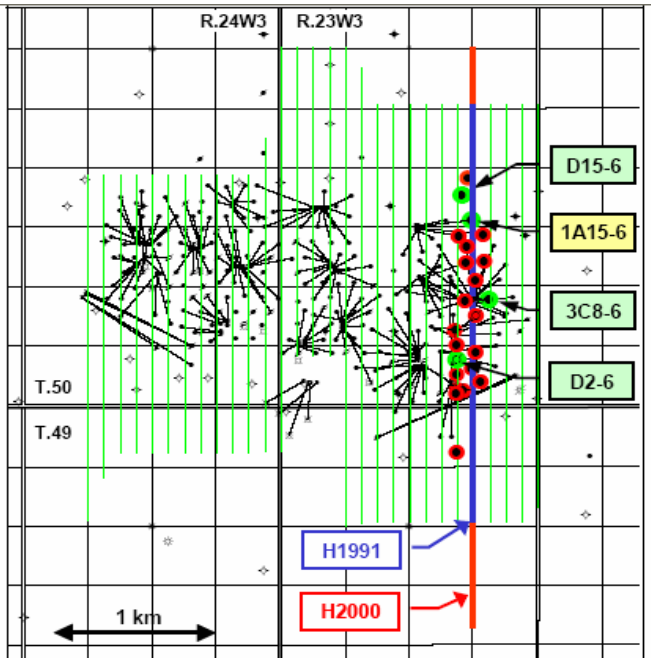

Figure 1.5. Map of the Pikes Peak field, Saskatchewan (Watson, 2004).

The data from 2000 were more noisy than 1991, because many more pump jacks were in operation during acquisition. Nevertheless, the increased fold from 30 to 66 helped to stack out much of this noise. Both sets of data were filtered and migrated.

Nine wells closest to seismic line (lying within 110 m of the 2D seismic line) were used in this thesis. A typical suite of logs includes: gamma ray (GR), P-wave sonic, spontaneous potential (SP), resistivity, neutron porosity and bulk density (Figure 1.6).

As mentioned previously, the SP and GR logs indicate a permeable sand interval (482-500m) with high porosity (30-32%) from the neutron and density logs. Resistivity logs indicate considerable oil saturation.

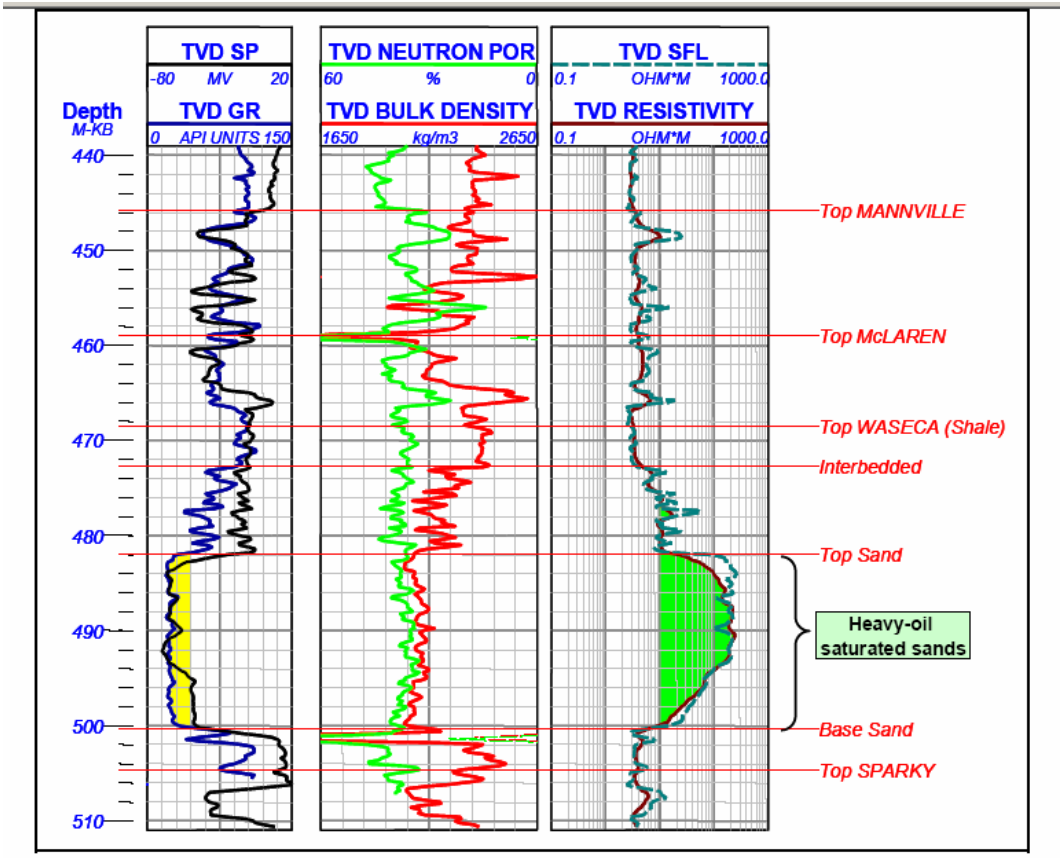

Figure 1.6. Typical log suite used for well log interpretation over the zone of interest. The well 3B9-6 is located 87 m east of the seismic line (Watson, 2004).

1.4 Software used

This thesis uses various Hampson-Russell software packages. With the help of the eLog package, the well logs were manually correlated to the seismic data. The AVO application was used to construct the synthetic seismograms and reflectivity curves with the offset. The ProMc package, designed for multicomponent data, was the main tool to create Vp/Vs sections and analyze PP and PS datasets simultaneously with one scale. Using Strata, both PP and PS coloured impedance sections were constructed and analyzed. Also the Emerge package was used to integrate the well log and seismic data in order to estimate some reservoir properties using multi attribute analysis.

The AccuMap system was used to verify the well locations and current data on production and operation. Finally, the dip and spectral maps for the seismic data were generated in Resolution software from Calgary Scientific Inc.

Chapter 2

Basic interpretation

2.1 Well log correlation to seismic data

The starting point of this geophysical interpretation is the correlation of the well logs to the seismic data. By convolving the reflectivity and wavelet at the well location, the synthetic traces (blue colour) are generated. Then each pick from the synthetic trace was correlated to each pick from real seismic data (red colour). The well log was datumed according to this correspondence (Figure 2.1).

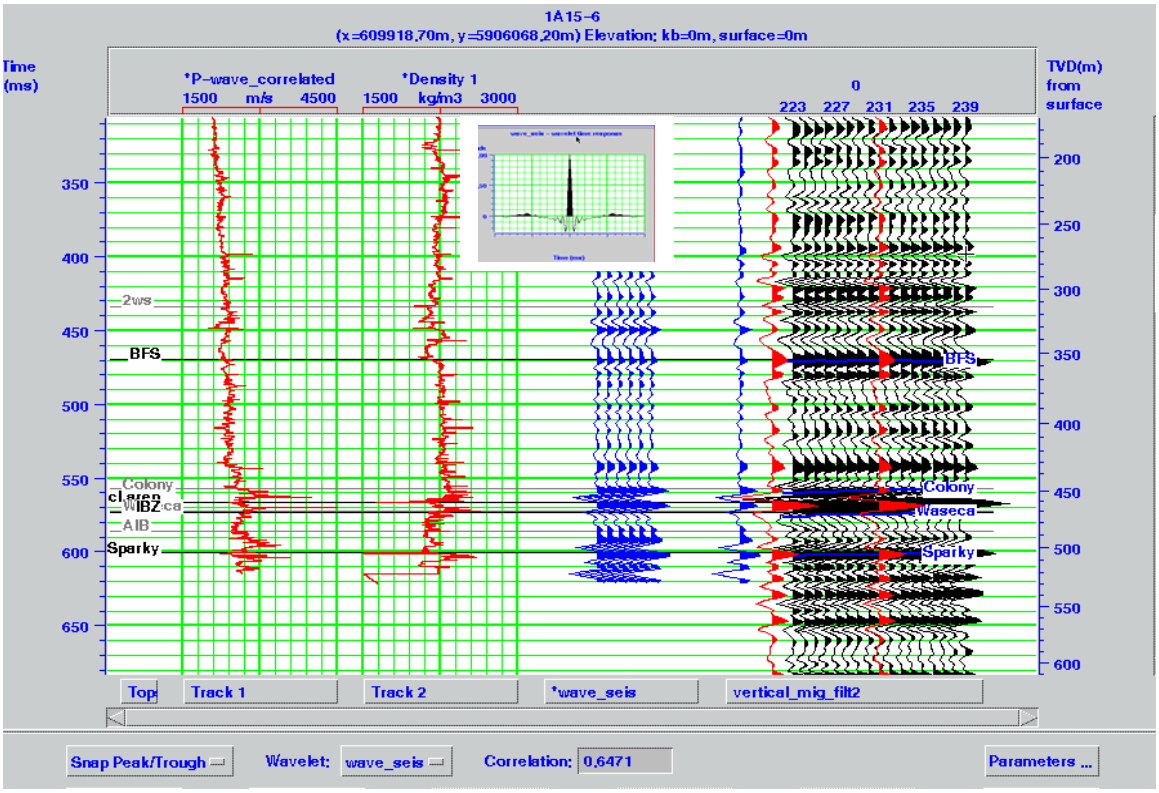

Figure 2.1.Well log, synthetic seismogram and surface seismic correlation for well 1A15-6.

Figure 2.1 demonstrates this application for well 1A15-6 corresponding to data around CDP 231 on the seismic line.

Six blue traces on the left represent the zero-offset synthetic seismogram for this well. After proper correlation, we can see that our synthetic trace (in blue) matches the real seismic trace, extracted at the well location (in red) reasonably well. The similarity between these two traces is shown in the window below (correlation – 64%).

The wavelet for the synthetic trace was extracted from the seismic data and we assume that it is constant with time and space. The wavelet parameters are:

- wavelet length – 200 ms
- taper length – 25ms
- sample rate – 2ms
- frequency spectrum 10-150 Hz (the same as the final filter used in the seismic data).

Taking a closer look at the well logs (Figure 2.1), we can observe the following:

P-wave sonic log

There is a slightly increase in velocities starting from the top of the Mannville (Colony formation). The Waseca formation has an average Vp velocity equal to 2500 m/s. The P-wave log for this well is not very informative in the case of event discrimination. However, the spikes on this log could be related to the facies boundaries, as confirmed by the calculated impedance log.

Density log

The Base of Fish Scales appears as a density increase from 2035 to 2235 kg/m^3. The next density increase from 2282 to 2330 kg/m^3 corresponds to the Colony event on the seismic section. The top of the Waseca formation corresponds to density decrease to 1900 kg/m^3. Then, at the beginning of the productive formation, the density increases to 2300 kg/m^3,

which corresponds to silty shale unit, and starts to get lower at the homogeneous sand formation – 2100 kg/m^3.

According to this correlation four possible layers have been identified (Table 2.1).

Formation Name	**Depth of Top (m)**
BFS (Base of Fish Scale)	357
Colony	453
Waseca	468
Sparky	504

Table 2.1. Four layers from correlating well 1A15-6 and the PP seismic data.

The well did not encounter the Devonian horizon. However, according to Hulten (1984), this formation would be found at about 640 m, and it is mainly represented by dolomite.

The gamma-ray log can be a good indicator of the natural radioactivity of the rocks. In sediments the log mainly reflects the shale content, because minerals containing radioactive isotopes tend to concentrate in clay and shale. Well 3C8-6 (Figure 2.2) has this type of log and crosses the productive formation.

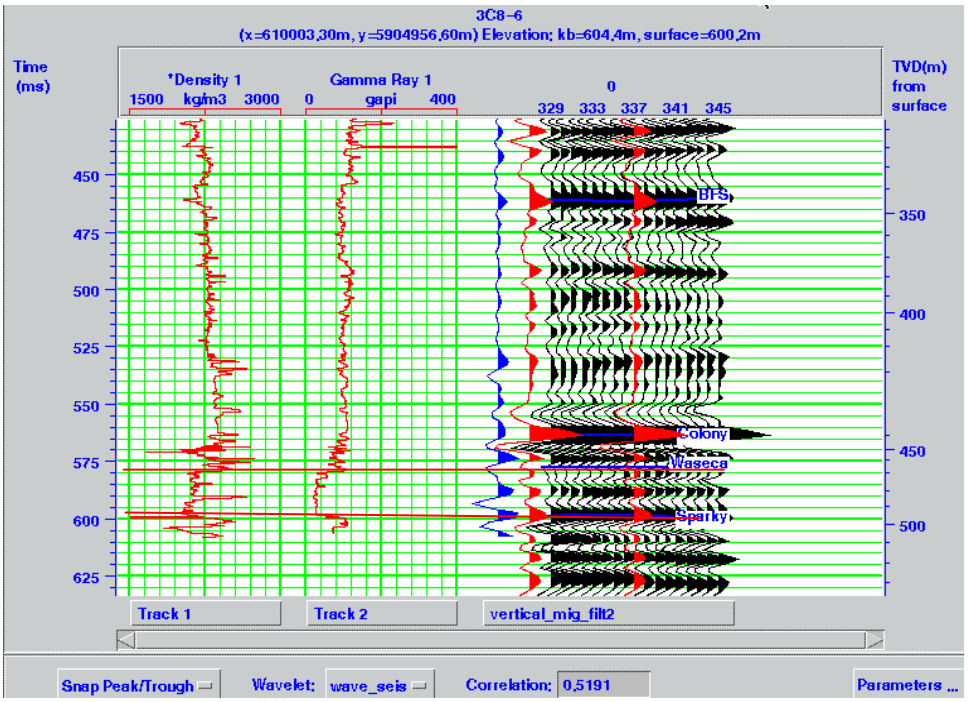

Figure 2.2. Density and gamma ray logs for well 3C8-6 correlated with the seismic data.

For this well, we can use the gamma ray log for sand and shale discrimination. Referring to the geology, the productive formation starts with the so-called shale cap, which corresponds to high values in the gamma ray log (80-90° API). When the log reaches the sand formation (oil- or water-saturated), its radioactivity drops to about 25° API. According to Figure 2.2, we can locate oil-saturated sands at depths from 470 to 495 m.

Similarly, the other wells were correlated to the surface seismic data and the correlation coefficient for well D15-6 (CDP 195) is 54%, and for well D2-6 (CDP 419) is 61%.

One can notice that well ties are imperfect. There are several reasons for this, including:

1) velocity dispersion
2) problems with sonic logs, such as cycle skipping or mud invasion
3) noisy seismograms
4) non zero-phase wavelets

5) polarity differences between synthetic seismograms and seismic data (Lines and Newrick, 2004).

Displaying correlated well logs on the seismic section (Figure 2.3) allows us to see how well they are calibrated to the seismic data.

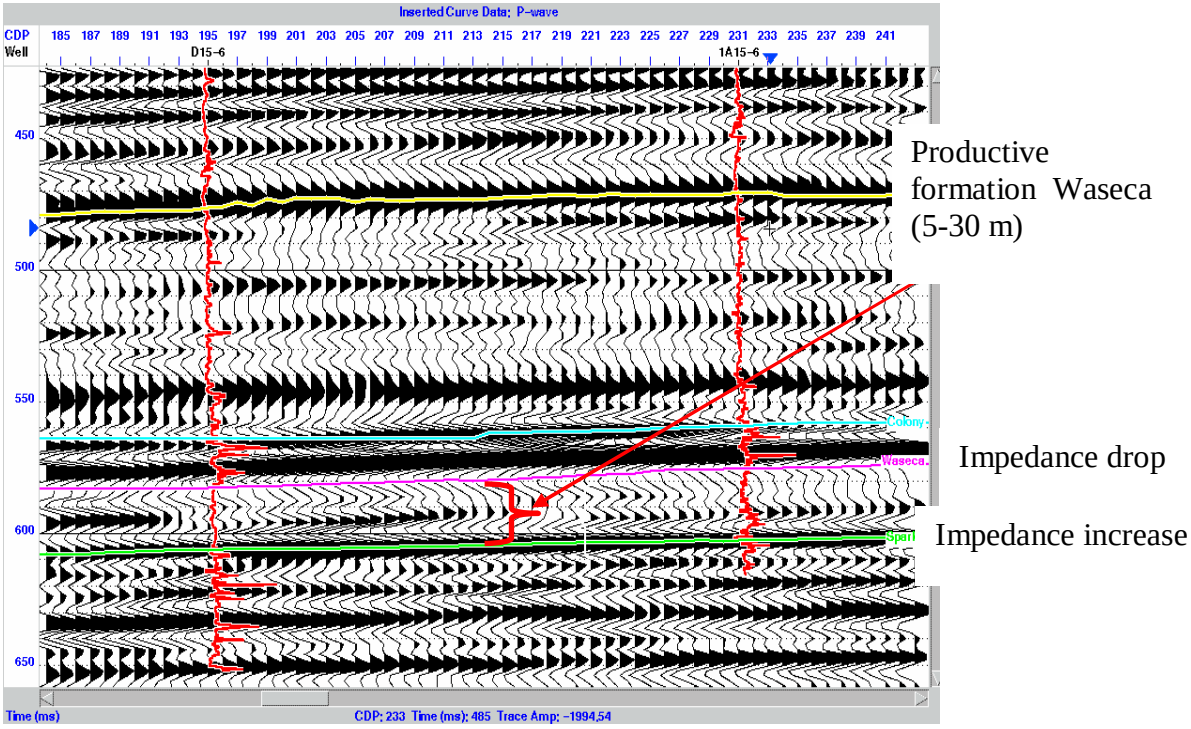

Figure 2.3. Interpreted fragment of the PP section with inserted P-wave sonic logs.

In general, the highest peaks on the logs should correspond to the brightest reflections. Figure 2.3 demonstrates that it is true for this case. The productive formation was found at a depth 500 m and its thickness varies from 5 to 30 m within the reservoir. Four main horizons were interpreted on the section: Base of Fish scale, Colony, Waseca and Sparky.

The top of the producing Waseca was recognised as an impedance decrease (trough on the seismic section) and at the bottom of the Waseca, impedance increases (peak on the seismic section). For this field, the density mainly contributes into the impedance changes.

Overall, the corresponding formations on the PS section have similar signatures (Figure 2.4) as for PP data, since the density and velocity are usually changing in the same direction for most of the oilfield.

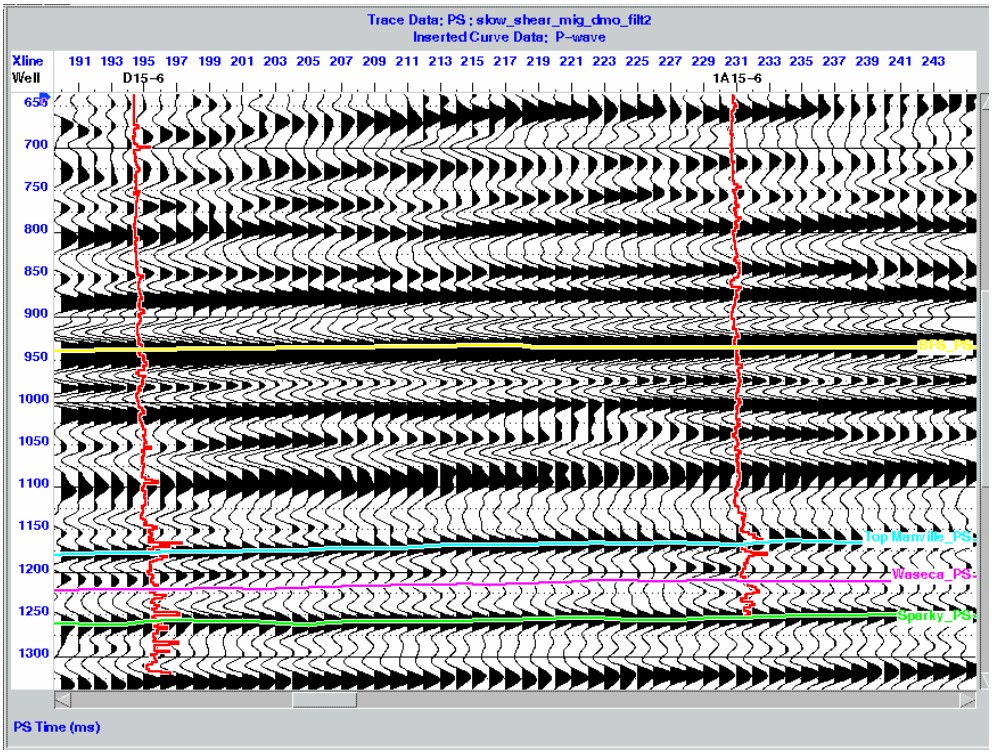

Figure 2.4. Interpreted fragment of the PS section in PS time with inserted P-wave sonic logs.

2.2 Synthetic modelling

It is well known that the measured seismic trace is modeled as a convolution of the source wavelet with reflectivity series:

$$S(t) = r(t) * w_s(t) \qquad (1)$$

In our case, P and S-wave logs are input values to calculate the reflectivity *r(t)* and the source wavelet w_s was extracted from the PP seismic data (Figure 2.5).

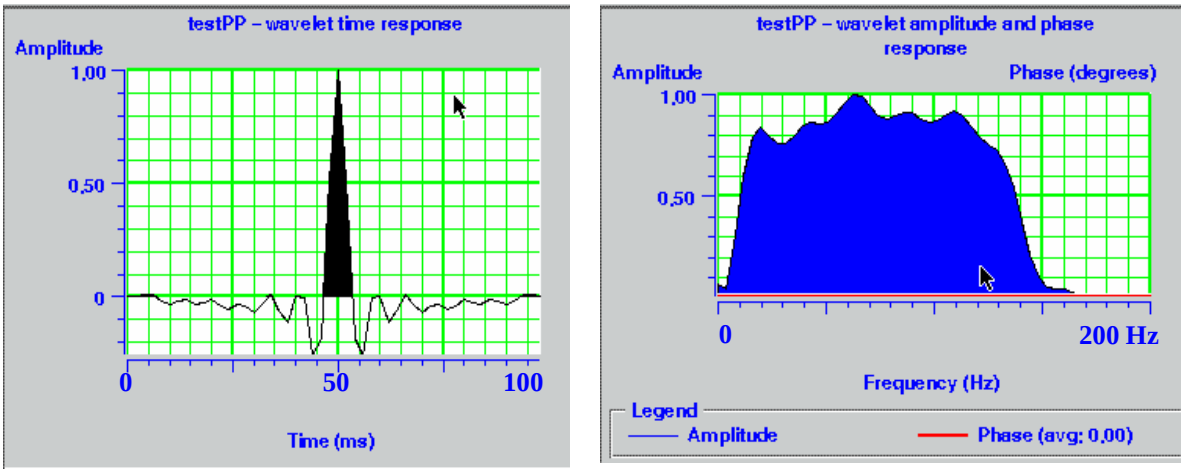

Figure 2.5. The amplitude of the wavelet with time (left) and frequency (right).

The wavelet *test PP*, extracted from the PP seismic data has the following parameters: wavelet length – 100 ms, taper length – 10ms, sample rate – 2ms, zero phase.

Note that the frequency band for this wavelet is about 15-150 Hz. These values correspond to the frequency content of the PP data.

I have chosen the Zoeppritz application in ProMc to create the synthetic seismogram (Figure 2.6). However, the solution of Zoeppritz's equation cannot be taken as the exact expected seismic response, because Zoeppritz's equation describes plane waves, while actual seismic waves are spherical (Lines and Newrick, 2004). In addition, the synthetic

seismogram is calculated in the absence of external effects such as transmission losses, attenuation, geophone coupling, coherent or random noise, etc.

The parameters for the PP synthetic seismogram are shown in Table 2.2:

number of offsets	30
minimum offset	0
maximum offset	500 m
sample rate	2 ms
start time	0
end time	700 ms
NMO corrected	

Table 2.2. Synthetic parameters.

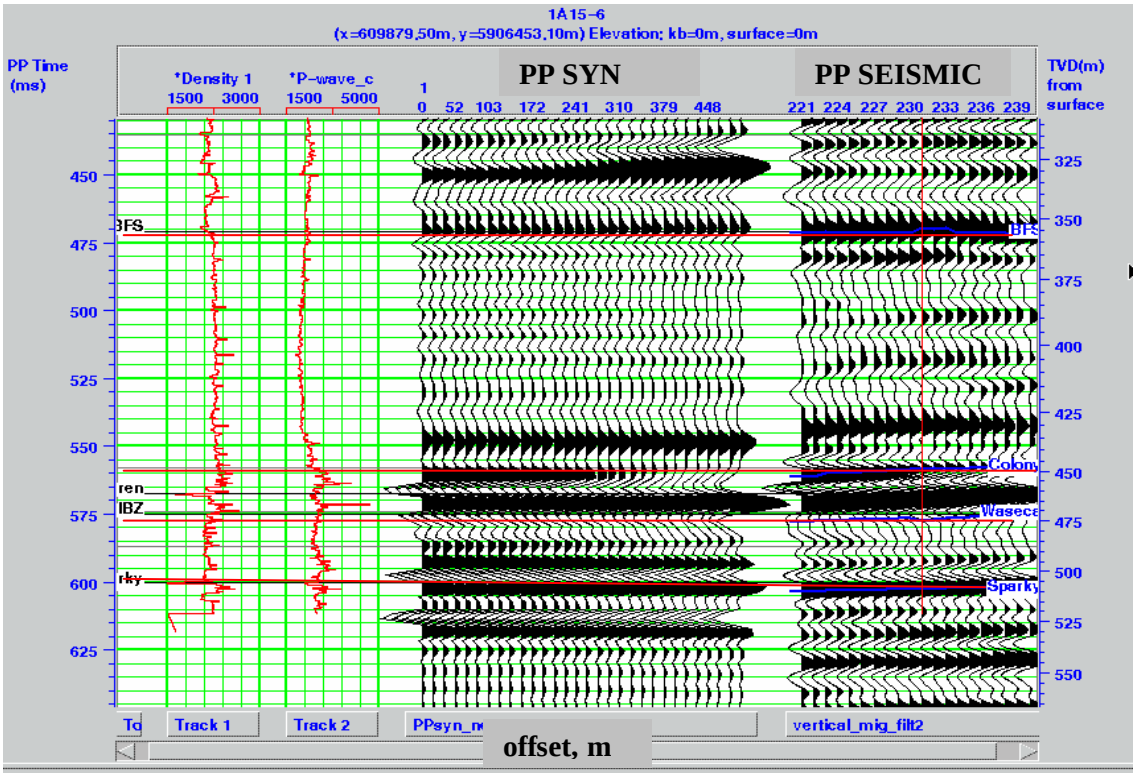

Figure 2.6. Well logs, PP synthetic and surface seismic data for well 1A15-6.

As we can see from the Figure 2.6, the main reflectors correlate reasonably well.

A Ricker wavelet was used to create the PS synthetic. Note the lower frequency content in Figure 2.7 that was chosen to match lower frequency PS seismic data.

Wavelet parameters are: wavelet length – 200 ms, taper length – 30 ms, sample rate- 2ms, phase type – constant phase.

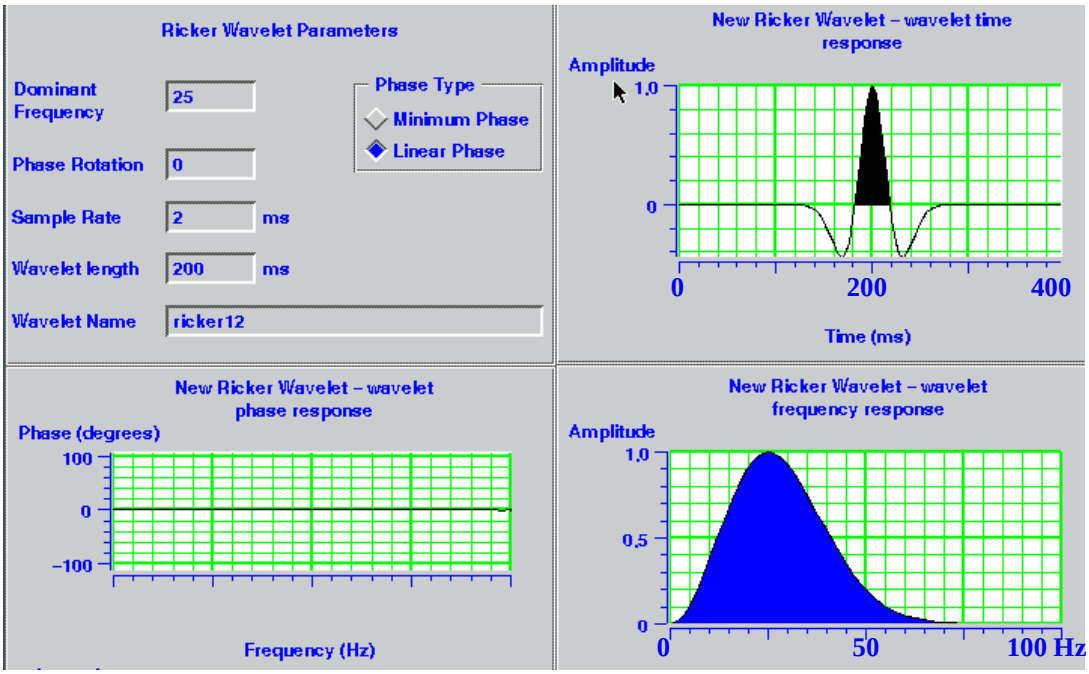

Figure 2.7. Ricker wavelet parameters for the PS synthetic seismogram.

As we can see from Figure 2.7, the dominant frequency is 25 Hz and the frequency band for the wavelet is about 8-45 Hz. The result of the PS modelling is shown on the Figure 2.8. The same input parameters as in previous case were used (Table 2.2), except that here a Ricker wavelet was used for the PS synthetic.

In this case, the well log curves are displayed in PS time and PS seismic and synthetic data are in depth. The first trace has no amplitude, because there is no conversion at zero offset. I have chosen a positive polarity for displaying the PS synthetic and frequency band for the

wavelet: 8-45 Hz. For this case, positive polarity can provide the better correlation of the events and help us avoid the erroneous event below 525 m.

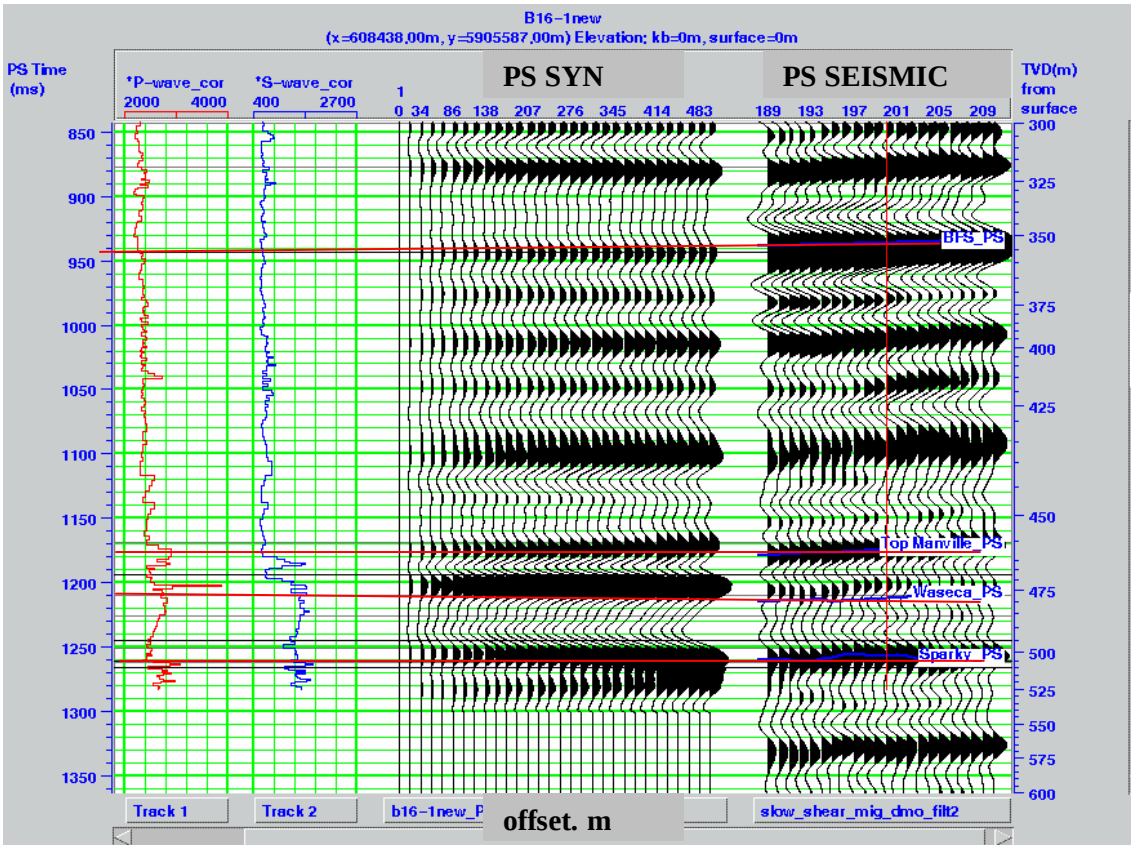

Figure 2.8. Well logs, PS synthetic and surface seismic data for the well B16-1.

We can assemble well logs, synthetic seismograms, VSP data, and surface seismic data into a composite plot, which often allows a more confident interpretation (Figure 2.9). The VSP at Pikes Peak was conducted in well D15-6, which is fairly close to our seismic line. This well was chosen because it had not been used for reservoir steaming, and it passed through all the major area formations (Osborne and Stewart, 2001). The energy source was a Vibroseis truck running a linear sweep from 8 to 200 Hz. Three-component receivers were spaced in the well every 7.5 m. The VSP included in Figure 2.9 is the P upgoing wave VSP with an offset of 180 m and a sample interval of 0.001s for a total recording time of 3s.

According to the acquisition parameters (Osborne and Stewart, 2001), the deepest geophone was clamped at a depth - 514.5m in the well. If we refer to Figure 2.9, we can see the last event registered by VSP, at zero offset, has about that depth.

As we can see from the Figure 2.9, the VSP supports our preliminary interpretation. All the main events correlate well with all types of information.

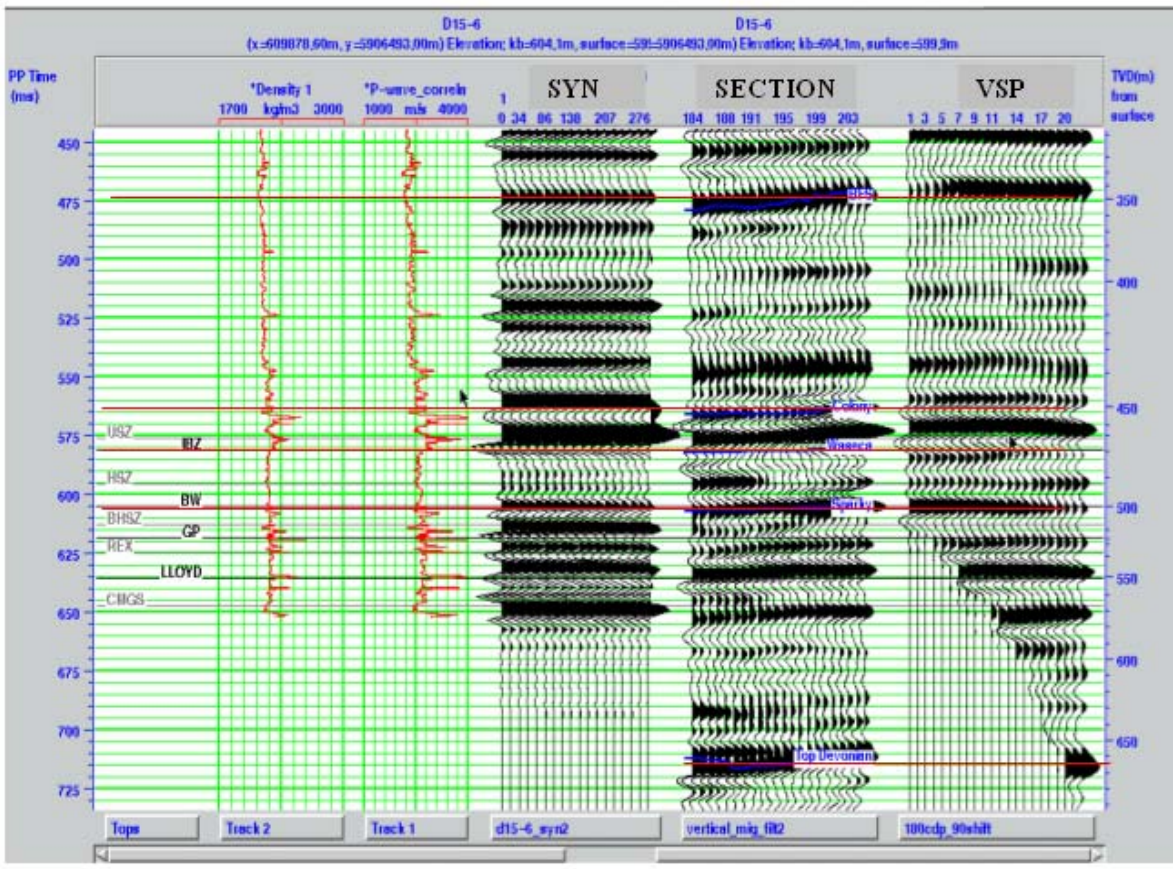

Figure 2.9. Composite plot for well D15-6 showing logs, synthetic seismograms, surface seismic and 180-m offset VSP; where the bandwidth for the synthetic and seismic data is 8-140 Hz and for VSP 8-120 Hz.

There is a noticeable bandwidth decrease as we move from the synthetic to VSP data (Figure 2.9). For example, some minor events between 500 and 550 ms are not pronounced on the VSP and surface seismic data because of their lower frequency content.

2.3 Interpreted data

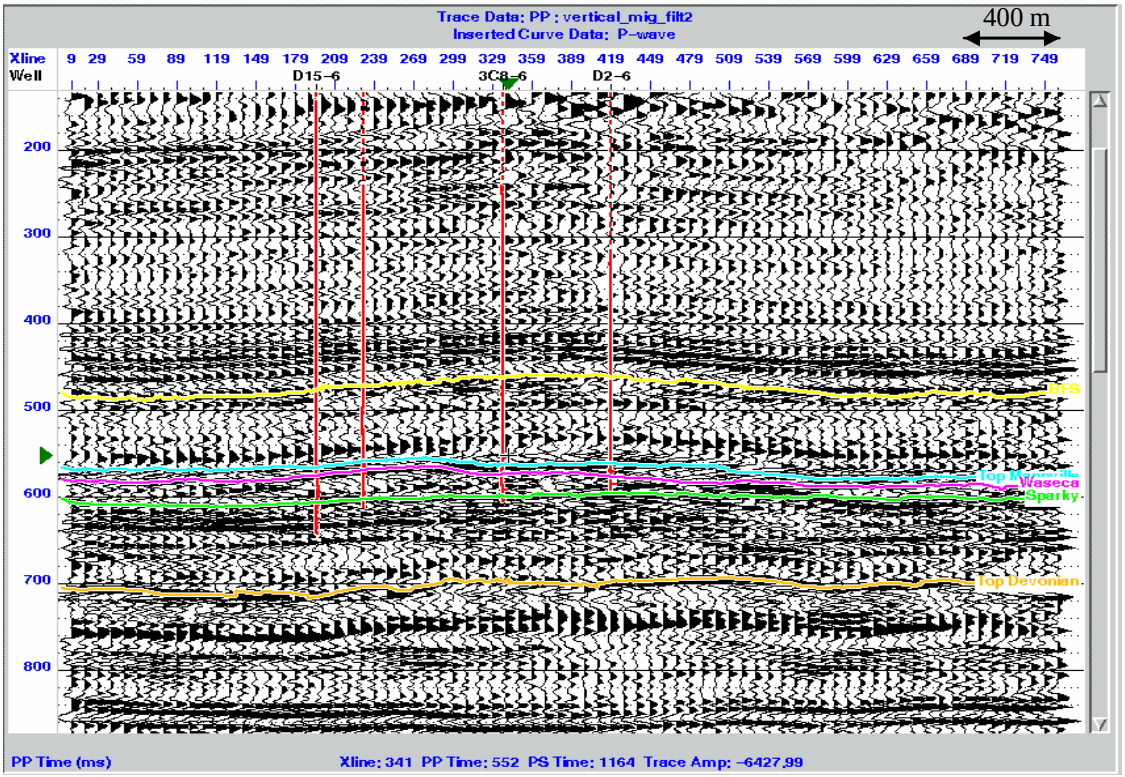

Figure 2.10. Interpreted PP section with indicated horizons.

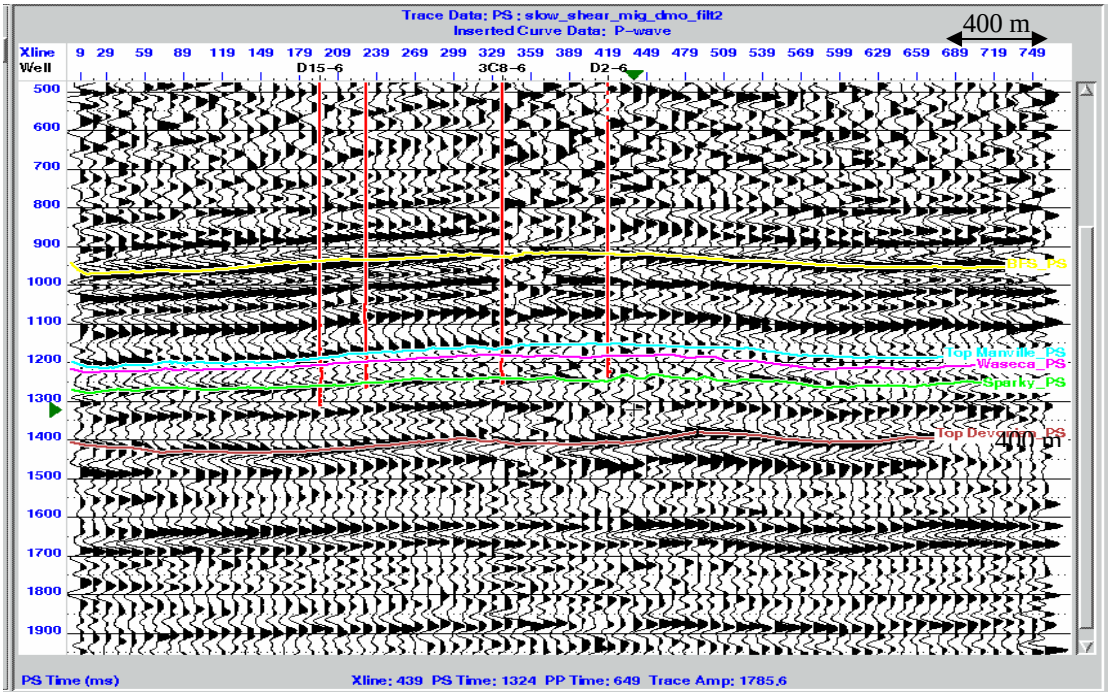

Figure 2.11. Interpreted PS section with indicated horizons.

The results of interpretation are shown on Figures 2.10 and 2.11. Every 10th trace is plotted to place all CDP's into one screen. We can trace almost all main horizons on both PP (Figure 2.10) and PS (Figure 2.11) sections. However, the Waseca event is not clearly recognizable on PS section, because of the lower frequency content of the data.

2.4 Vp/Vs estimation

Dividing P-sonic velocities with the S-sonic velocities provides a Vp/Vs value (Figure 2.12), which is important for lithology discrimination. The productive formation has a Vp/Vs value noticeably lower (1.7) than the overlying formations (around 4.4).

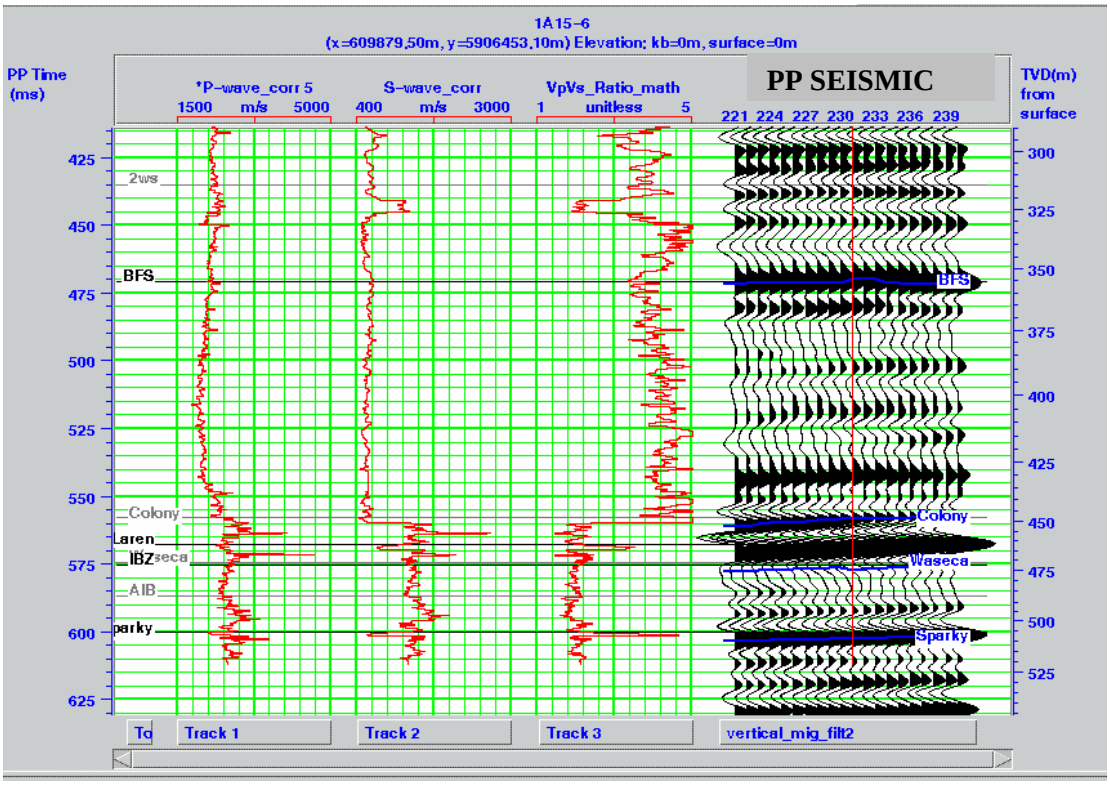

Figure 2.12. Calculated Vp/Vs value for well 1A15-6.

Since we have now interpreted both PP and PS horizons, we can link the corresponding horizons in the multicomponent seismic interpretation package, ProMc. The program

calculates a Vp/Vs value between the horizons and plots the colour section of Vp/Vs along the entire line. This colour Vp/Vs overlay is shown with a PS line in Figure 2.13.

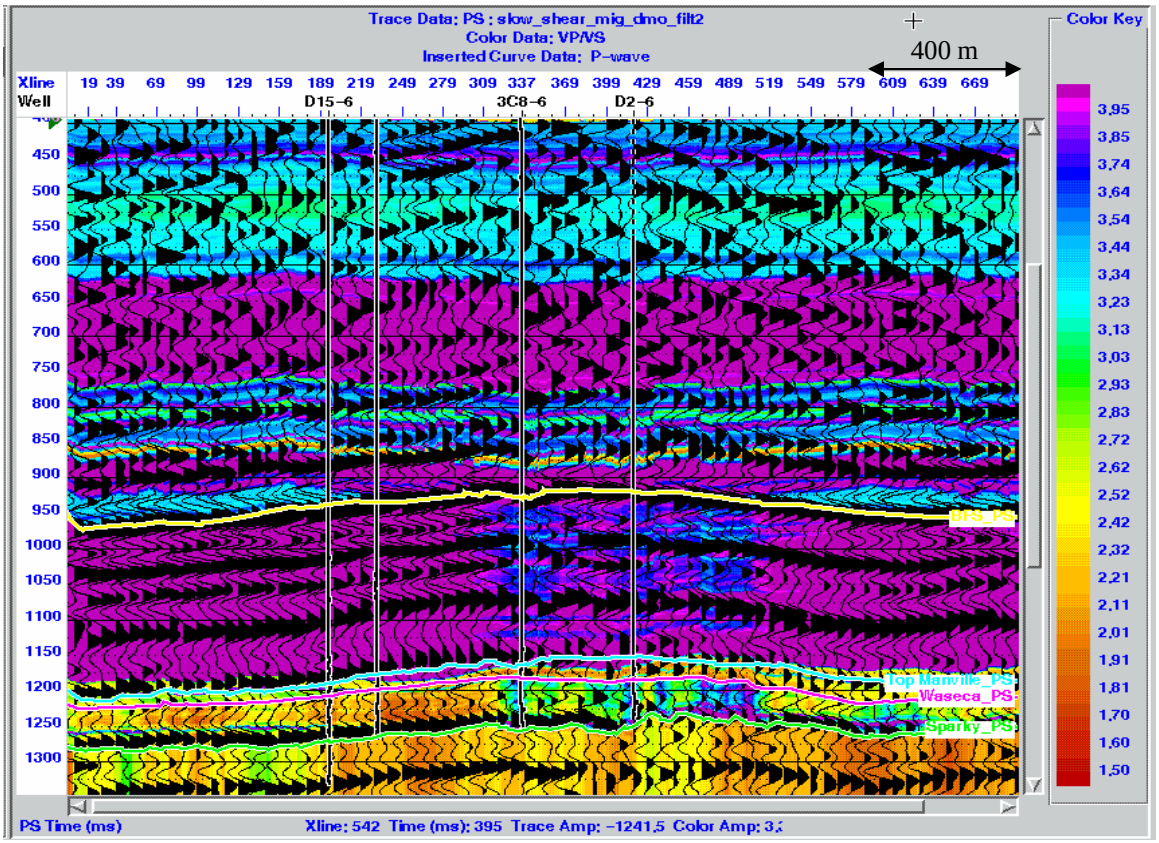

Figure 2.13. Vp/Vs value, computed from time thickness, overlain with the PS section.

To compute the Vp/Vs along the seismic line we use the following formula:

$$\frac{V_P}{V_S} = \frac{2*\Delta t_{PS}}{\Delta t_{PP}} - 1 \ , \qquad (2)$$

where Δt_{PP} and Δt_{PS} are the time thicknesses between the interpolated horizons on PP and PS data set accordingly. A derivation of the above equation was described by Watson (2004). One of the limitations in equation (2) is that it is an average over the time thickness interval.

A drop from 4.4 to 3.6 between 950 and 1100 ms in the seismic Vp/Vs value may be explained by the effect of steam injection into the wells. It was shown by Watson (2003)

that the injection of the steam causes increases in travel time and decreases in both Vp and Vs velocities. However, Vp decreases at a greater rate than Vs, which causes a Vp/Vs drop near the recently injected wells 3C8-6 and D2-6. Wells D15-6 and 1A15-6 do not exhibit any anomalies since they had not been recently injected.

We can trace the general tendency of Vp/Vs: it is quite high in the Mannville shale (around 4) and goes down in the productive sand interval with the exception of coal layers. The coal layers typically have higher Vp/Vs. In our case, this value goes up to almost 4 within thin coal layers of Waseca (at about 600 ms at the PP section). The productive interval has a Vp/Vs at around 1.5 which is in reasonable accord with the well log data (Figure 2.12).

The Waseca-Sparky time interval of almost 25 ms correlates to a depth thickness of around 35 metres. Note that the Vp/Vs value represents an average across this depth interval.

Chapter 3

AVO analysis and inversion at Pikes Peak

3.1.1 Synthetic AVO example

AVO analysis consists of an examination of reflections at varying source-receiver offsets and the search for an anomalous seismic response. According to Rutherford and Williams's classification (1989), there are three main classes of AVO anomalies: Class 1 – dim out, Class 2-phase reversal and Class 3 – bright spots. Since the Pikes Peak field is considered as a low impedance reservoir, it should be related to the Class 3 and exhibit a reflectivity decrease with the offset (Figure 3.1.)

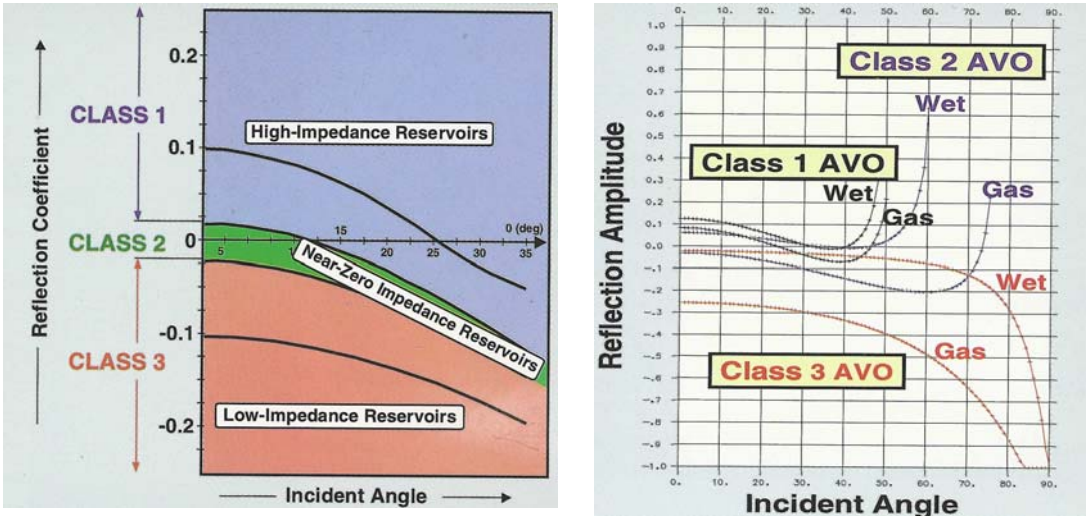

Figure 3.1. Classification of AVO responses (left) with corresponding linear approximation (right), after Rutherford and Williams (1989).

The AVO Software package allows us to create a synthetic AVO response for a particular well. For this example, I took the density and P-wave sonic logs for the well 3C8-6 and then calculated the S-wave log, using Castagna's equation. A wavelet was extracted from the seismic data using the well log (Table 3.1).

Time from	0 – 2000 ms
Number of offsets	30
Wavelet length	150 ms
Taper length	20 ms
Sample rate	2 ms
Extraction type	Full wavelet

Table 3.1. Wavelet extraction parameters

Observing the Zoeppritz synthetic seismograms (Figure 3.2), we can notice that some reflections exhibit an amplitude decrease with offset. For this well, a decrease in the amplitude with offset at around 580 ms corresponds to the oil sands.

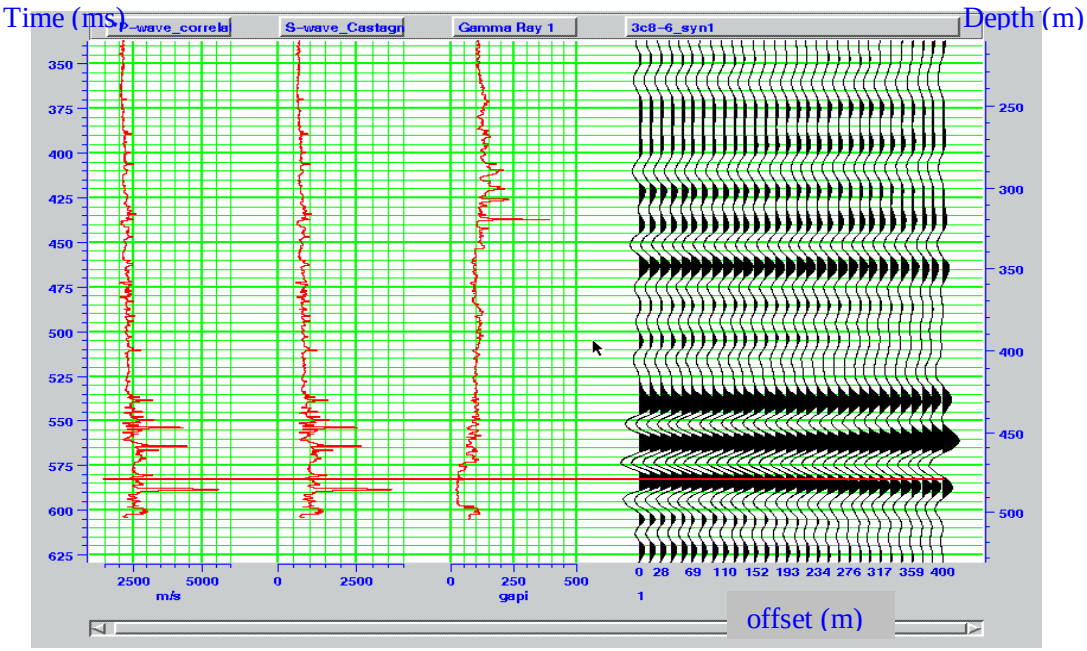

Figure 3.2. P-wave sonic, calculated S-wave sonic, gamma-ray log and PP synthetic for well 3C8-6. Note the amplitude decrease with offset at 580 ms.

Zoeppritz's equation can predict the change in amplitude for any combination of rock properties. For example, when at a particular depth point both impedance and Poisson's

ratio increase (or decrease simultaneously), then reflectivity is increasing (Figure 3.4.c). When they change in different directions, then the reflectivity is decreasing (Figure 3.4.b). In the case of constant Poisson's ratio, the AVO response is almost flat (Figure 3.4.a).

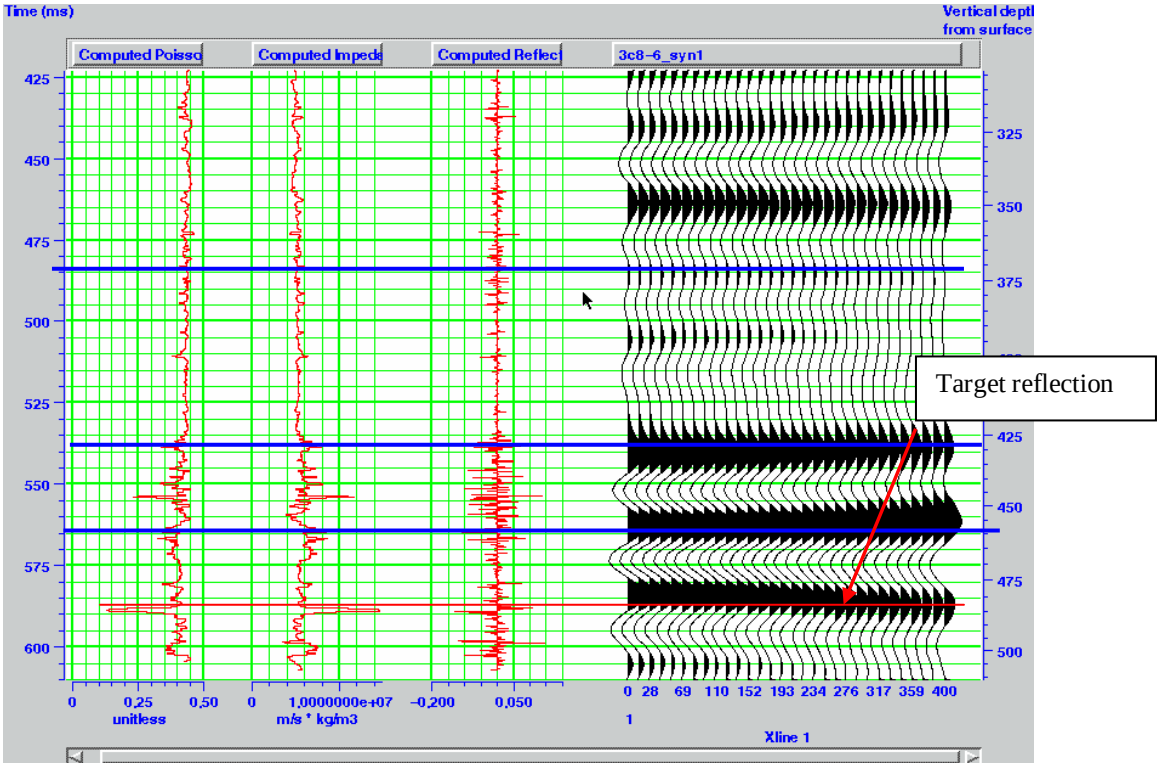

Figure 3.3. Computed Poisson's ratio, impedance and reflectivity for well 3C8-6, where the target reflector exhibits the amplitude decrease with offset.

A theoretical relationship between the reflection amplitude and lithology was previously described by Shuey (1985) and modified by Hilterman (1990):

$$RC(\theta_1) = \frac{1}{2}\left(\frac{\Delta\alpha}{\alpha}+\frac{\Delta\rho}{\rho}\right)\left(1-\frac{4\beta^2}{\alpha^2}\sin^2\theta\right) + \frac{\Delta\sigma}{(1-\sigma)^2}\sin^2\theta + \frac{1}{2}\frac{\Delta\alpha}{\alpha}\left(\tan^2\theta-\frac{4\beta^2}{\alpha^2}\sin^2\theta\right) \quad (3)$$

Acoustic impedance $0^o \rightarrow 90^o$ — Poisson's ratio $15^o \rightarrow 90^o$ — P-wave velocity $30^o \rightarrow 90^o$

where RC – reflection coefficient, θ - incident angle, α - P-wave velocity, β - S-wave velocity, ρ - density, and σ - Poisson's ratio.

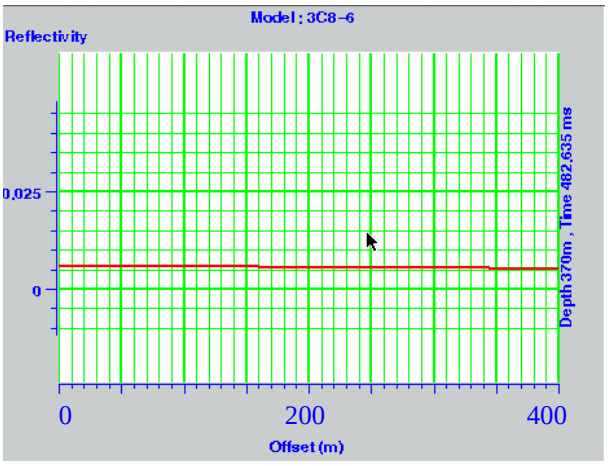

Figure 3.4.a AVO curve created for 370 m depth

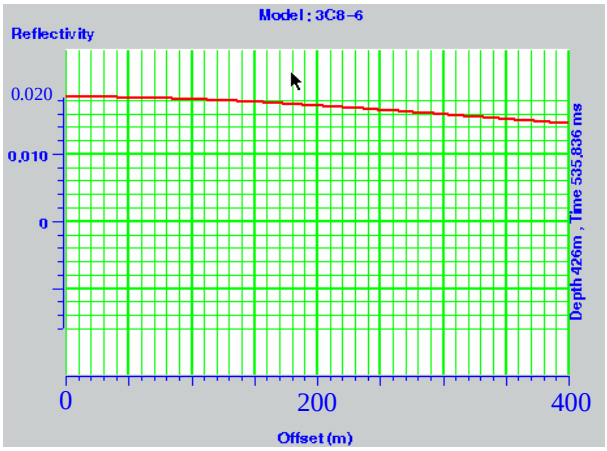

Figure 3.4.b AVO curve created for 426 m depth

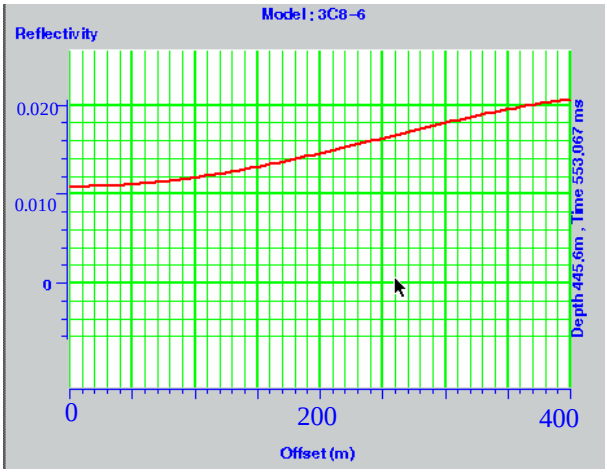

Figure 3.4.c AVO curve created for 445 m depth

Figures 3.4a-c demonstrate how the P-wave reflectivity is changing with the offset from 0 to 400 m. According to the Figure 3.3, the computed reflectivity ranges from -0.1 to 0.15. Since there is a large difference in frequency content of the synthetic and well log (reflectivity) data, we can trace just the general trend of reflectivity, whereas small changes in the coefficient are not seen on the synthetic data.

3.1.2 Fluid replacement modelling

When shear logs are not available, we can attempt to estimate Vs using P-wave velocity logs. Castagna's equation is the most commonly used technique:

$$V_s = C_1 V_p + C_2 \qquad (4)$$

where $C_1 = 0.86190$, $C_2 = -1172$.

This equation is used for the wet-sand model. So, our estimated log might be not completely accurate for oil sands. The Fluid Replacement Model (FRM) allows modelling gas or oil saturated sands. Within the FRM module, the Biot-Gassman equations are used to convert the actual P-wave log from 50% to 100% water saturation (Russell, 2001). Then, with the help of Castagna's equation, the shear-wave velocity for this water saturation is calculated. Finally, the Biot-Gassman equations are used again to correct from 100% water saturation back to 50%. Figure 3.5 shows the original P and S-wave logs (blue) and those, calculated for 50% hydrocarbon saturation (red). The P-wave logs are identical; the S-wave log, calculated in FRM module has slightly higher velocities (red curve), but keeps the same trend. As a result, the FRM synthetic seismogram for this well looks very similar to the wet synthetic.

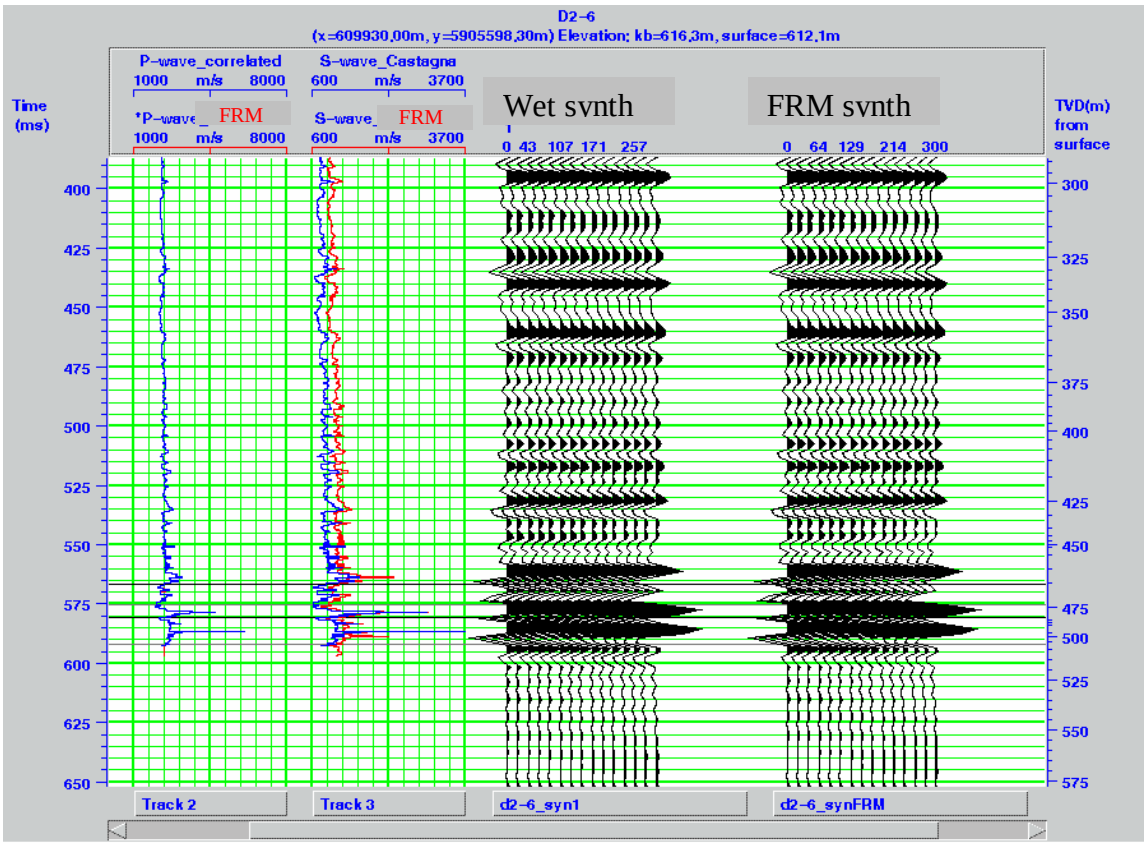

Figure 3.5. P-wave and S-wave Castagna's logs, wet synthetic and 50% oil synthetic seismogram for well D2-6.

The reason for this similarity is the comparable petrophysical characteristics of oil and water (Table 3.2).

Parameter	Water	Oil
Density	1.00 g/cc	0.95 g/cc
P-wave velocity	2300 m/s	2100 m/s
Poisson's ratio	0.5	0.5
Bulk moduli	2.2 GPa	1.62 GPa

Table 3.2. The averaged petrophysical characteristics for oil and water at normal temperature and pressure ($20°C$, $50 Atm$) (Prohorov, 1990).

3.1.3 Intercept and gradient analysis using CDP gathers at Pikes Peak (array data)

AVO processing should preserve or restore relative trace amplitudes within CMP gathers (Allen, 1993). To improve the data quality (reduce ground roll and surface waves), vertical geophone arrays were used at Pike Peak. The group interval for the arrays was 20 m, with maximum offset 1330 m (Hoffe et al., 2000 and Appendix 1).

The presence of gas and oil sometimes results in high-amplitude reflections known as "bright spots". In the Pikes Peak case, we can see the strong reflection at a time about 580 ms (Figure 3.6), which corresponds to the top of productive Waseca formation.

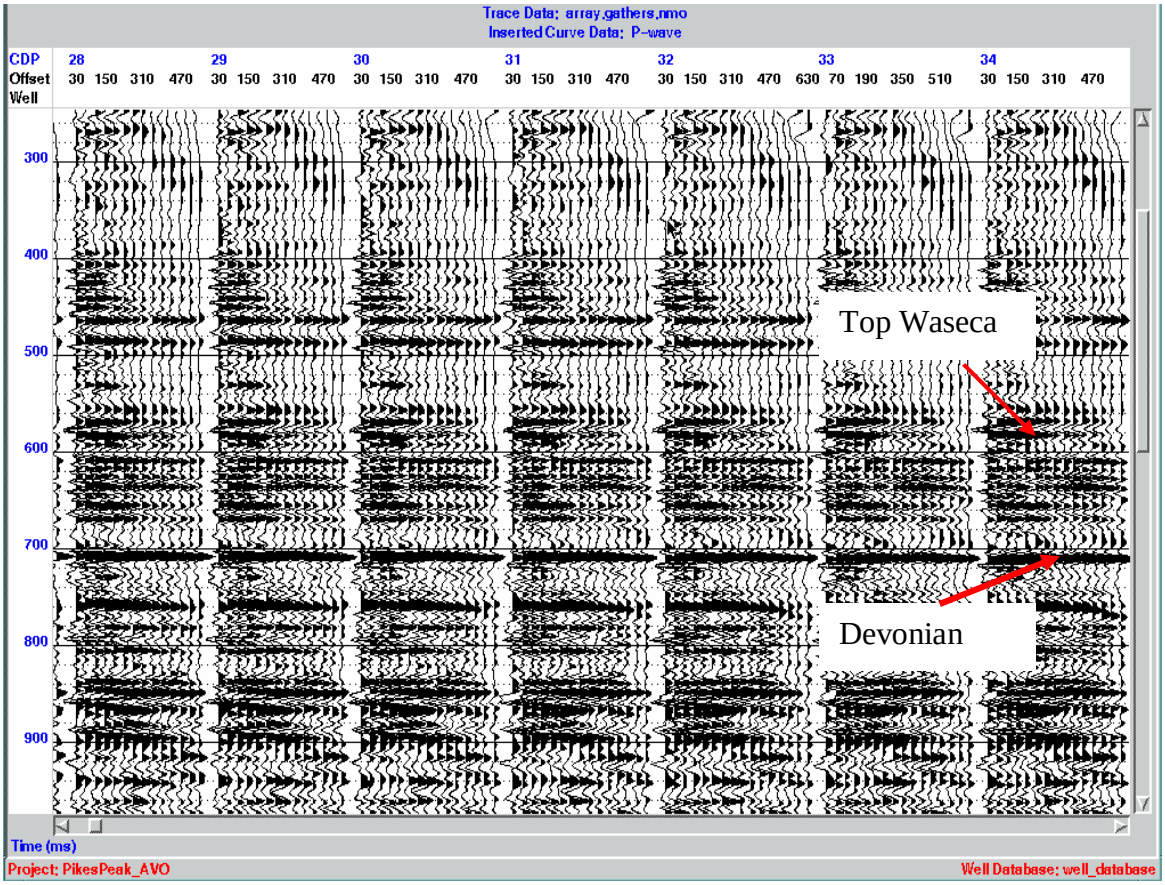

Figure 3.6. NMO corrected CDP gathers from the array data (year 2000).

For the Class 3 environment, the intercept and gradient can be used to support the presence of hydrocarbons. Here, under the intercept (A) we assume a normal incident reflectivity, and gradient or slope (B) is a function of P-wave velocity, S-wave velocity and density (Hilterman, 2001). Since the productive zone is located at around 586 milliseconds, I chose this time for the intercept and gradient calculation (Figure 3.7). The actual reflectivity is shown as a squared line, and the smoothed version of reflectivity is shown as a solid line.

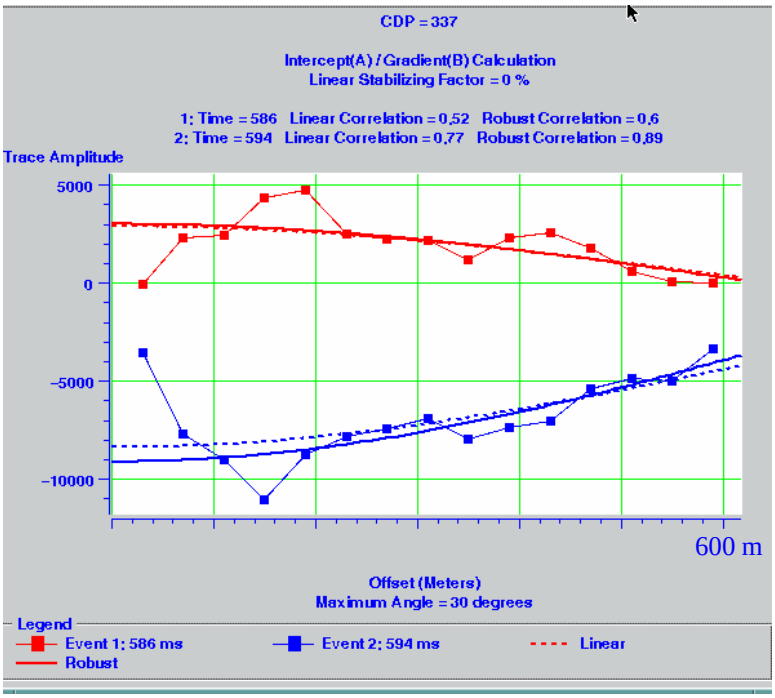

Figure 3.7. Intercept and gradient calculation for two events (586ms, red and 594ms, blue) from the seismic data. The P-wave sonic log from well 3C8-6 (CDP 337) and the array gathers are used as an input.

As it is seen from the graph (Figure 3.7), the reflectivity of the target event (red) decreases with the offset, which corresponds to the reflectivity changes on the synthetic seismogram for well 3C8-6 (Figure 3.3).

To maximize the indicator of possible pore fluids, the product of intercept and gradient is often used (Figure 3.8).

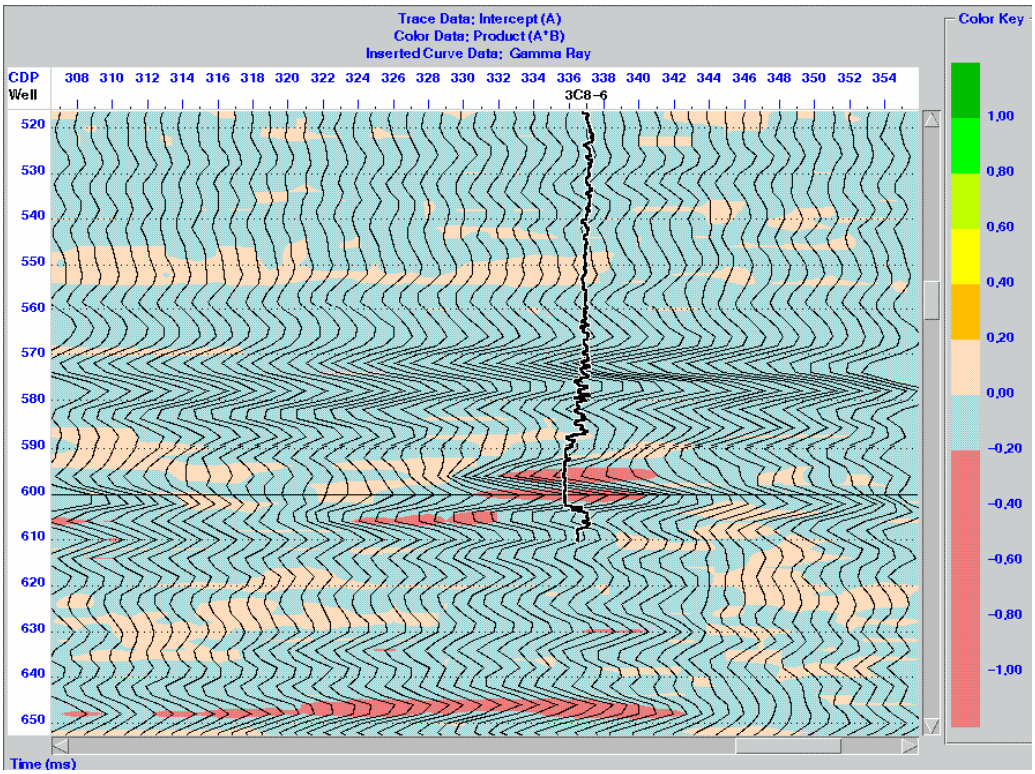

Figure 3.8. Coloured section showing the product of intercept and gradient and inserted gamma ray log for well 3C8-6. Note that the anomaly coincides with the sand channel, characterized by the gamma ray log decrease.

The CDP gathers (Appendix 1) and P-wave velocity from well 3C8-6 are used as an input to create this coloured section (Figure 3.8). The maximum number of CDP locations is also specified. Here, the wiggle traces are intercept traces, the colour attribute is the product of intercept and gradient, A*B. In this case, we can see a strong red (negative) response at the well location at about 580 milliseconds, which correlates with the inserted gamma ray log for well 3C8-6 (CDP 337).

Finally, we can cross-plot the intercept and gradient for a particular time interval (Figure 3.9). The interval 480-680 milliseconds is chosen to fit the productive zone in the middle of it. After delineating four zones with the similar intercept/gradient values, we can apply this result to the cross-section (Figure 3.10).

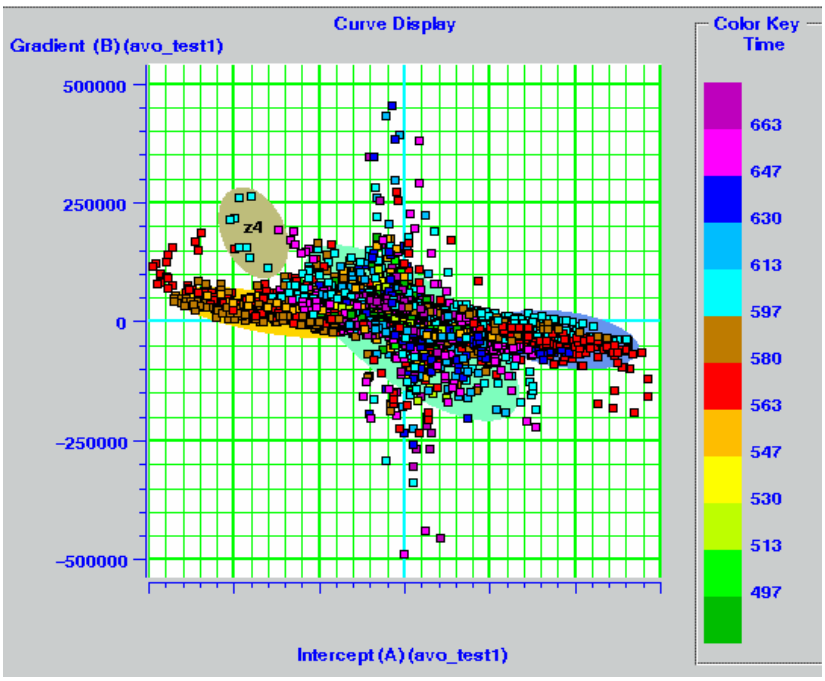

Figure 3.9. Cross-plot of intercept and gradient where different coloured points represent different times.

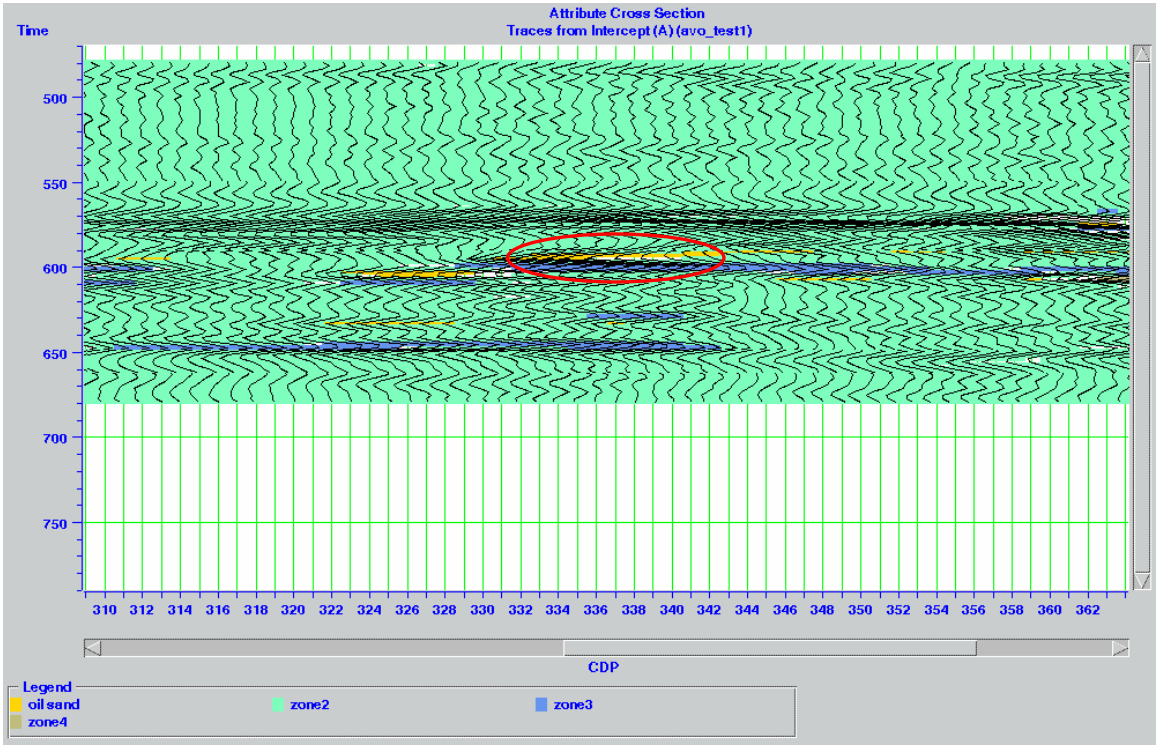

Figure 3.10. Fragment of the PP seismic section, showing zones with different intercept/gradient values, where the yellow colour corresponds to the oil sands.

Note that the anomaly is fairly well defined and its location matches CDP 337 where the producing well 3C8-6 was drilled.

It is important to remember about the limitations of amplitude versus offset analysis. Since the AVO theory is based on linearized approximations of Zoeppritz equations (Downton, 2000), the seismic data must be properly processed, otherwise the AVO anomalies can not be related to the hydrocarbon zones. The relationship between the elastic parameters and the rock properties is non-unique. There are many rocks and fluids that may influence the elastic parameters, therefore, understanding the geology in the area of interest is crucial for the successful AVO interpretation.

3.2 Inversion of seismic data

Inversion can be defined as a procedure for obtaining models which adequately describe a dataset (Treitel and Lines, 1994). For this seismic case, post-stack migrated data plays the role of the dataset to be inverted and the acoustic impedance is a desired property to estimate. Our zone of particular interest is the Waseca formation, which is going to be analyzed in detail in terms of the impedance anomalies. Since all inversion algorithms suffer non-uniqueness, it is important to use some external information to limit the number of possible models, which agree with the input seismic data. Well log data provides the additional information to constrain our model and to make the inversion result more accurate.

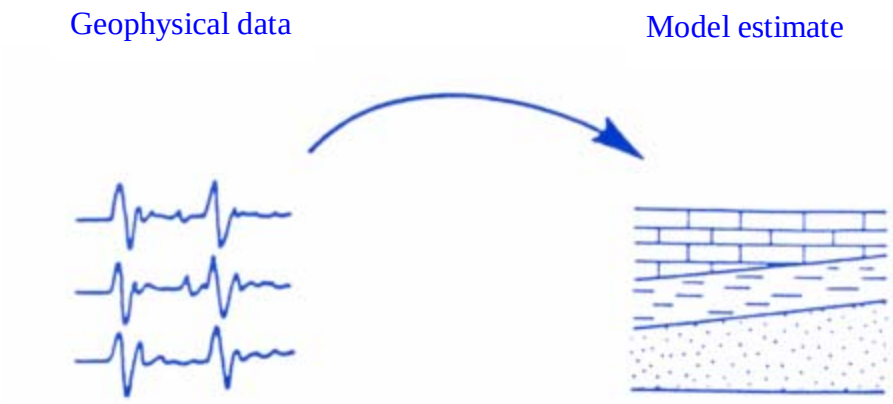

Figure 3.11. An illustration of inversion (from Treitel and Lines, 1994).

3.2.1 PP inversion

With our wells now correlated to the seismic data, we can proceed with the inversion. Using the convolution model of seismic traces, $S(t) = r(t) * w_s(t)$, and the wavelet, we begin the inversion process.

There are two different approaches to estimate the wavelet:

a) Statistical

This method estimates the wavelet from the seismic data alone and can be described as following:

1) calculate the autocorrelation over a chosen window
2) calculate the amplitude spectrum of autocorrelation under the white reflectivity assumption
3) take the square root of the autocorrelation spectrum which approximates the amplitude spectrum of the wavelet
4) compute the desired phase (zero, constant, minimum)
5) take the inverse FFT to produce the wavelet (Todorov, 2000)

b) using a well log

This method combines the well log (density and velocity) and seismic information. The reflectivity at the well location is computed from the density and sonic logs, then deconvolving the reflectivity from the seismic data, we obtain the wavelet. (Lines and Treitel, 1985). In theory, the exact phase information can be obtained at the well locations.

So, the choice of the wavelet is crucial for the correct impedance model.

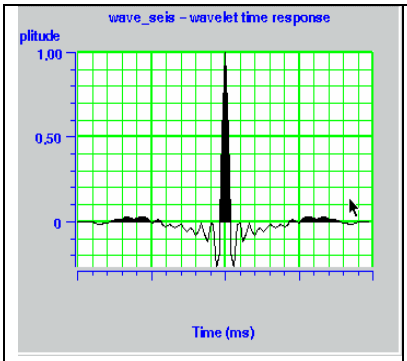

Time axis: -100 – 100ms

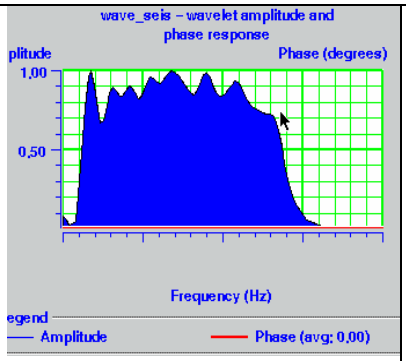

Frequency axis: 0 – 200 Hz

Wavelet parameters:

Wavelet name: wave_seis
Wavelet length: 200 ms
Taper length: 25 ms
Sample rate: 2 ms
Phase rotation: 0 degrees
Phase type: Constant phase

The number of traces used for wavelet extraction: 759

Figure 3.12. Wavelet extracted from seismic data.

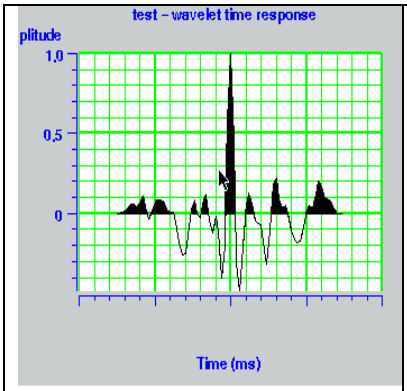

Time axis: -100 – 100ms

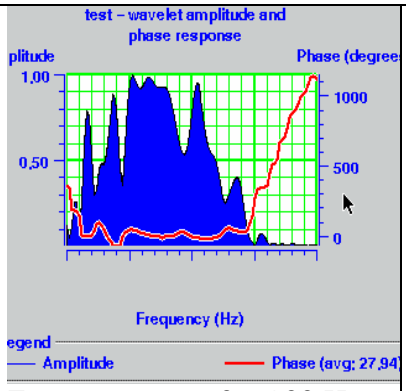

Frequency axis: 0 – 200 Hz

Wavelet parameters:

Wavelet name: test
Wavelet length: 150 ms
Taper length: 20 ms
Sample rate: 2 ms
Extraction type:
Full wavelet

The number of traces used for wavelet extraction: 759

Figure 3.13. Wavelet extracted from seismic data using all wells in the project.

Figures 3.12 and 3.13 illustrate the application of these two methods of wavelet extraction. Since the wavelet extracted from the seismic data alone (Figure 3.12) looks less complicated, it was chosen for the inversion modelling.

Multi-well analysis allows us to check the total correlation between the synthetic and seismic traces at the well location (Figure 3.14). Four calculated impedance logs (blue) along with the seismic trace (black) and synthetic (red) trace, extracted at the well location, are shown in one window. By reducing the correlation window, we can improve the quality of correlation. For this case, I reduced the window to 250-620 ms to get the total correlation coefficient 57%.

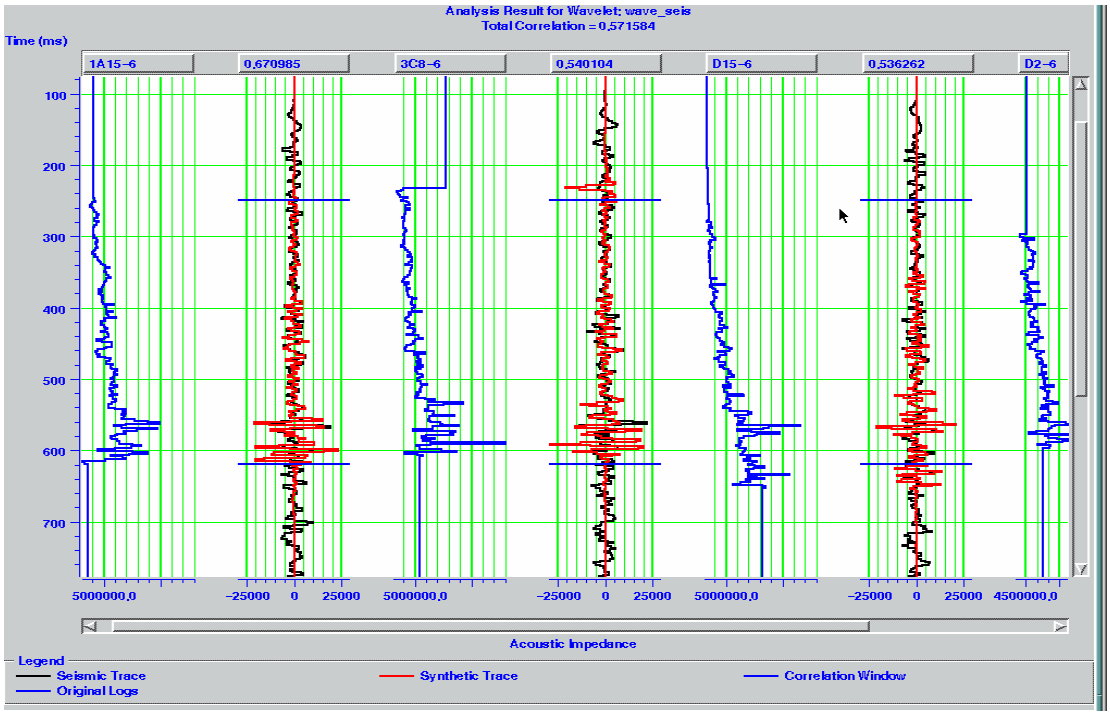

Figure 3.14. Multi-well analysis window showing the calculated impedance log (blue), seismic trace (black) and synthetic trace (red) extracted at the well location.

The correlation plot (Figure 3.15) allows us to check the correlation coefficient for the particular well. Unsatisfactory wells can be excluded from the analysis.

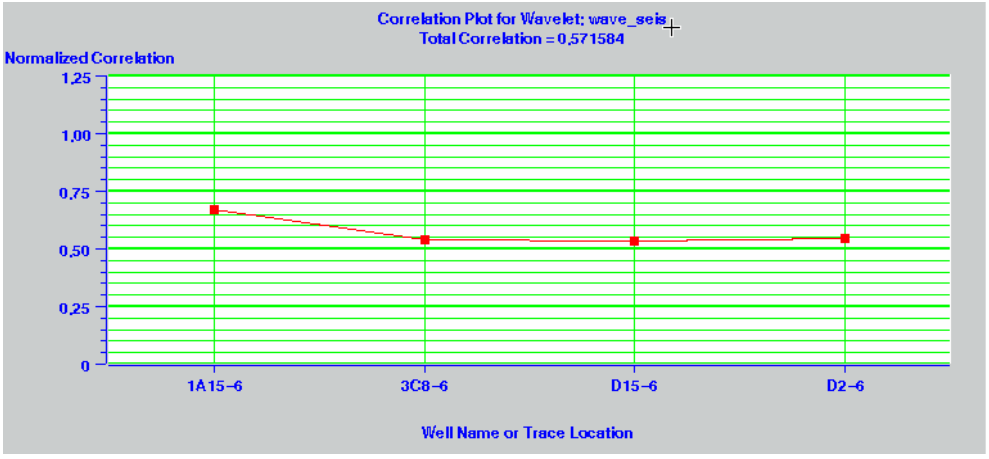

Figure 3.15. Correlation plot for four wells.

The initial background model (Figure 3.16) is formed by blocking an impedance log from the wells and interpolating the values between the wells. The colour bar on the right gives a total impedance range for this section. Since the impedance is a product of density and velocity it is measured in [m/s* g/cc].

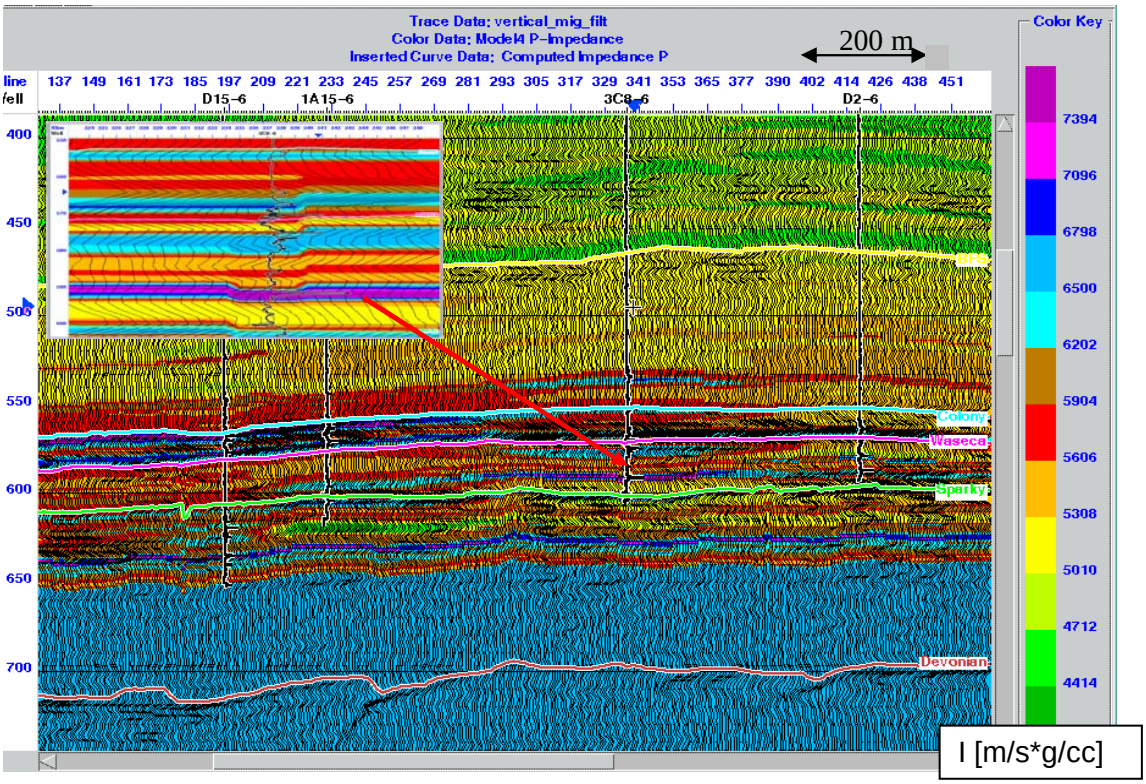

Figure 3.16. Initial/background P-wave impedance model constructed from 4 wells and PP seismic data.

As it is expected, the impedance increases with depth with the exception of the productive zone (yellow in the picture). The inserted impedance logs are shown on the section. An enlarged plot for well 3C8-6 allows us to check the quality of prediction.

I performed three types of inversion for these data: model-based, sparse spike and recursive. Model-based inversion (Figure 3.17) produced the highest frequency result, but this high frequency comes largely from the initial guess model, not from the seismic data.

The sand channel can be traced here as a low impedance anomaly (yellow in the picture). This anomaly (circled in the white oval) coincides mainly with the well locations.

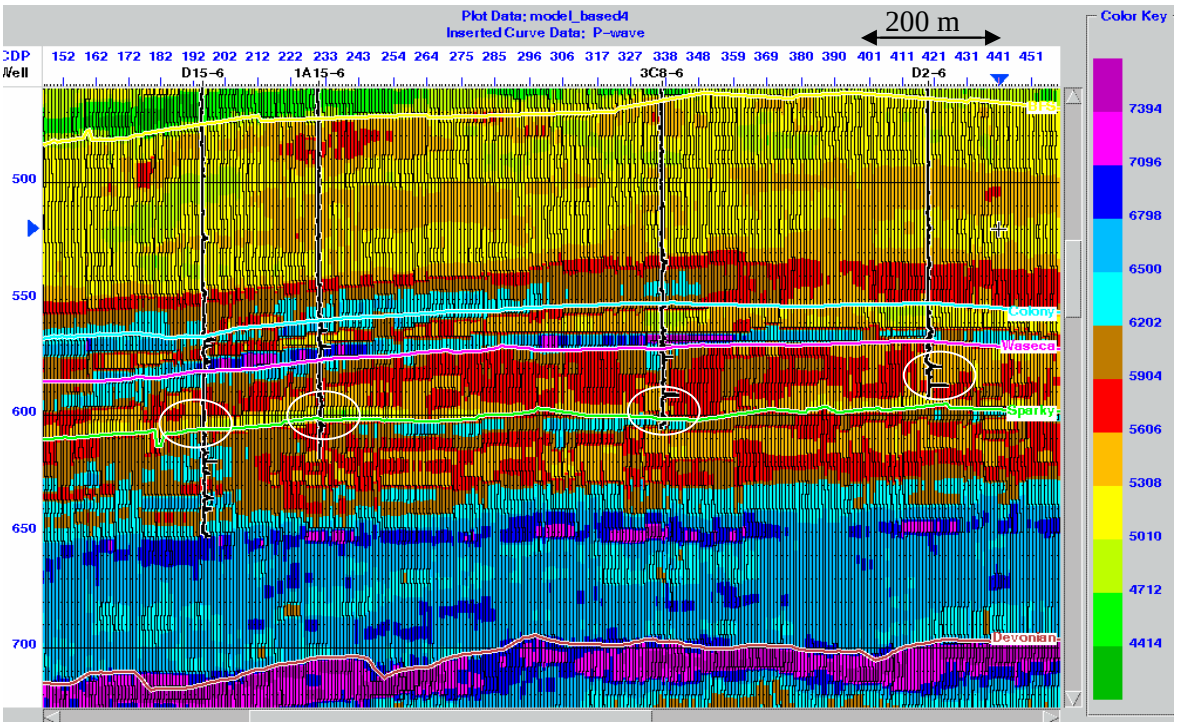

Figure 3.17. Model-based inversion of PP seismic data to impedance.

A visible impedance drop is observed at about 580-600 ms (yellow), where the productive formation lies.

The algorithm for the model-based inversion (Figure 3.18) has been described by Russell (1988) and consists of the following steps:

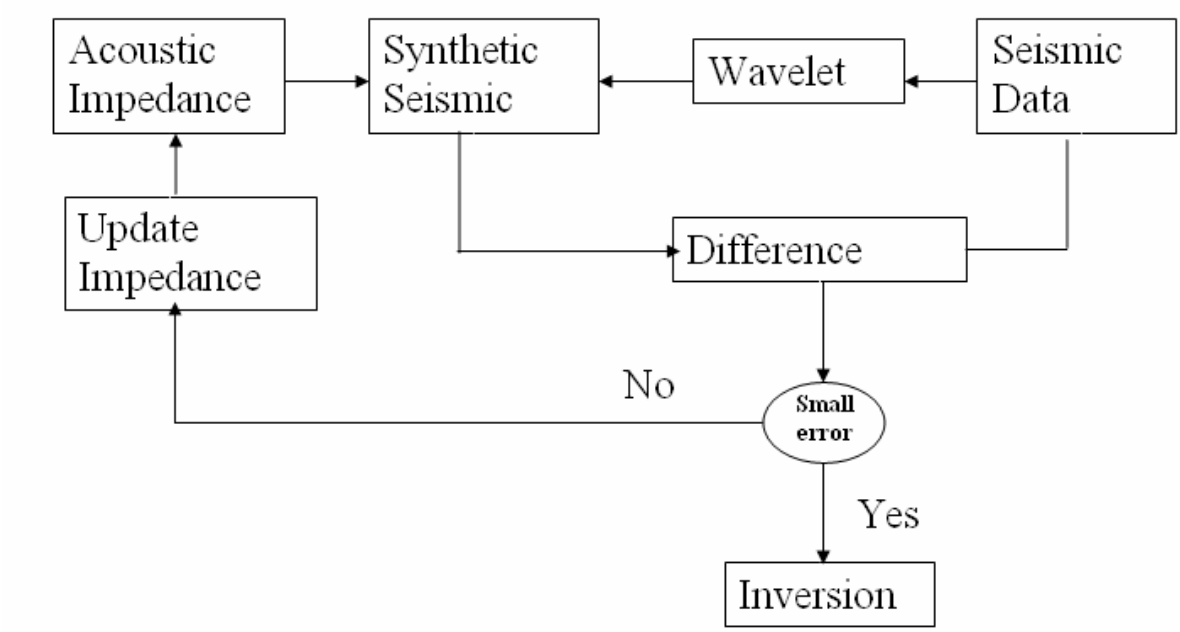

Figure 3.18. Algorithm for the model-based inversion (Russell, 1988).

The parameters chosen for the model based inversion are shown below:

- inversion option – constrained
- average block size – 6 ms
- number of iterations – 5
- processing sample rate – 2 ms
- separate scaler for each trace
- single trace inversion

Two main problems related to this type of inversion are a strong sensitivity on the wavelet and non-uniqueness of the result.

The sparse-spike inversion (Figure 3.19) is based on a maximum-likelihood deconvolution algorithm. It is assumed that the wavelet in the seismic data is known and the earth's reflectivity is composed of a series of large events superimposed on a Gaussian background

of smaller events. For each trace, a sparse reflectivity sequence is estimated. Then, the broadband reflectivity is gradually modified until the resulting synthetic trace matches the real trace with some minor error (from Strata, 2006). It produces a broadband and high-frequency result, which looks quite similar to the model-based inversion (Figure 3.17). The main difference is that, the sparse spike puts events only where the seismic section demands, and model-based is biased to putting events where the initial guess model indicates.

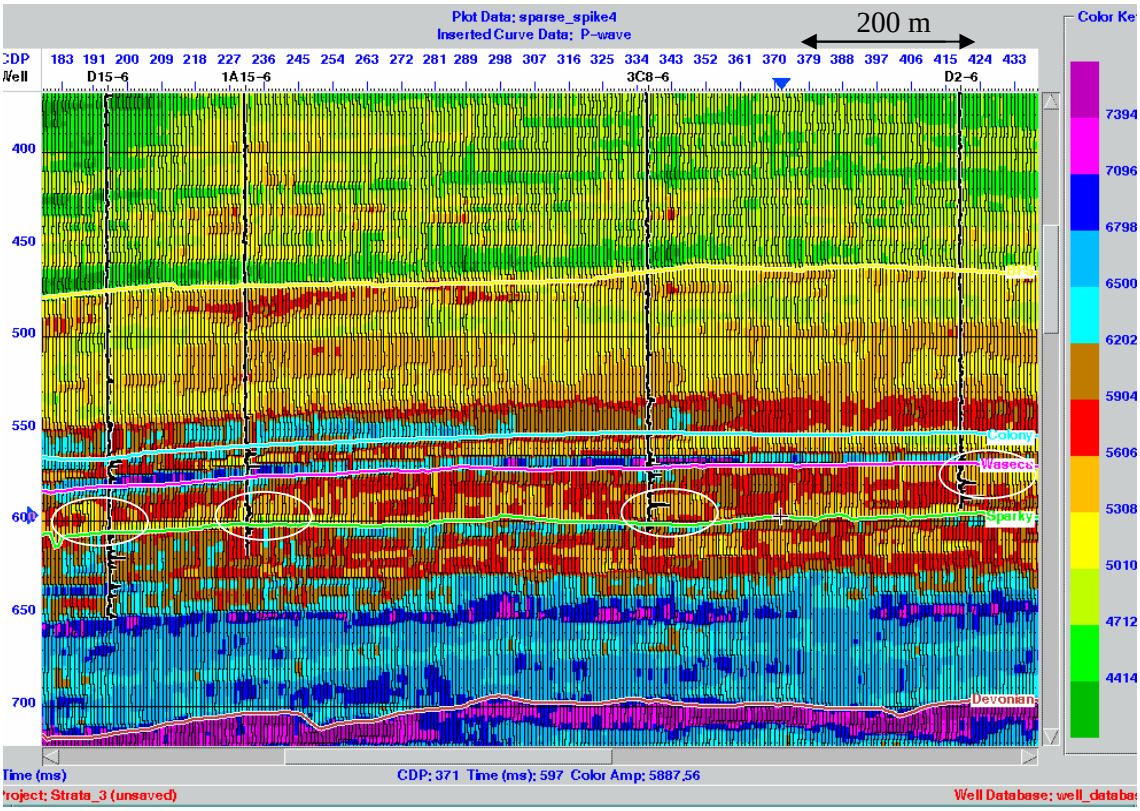

Figure 3.19. Sparse spike inversion (maximum likelihood).

Geologically, the large events correspond to unconformities or the major lithologic boundaries (Figure 3.19). Similarly, the productive zone here is seen as a low impedance anomaly at around 600 ms.

The recursive inversion is also called band-limited because it produces a result (Figure 3.20) confined to just a limited range of frequencies. This frequency range is determined by

the input seismic data (20-150 Hz in this case). The assumption is that the seismic trace itself can be thought of a series of reflection coefficients that have been filtered by a zero-phase wavelet (Strata, 2006); and samples are scaled properly, so reflection coefficients must be the number between -1 and +1.

According to its algorithm, the initial background model is formed by filtering an impedance log from a well (10 Hz high cut); the recursive equation is applied to each trace; then we need to add a low frequency component from the well to get the final result (Figure 3.20).

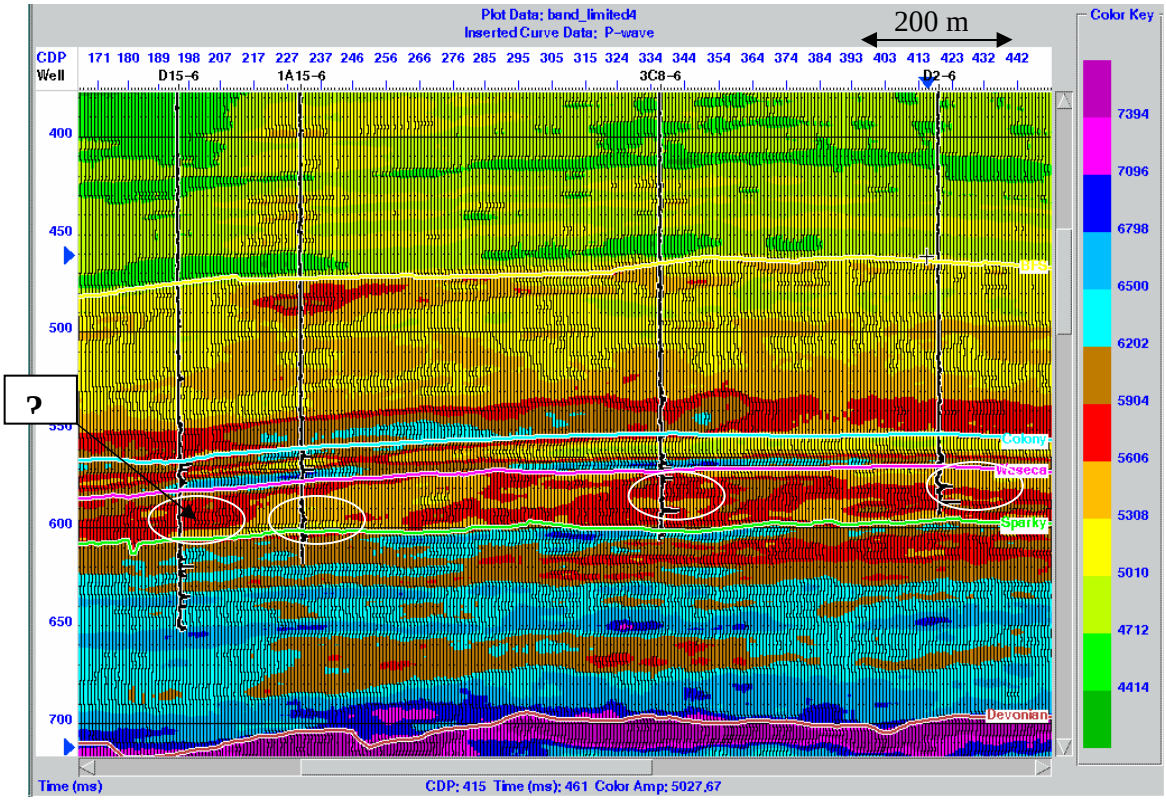

Figure 3.20. Recursive (band-limited) inversion (CDPs 170-445).

The known sand channel ideally should correlate with the low impedance values (yellow). However, the producing well D15-6 is not located in a low-impedance area, which means that the PP inversion may be ambiguous. The reasons for this mismatch could include:

- band-limited character of the seismic data
- existence of noise
- some errors in the wavelet estimation.

In general, the oil wells are located in a low impedance anomaly at around 580-600 ms. (I~5400 g/cc m/s). Figure 3.21 demonstrates the recursive inversion result for the southern part of the seismic line.

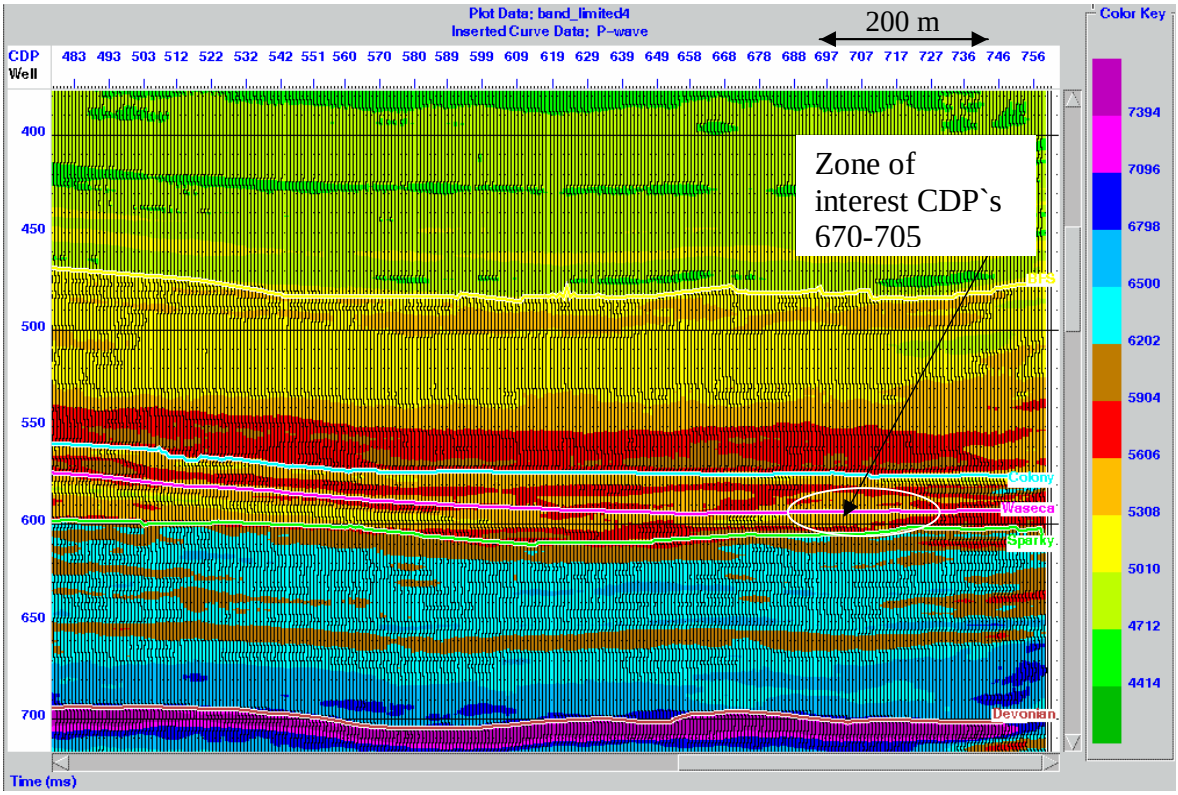

Figure 3.21. Recursive inversion (CDP's 482-756).

An anomalous zone could be observed between 670 and 705 CDP, where no wells have been drilled so far.

3.2.2 PS inversion

First, we transform the PS dataset to the PP time domain. After picking the horizons and extracting the wavelet for PS data (Figure 3.22), we employ the same inversion procedure as with the P-wave case to invert the data using S-wave reflectivity.

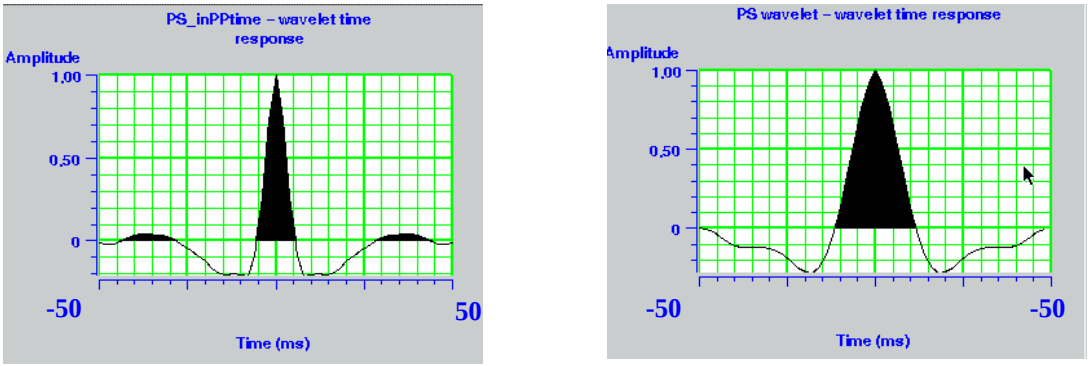

Strata **ProMc**

Figure 3.22. PS wavelet from Strata (PP domain) and ProMc (PS domain).

Thus PS inversion flow is mainly a repeat of the PP inversion flow with the difference that the initial model is created using an S-impedance. Since at Pikes Peak only one well from the vicinity of seismic line had an S-wave sonic log, this log was used to construct the initial model. PS horizons in PP time were also included into the model.

The initial/background model (Figure 3.23) looks pretty flat because only one well containing S-wave sonic was used.

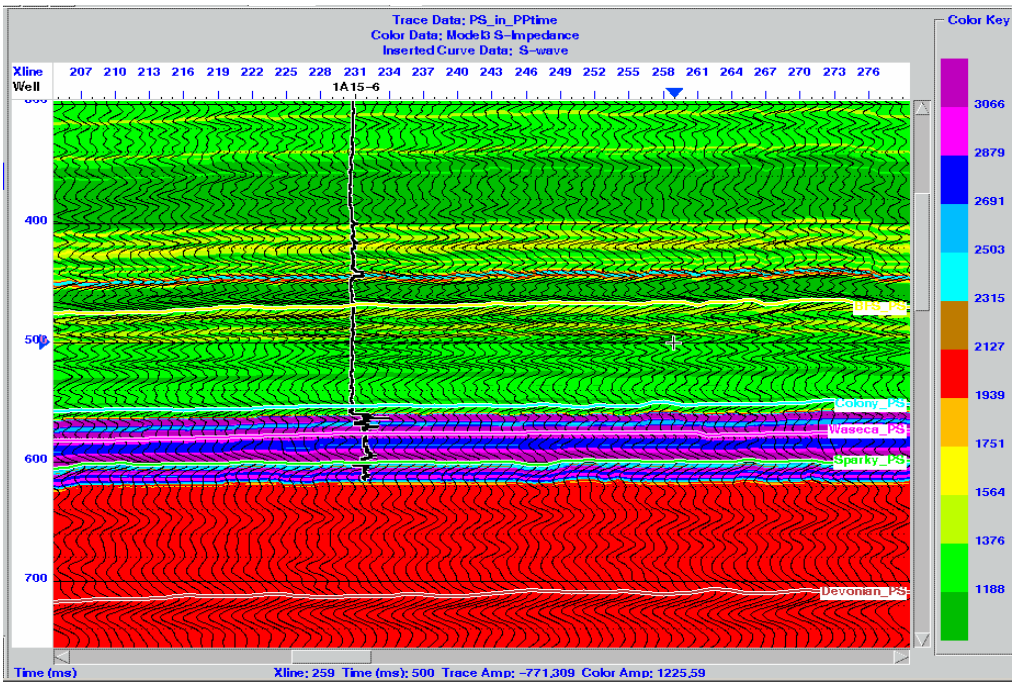

Figure 3.23. The initial/background model for PS data, where the wiggle traces are PS data in PP time and the color attribute is S-impedance.

The inversion analysis window (Figure 3.24) allows us to experiment with the different inversion types, in order to select the most reliable one.

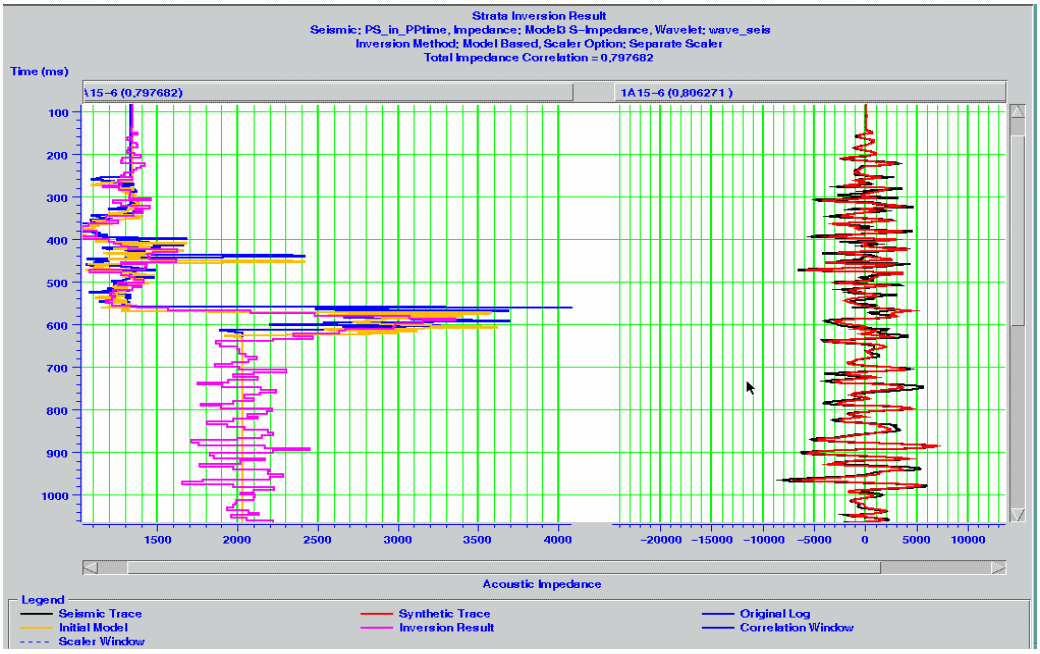

Figure 3.24. Inversion analysis window showing the calculated S-impedance log (blue), initial model trace (yellow) and inverted trace (purple) at well 1A15-6 location.

Figure 3.24 demonstrates the total impedance correlation after the model-based inversion. According to the annotations, the blue trace represents S-wave impedance log from the well 1A15-6, the yellow trace gives us the smoothed version of S-wave impedance log, and the result (purple) repeats the shape of the initial model but also contains the high-frequency component obtained from the seismic trace (black). The total correlation between the real and predicted impedance traces is 79%.

The result of the model-based inversion with the corresponding well is shown on Figure 3.25. Here the productive formation is recognised as an impedance increase (as opposed to a decrease in the PP case). The reason for this is a considerable increase in S-wave velocity within the Waseca formation (Figure 3.26). This velocity contrast will result in an abrupt impedance change at the top and the bottom of the oil sands (even though density is decreasing). The same tendency can be traced laterally across the whole section.

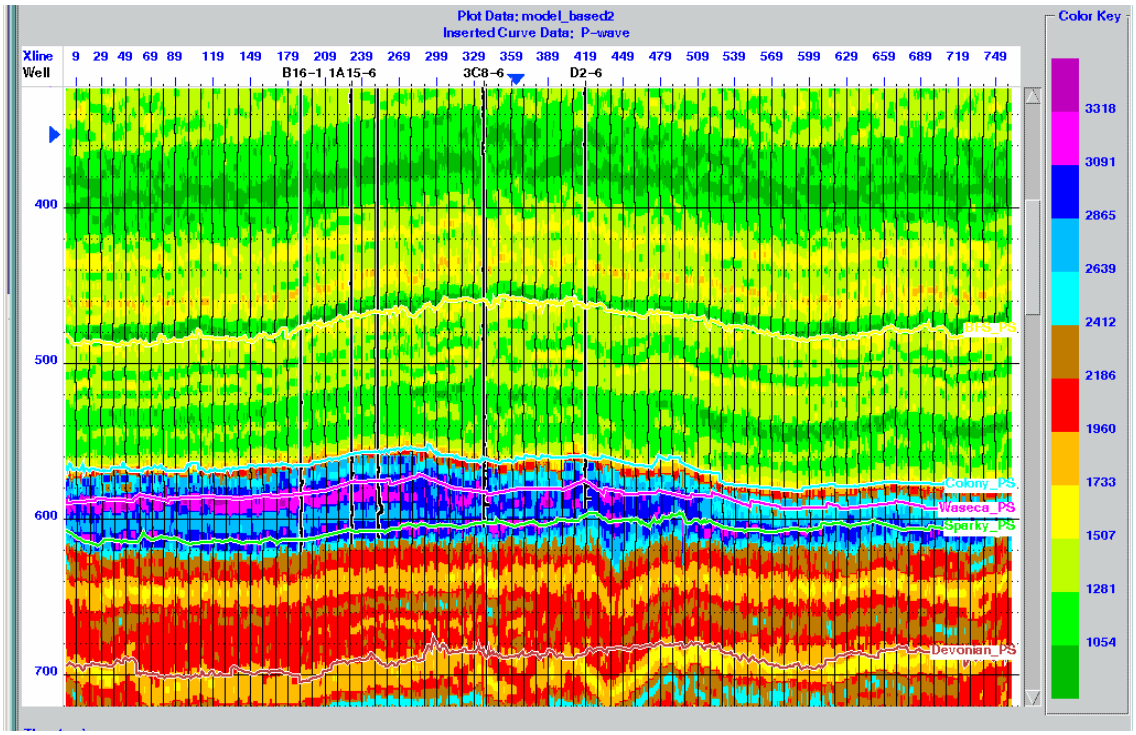

Figure 3.25. Model-based inversion result.

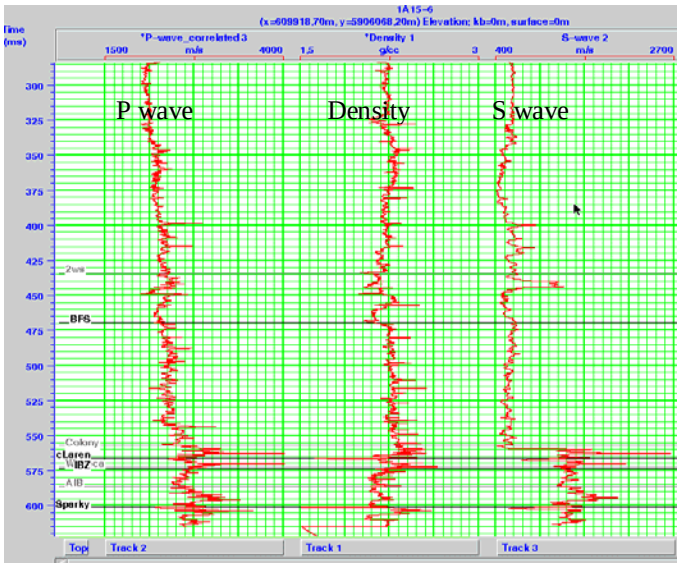

Figure 3.26 The P-wave sonic, density and S-wave logs for well 1a15-6 used in PS inversion process.

The high impedance zone in Figure 3.25 is wider than the Waseca interval. The reason for this would be the behaviour of S-wave sonic log, which gives the higher velocities in Colony, Waseca, and also at the top of the Sparky. The result shown in Figure 3.25 is quite approximate, as we are assuming that PS reflectivity is directly proportional to pure S reflectivity, and only serves as an indicator of S-wave velocity changes.

Since we now have inverted both PP and PS data, it is possible to take a ratio of them. Figure 3.27 was obtained dividing the inverted PP dataset with corresponding PS dataset.

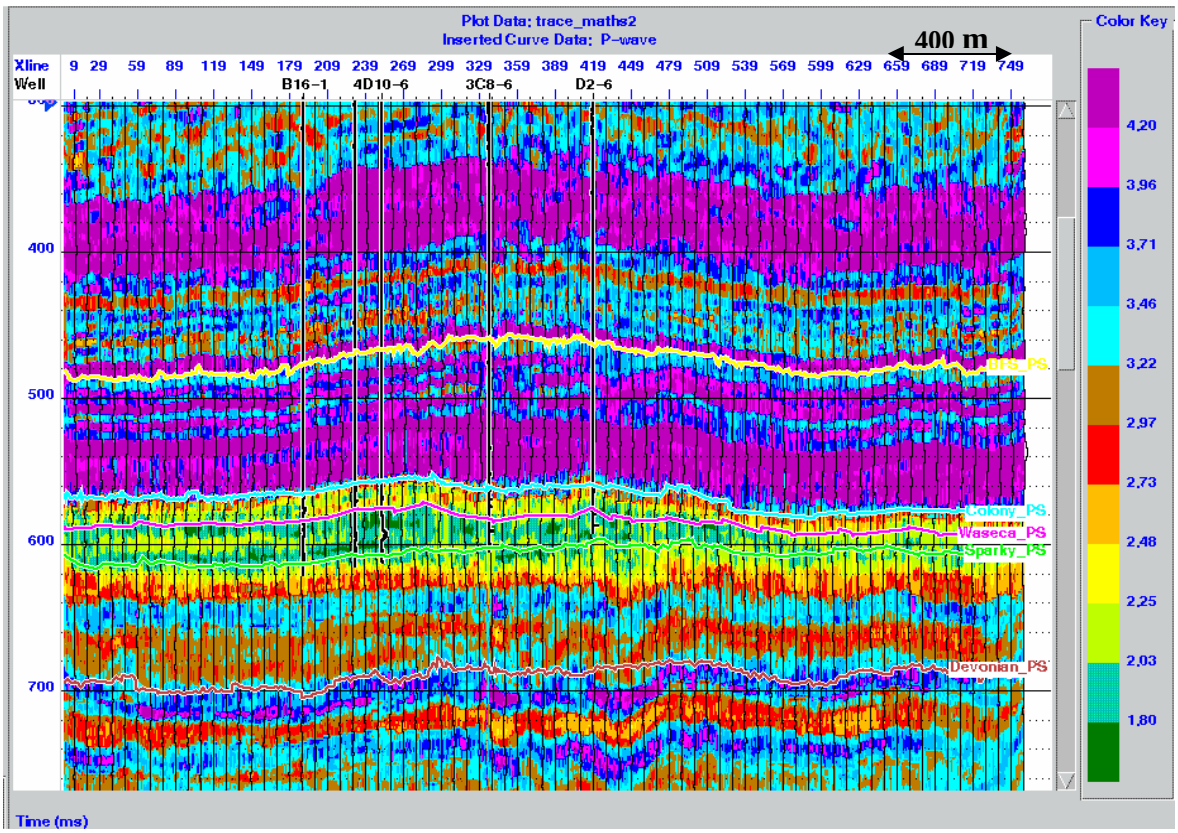

Figure 3.27. The ratio of the PP inversion to the PS inversion in PP time (trace increment equal 10).

We can observe some similarity between this image and Figure 2.13 (coloured Vp/Vs section). The productive formation is recognizable on both sections as having low values of Vp/Vs (Figure 2.13) and low values for the impedances ratios (Figure 3.27).

Chapter 4

Reservoir property prediction using well logs and seismic data

Mapping the physical properties of a reservoir is important for assessing and developing the reservoir's hydrocarbon content. The Pikes Peak heavy oilfield is a heterogeneous reservoir, so we employ geostatistical methods to predict the rock properties between drilled wells. The geostatistical idea is to find and quantify the relationship between the log and seismic data at the well location and use this relationship to predict or estimate the log property at all locations of the seismic line using cokriging techniques.

In this thesis, I examine the prediction of density and porosity logs along the seismic line using multi-attribute analysis.

4.1 Density prediction

Our aim is to find an operator which can predict the density logs from the neighbouring seismic data. The desired operator can be found by analysing different seismic attributes. In this case from Pikes Peak, I find that the most important internal attributes are the:

- integrated trace
- interpolated absolute amplitude of trace
- AVO intercept/gradient
- frequency and seismic velocity.

Geostatistical methods sometimes use external attributes to improve the final prediction. Since we have two inverted datasets (for PP and PS data), it might be helpful to use one of them as an external attribute.

4.1.1 Application to the PP data

Single attribute analysis is conducted for both the PP and PS datasets. First, I consider the density estimate using only P-wave data. The PP inversion result was chosen as an external attribute to predict the density along the seismic line (Figure 4.1).

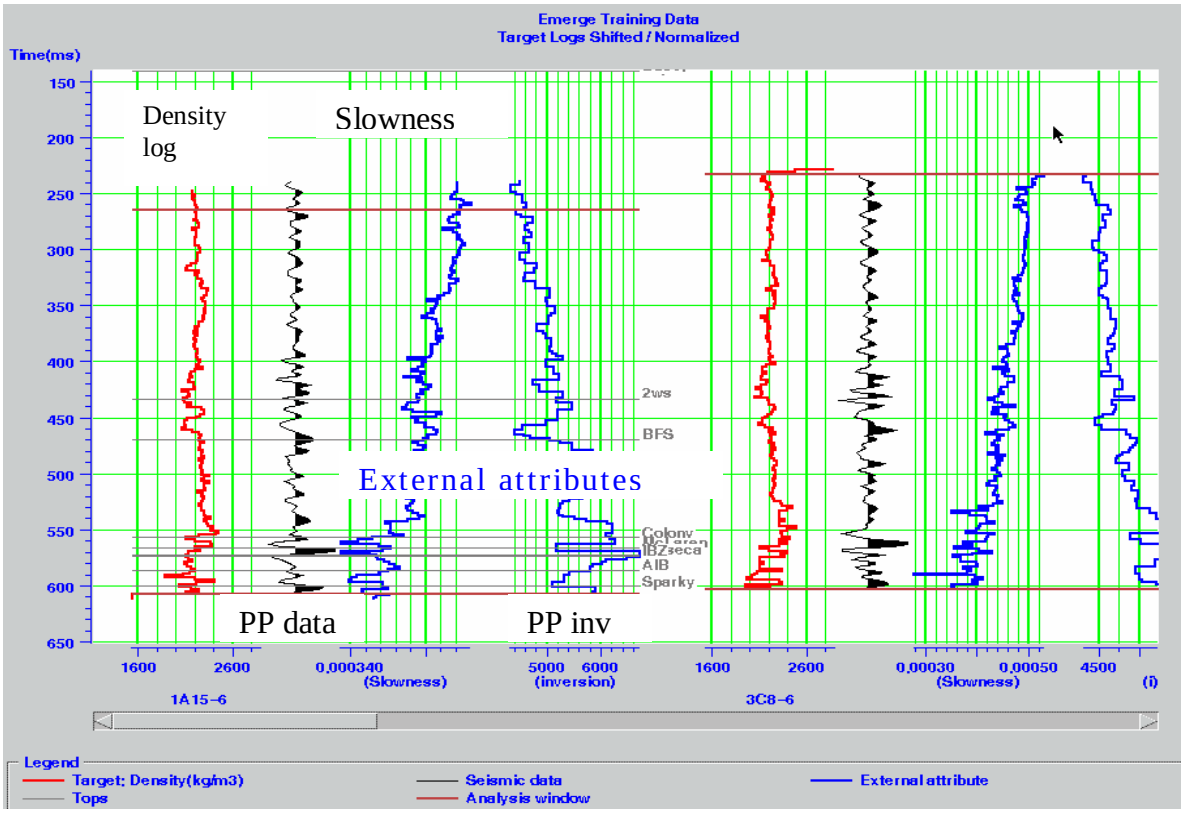

Figure 4.1. Data window with density log (red), seismic trace extracted from the PP dataset at the well location (black), slowness and PP inversion trace (blue).

First of all, we are going to use the wells which contain the density logs and are located close to the seismic line H00-131. Since the procedure requires sufficient well control, seven density logs were loaded into the project (Figure 4.1). The same window contains an extracted seismic trace (from PP dataset) at the well location and two external attributes: the slowness and PP inverted trace.

Considering the geology of this region, we should expect a moderate density for the tight shale of the upper Mannville group and a lower density zone will correspond to the Waseca

sand formation. The density drop at about 570 ms roughly corresponds to the productive zone. As mentioned before, the software will be analyzing the seismic attributes and the seismic traces. Several attributes are plotted for well 1A15-6 in Figure 4.2.

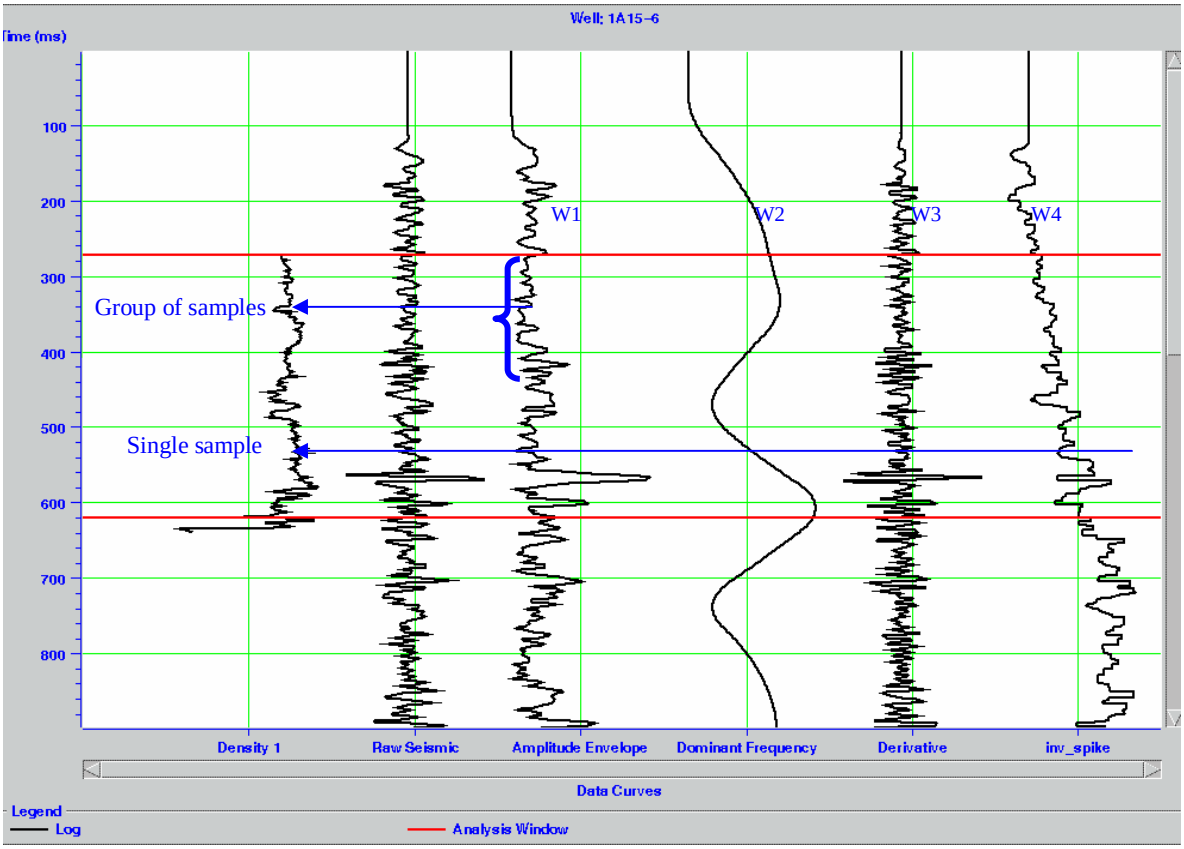

Figure 4.2. Density log and seismic attributes for well 1A15-6.

Here I have chosen to display amplitude envelope, dominant frequency, derivative and the PP inversion result for the well 1A15-6. Hampson (1988) modelled each target log sample as a linear combination of attribute samples at the same time:

$$\rho(t) = w_0 + w_1 A_1(t) + w_2 A_2(t) + w_3 A_3(t) + w_4 A_4(t), \qquad (5)$$

where A - is a seismic attribute and w - its weight.

Equation (5) can be written as a series of linear equations or in matrix form. The solution is optimal in a least-square sense.

The problem is that the frequency content of the target log is much higher than that of the seismic attribute (Figure 4.3), therefore the convolution operator is recommended to resolve the difference.

$$\rho(t) = w_0 + w_1 * A_1(t) + w_2 * A_2(t) + w_3 * A_3(t) + w_4 * A_4(t) \quad (6)$$

In this case, each target sample is predicted using a weighted average of a group of samples on each attribute (Figure 4.3). This could be done in multi-attribute analysis, by setting the operator length equal 7 (In the case of a single sample weighting, it equals 1).

So we need to analyse our attributes to determine which combination of attributes is more reliable for density prediction. The analysis was performed using a step-wise regression method.

On the prediction error graph (Figure 4.3), the average error is plotted versus attribute number for two datasets: a training dataset (in black) and a validation dataset (in red). The operator for a training dataset was created using all wells in the project. To estimate the validity of the result, the target well (for example well 1A15-6) was "hidden", and the operator was calculated from the other wells. The derived operator then used to predict the values at well 1A15-6. As we add attributes, the training error decreases. But the validation error at some point starts to increase. So in our case, the optimum number of attributes to use is 6 to avoid overtraining the data.

Table 4.1 shows the list of attributes selected by the step-wise regression as the best predictors of density. Each row includes all the attributes above. (Row 1 – best single attribute, 2 – best pair, 3 – best triplet, etc.) The corresponding training error and validation error are given in kg/m^3.

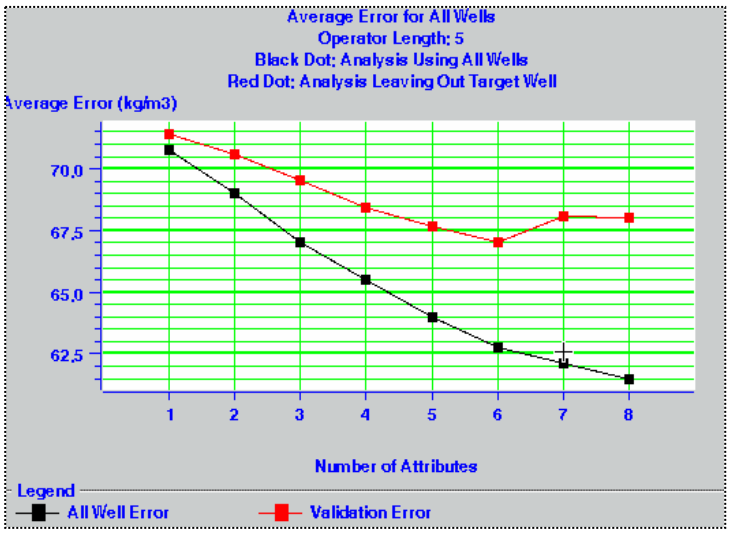

Figure 4.3. The prediction error plot, where the prediction error is the error between the predicted and real logs.

	Target	Final attribute	Training error	Validation error
1	Density	Amplitude Weighted Cosine Phase (inversion)	70.75	71.38
2	Density	Derivative	69.01	70.60
3	Density	1/(Slowness)	67.04	69.52
4	Density	(inversion)**2	65.49	68.42
5	Density	Quadrature trace (inversion)	63.98	67.67
6	Density	Amplitude Weighted Frequency	62.75	67.02
7	Density	Integrate (inversion)	62.09	68.11
8	Density	Cosine Instantaneous Phase (inversion)	61.50	68.04

Table 4.1. Multi-attribute list with corresponding error for PP data.

One more way to check the quality of prediction is to cross-plot the actual density versus predicted density (Figure 4.4). If we compare the actual correlation and error (at the top of Figure 4.4), we can see that the result of using 6 attributes (Table 4.1) is better than that with 5 attributes .

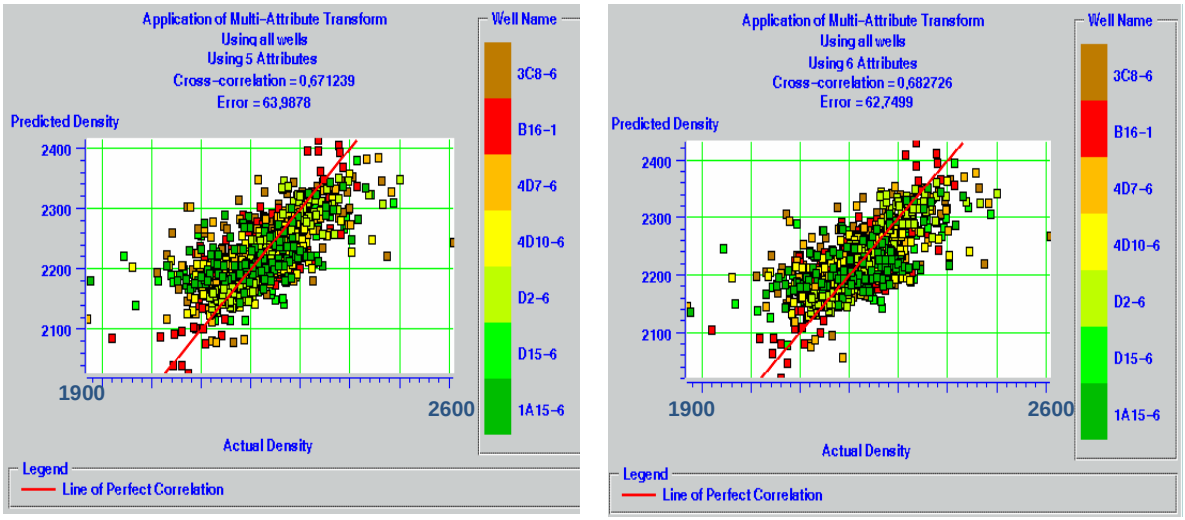

Figure 4.4. Cross-validation of predicted and actual density using 5 (left) and 6 (right) attributes.

The different colours of the points represent different wells and the red line is a line of perfect correlation.

Now, we can check how the program predicts the logs from the seismic data. In other words, each predicted log has used an operator calculated from the other well and we can see how well the process will work on a new well. Figure 4.5 demonstrates this application using 5 attributes, and Figure 4.6 using 6 attributes. The correlation of predicted (red) and real (black) density logs using 6 attributes (Figure 4.6) is 68 %. Although the predicted log looks smoother than the real one, the main log futures are preserved reasonably well. Thus each well exhibits the density drop at around 570-600 ms, which corresponds to the Waseca oil sands.

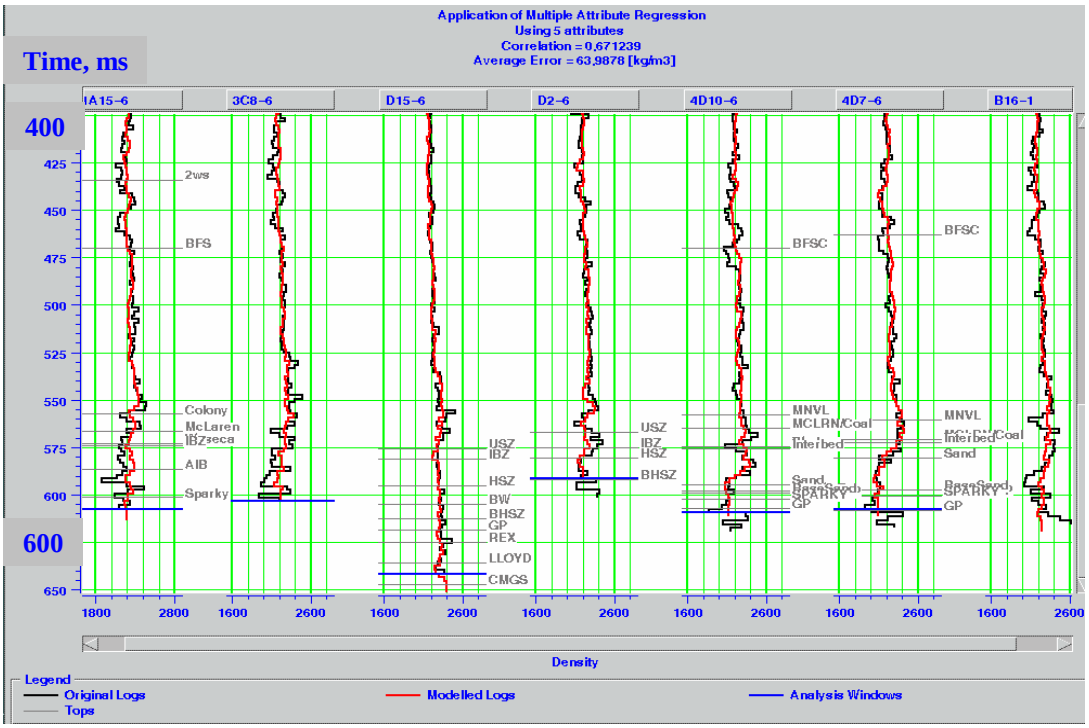

Figure 4.5. Application of multi-attribute regression using 5 attributes, where the predicted density log (red) is plotted versus the original log (black). The correlation is 0.67.

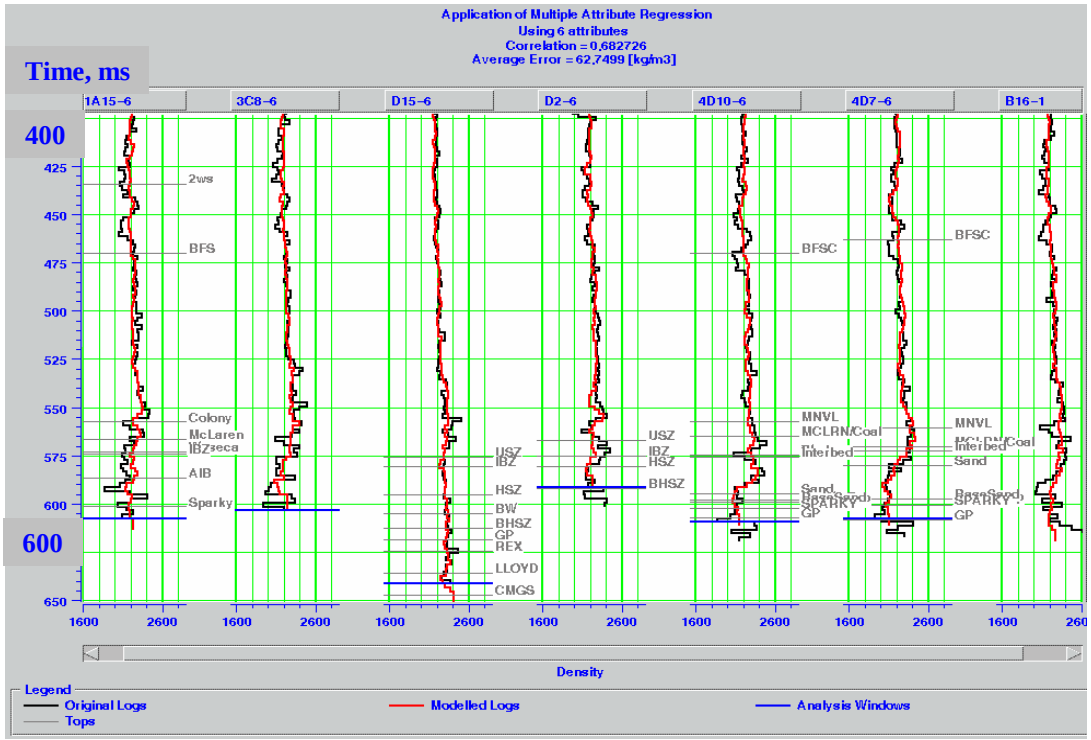

Figure 4.6. Application of multi-attribute regression using 6 attributes, where the predicted density log (red) is plotted versus the original log (black). The correlation is 0.68.

Ultimately, we are able to apply our attributes to the seismic data. Figures 4.7 and 4.8 show the density, predicted along the seismic line. In this case, geostatistical methods helped us to predict the reservoir property between the drilled wells. The productive zone here is seen as a density decrease at about 600 ms (red and yellow colours). If we assess the southern part of the line, a density anomaly is observed between CDPs 685 and 700. Also, this low-density zone correlates with a low impedance anomaly on the PP impedance section (see recursive inversion result, Figure 3.16). No wells have been drilled at this location (Figure 1.5). Geologically, this site could be prospective for oil accumulation as the predicted density here is noticeably lower than for the surrounding area.

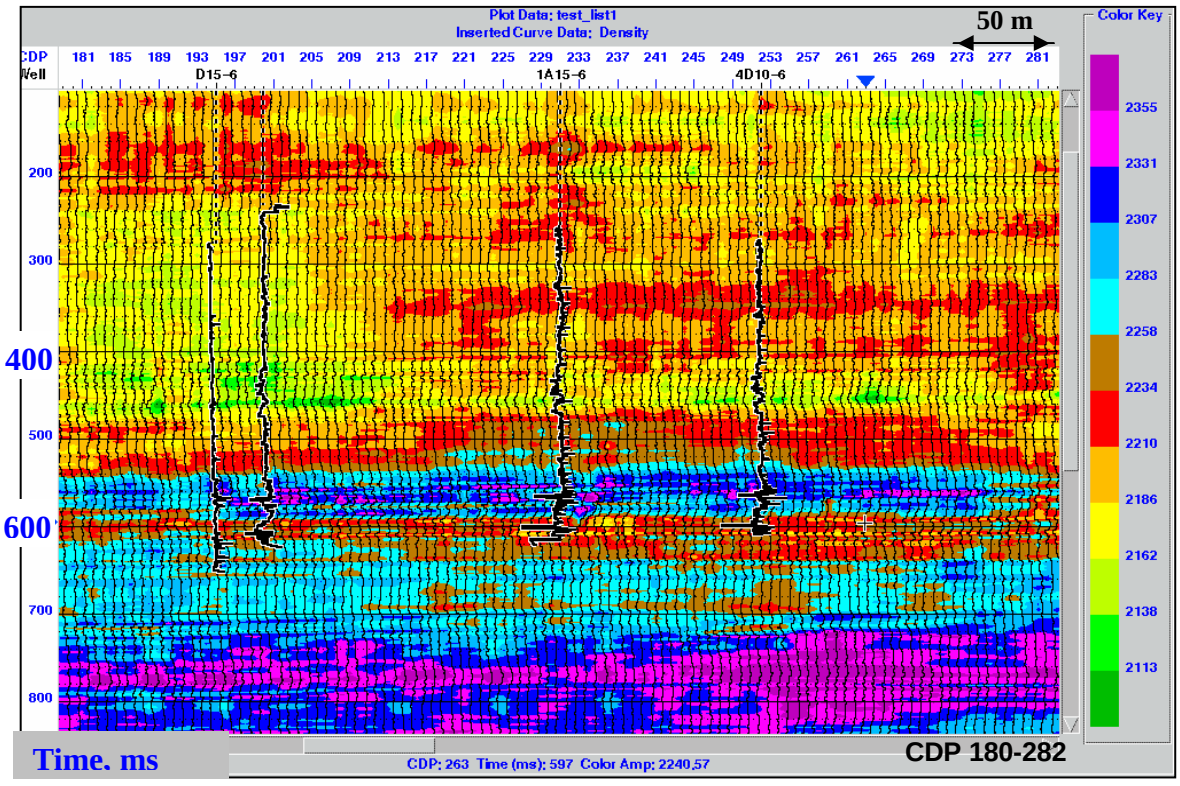

Figure 4.7. Coloured density section along the PP seismic line with inserted density logs. CDP 180-282.

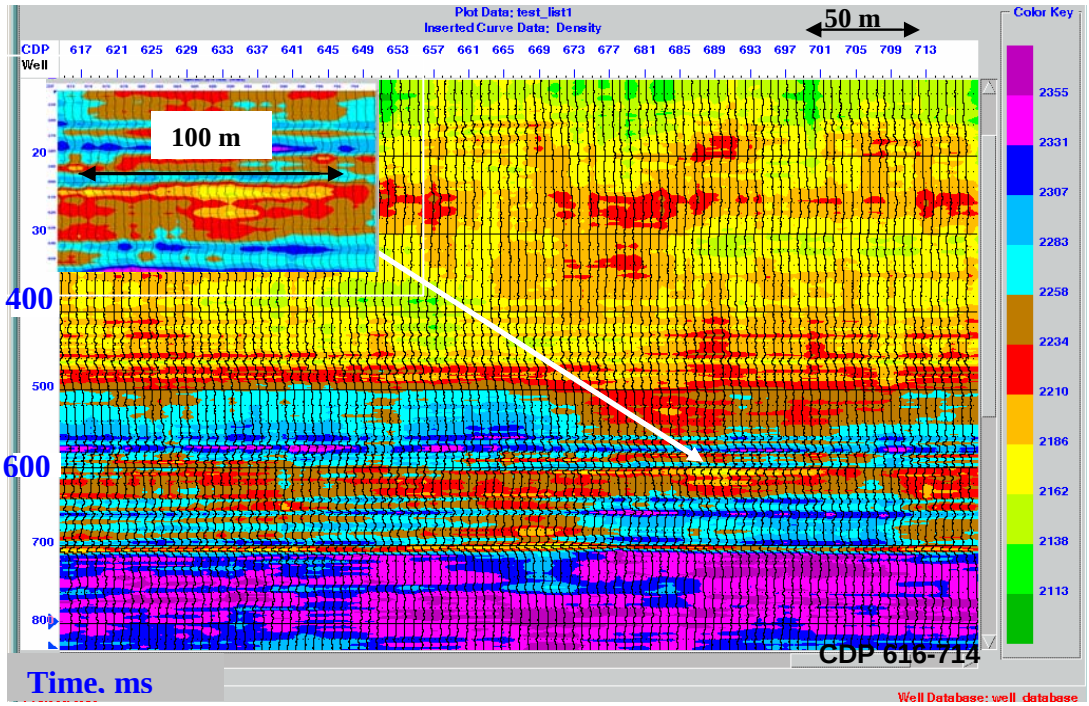

Figure 4.8. Coloured density section along the PP seismic line with enlarged zone of interest. CDP 617-714.

4.1.2 Application to the PS data

To further assess the seismic, I repeated the full process described in Chapter 4.1.1 for the converted wave data. Here, the PS data in PP time were used as a basic seismic volume, and the PS inversion result – as an external attribute. The PP data were not included in this experiment. According to the multi-attribute analysis, the minimum validation error that can be achieved for these data is 60.74 kg/m^3 (Table 4.2). Application of the multi-attribute regression to the seismic data using 5 attributes shows the density predicted along the line (Figure 4.9). Similar to the previous case, the producing wells are concentrated in the low-density zone (yellow); and the southern part of the line reveals the anomaly at around CDP 700.

	Target	Final attribute	Training error	Validation error
1	Density	Time	66.81	72.37
2	Density	(PS inv)**2	61.76	66.54
3	Density	Amplitude Envelope	57.69	61.47
4	Density	Filter 15/20 – 25/30	56.33	60.77
5	Density	Filter 5/10 – 15/20	55.76	60.74
6	Density	Quadrature trace	55.23	60.79
7	Density	Filter 35/40 – 45/50	54.95	60.81
8	Density	Apparent Polarity	54.74	61.53

Table 4.2. Multi-attribute list with corresponding error for PS data.

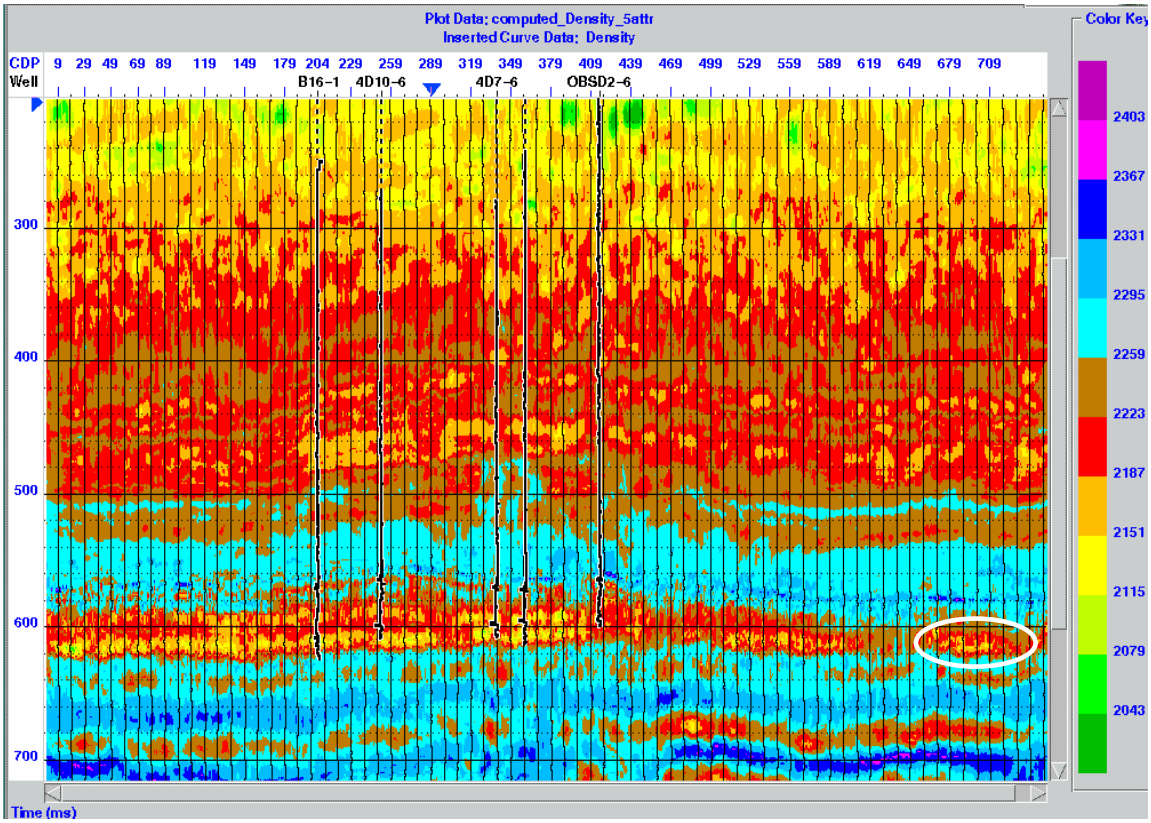

Figure 4.9. Coloured density section along the PS seismic line (in PP time) with inserted density logs and circled zone of interest. Trace increment - 10.

4.1.3 Application to the PP and PS data and their inversion results

In an attempt to reduce the validation error, we can include all available information into the process of density prediction. Figure 4.10 demonstrates the Emerge input data, where the target log is shown in red, the row seismic (PS data in PP time) – in black, and the three external attributes are in blue.

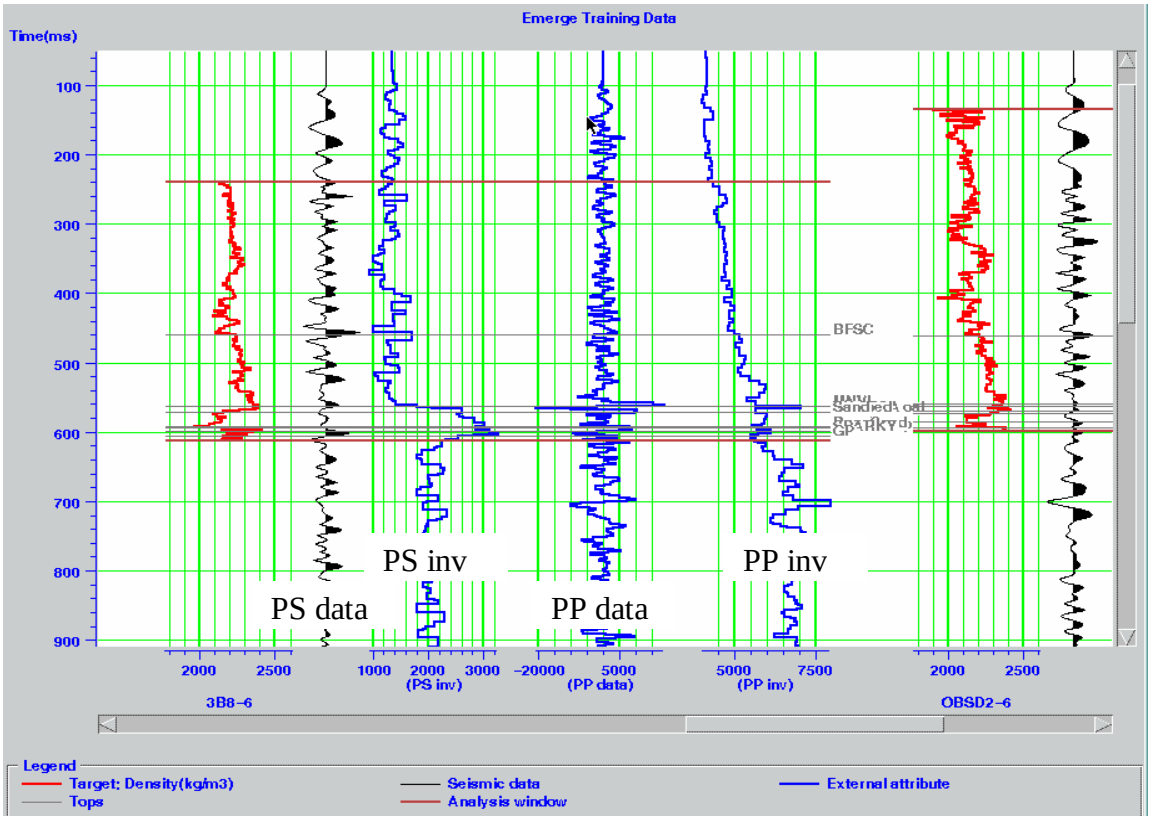

Figure 4.10. Data window with density log (red), seismic trace extracted from the PS dataset at the well location (black), PS inversion trace, PP data and PP inversion trace (blue).

After multi-attribute analysis we can check how the step-wise regression sorted the attributes (Table 4.3). Here, the maximum number of attributes to use is 10, and the best single attribute is 1/PP inversion. The minimum validation error is achieved when using 6 attributes.

	Target	Final attribute	Training error	Validation error
1	Density	1/(PP inv)	62.48	68.86
2	Density	(PS inv)**2	54.63	60.06
3	Density	Amplitude Envelope	53.50	59.64
4	Density	Integrate	52.65	59.79
5	Density	Time	52.05	58.66
6	Density	Amplitude Weighted Frequency	51.58	58.09
7	Density	Filter 15/20-25/30	51.24	59.09
8	Density	Dominant Frequency	50.89	61.69
9	Density	Apparent polarity	50.58	62.81
10	Density	(PP data)**2	50.30	62.82

PS data

Table 4.3. Multi-attribute list with corresponding error for PP and PS data.

Therefore, I used 6 attributes to estimate the density values at all locations of the seismic line (Figure 4.11). As expected, the predicted density section looks very similar to that using PS data alone. However, the zone of interest is characterised by the slightly higher density values, which could be explained by the different attributes used in the process.

Summarizing the results (Chapters 4.1.1-4.1.3), we can see that the combination of PP and PS data and their inversion results gives the minimum validation error (Table 4.4), and thus makes the density prediction more reliable.

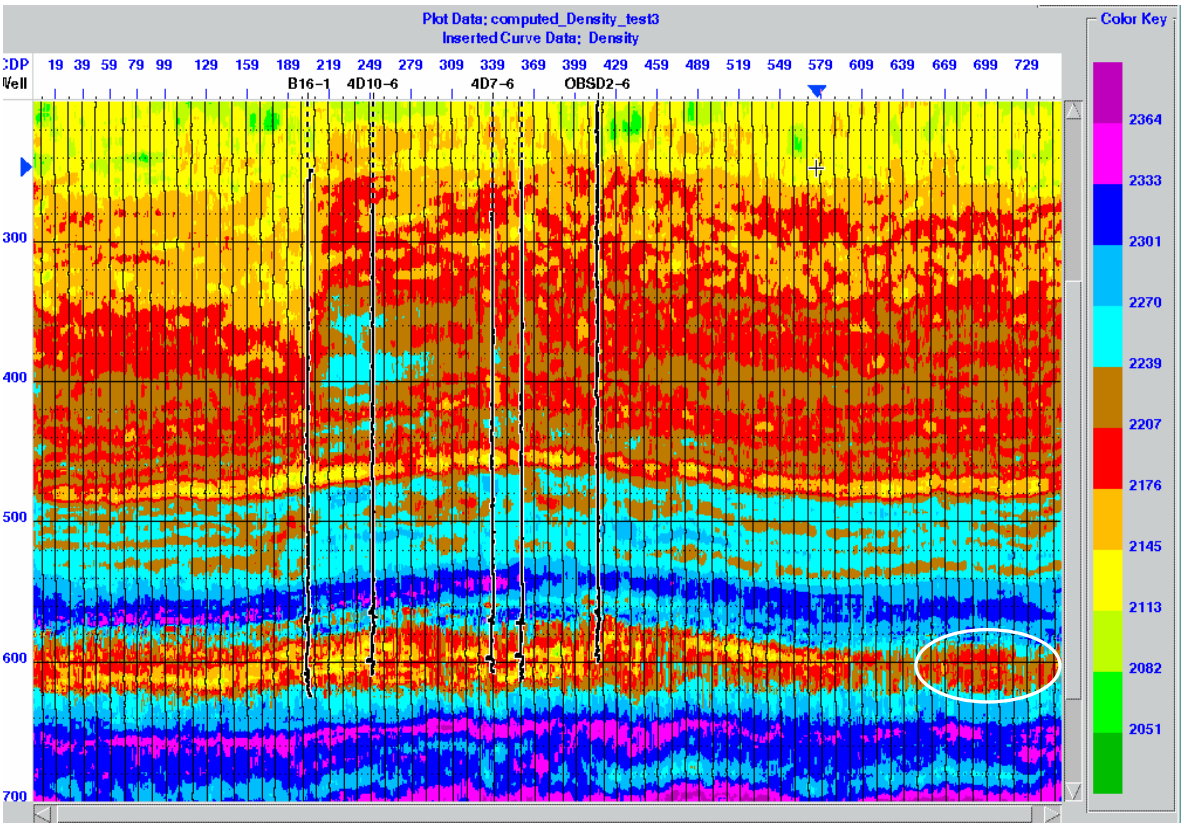

Figure 4.11. Coloured density section along the PS seismic line (in PP time) with inserted density logs. Trace increment - 10.

Seismic data used for density prediction	**Minimum validation error (kg/m^3)**
PP data and PP inversion	67
PS data and PS inversion	60.7
PP and PS data, PP and PS inversion	58.1

Table 4.4. Dataset for density prediction and its corresponding minimum validation error.

4.2 Porosity prediction

In terms of exploration and development, the porosity and permeability are reservoir properties of considerable interest, since they determine the volume of fluids and its ability to flow. Since neutron-porosity logs were not conducted at the Pikes Peak area, we approximate the porosity in the area using the density log. To make the result more realistic, I decided to use different wells than those used in the density prediction (Appendix 2, wells marked in black). All of these wells are located within 150 m from the seismic line.

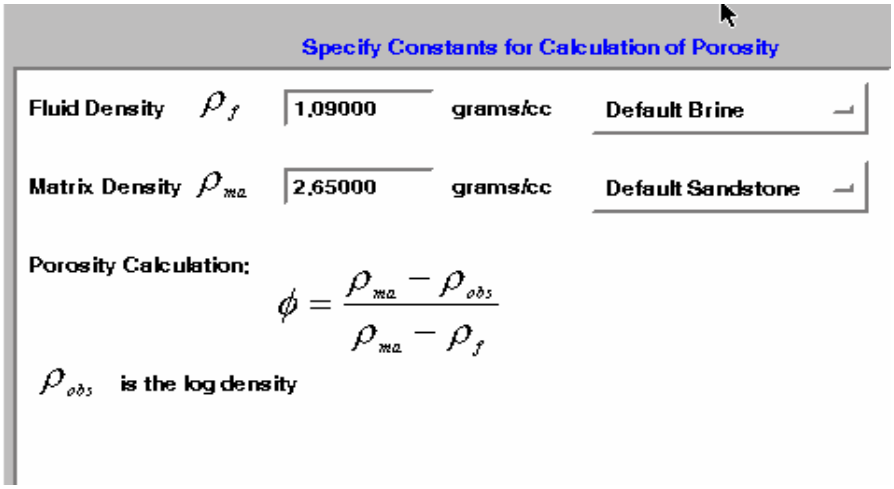

Figure 4.12. Constants used in prediction porosity from density.

New density-porosity logs were calculated using the standard formula (Figure 4.12), where the fluid density and matrix density were defined according to the lithology and the observed density was taken from the conventional density log. After experimenting with different matrix density values (Figure 4.13), it was determined that a matrix density of 2.4 g/cc (yellow colour) gives the best approximation for the calculated density porosity log, since this value corresponds to the sandstone matrix.

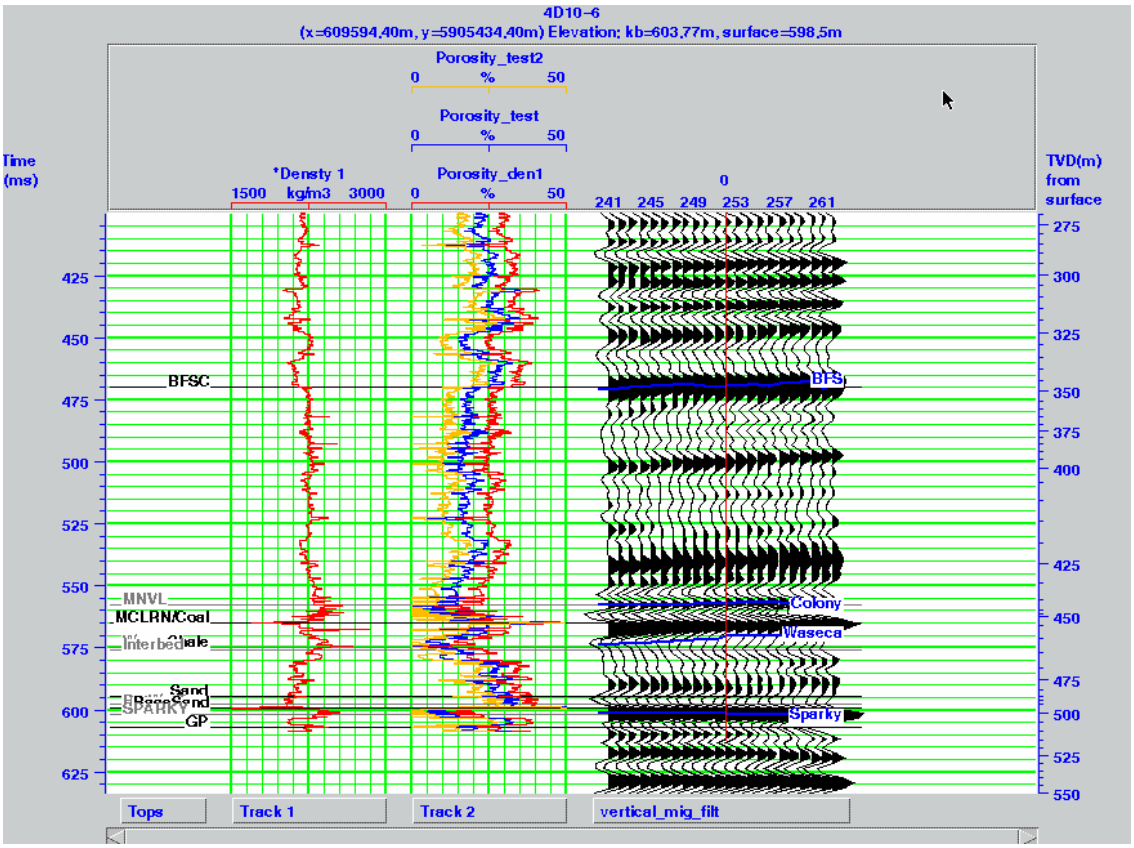

Figure 4.13. Density, three porosity logs and seismic data for well 4D10-6.
Porosity_test2 – matrix density – 2.40 g/cc (yellow),
Porosity_test – matrix density – 2.50 g/cc (blue),
Porosity_den1 – matrix density – 2.65 g/cc (red),

4.2.1 Application to the PP data

Using the same procedure as for the density prediction, seven porosity logs were processed along with the surface seismic and PP inversion result (Figure 4.14). Here, the Mannville shales are recognizable as a moderate porosity zone (up to 15%) and the Waseca sand formation is seen as a considerable porosity increase (25-30%). Note that the P impedance, in general, increases with time and exhibits a low impedance anomaly at around 590 ms. After multi-attribute analysis, the software selected the following attributes, as the best porosity predictors (Table 4.5).

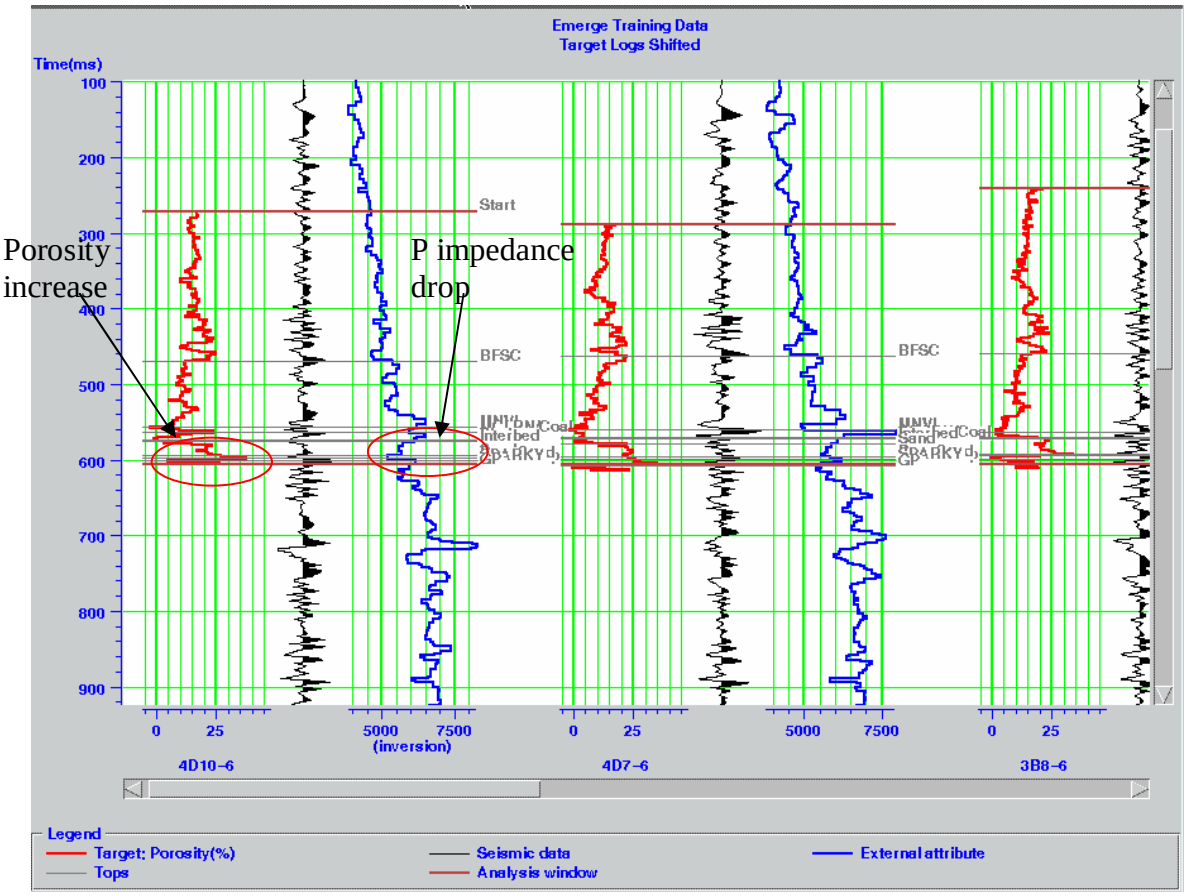

Figure 4.14. Training data window with porosity logs (red), seismic trace extracted at the well location (black) and the PP inverted trace (blue).

	Target	Final attribute	Training error	Validation error
1	Porosity	1/ (inversion)	5.71	6.06
2	Porosity	Dominant Frequency	5.61	6.20
3	Porosity	Average Frequency	5.32	5.88
4	Porosity	Amplitude Envelope	5.21	5.82
5	Porosity	Integrated Absolute Amplitude	5.10	5.84
6	Porosity	Amplitude Weighted Frequency	4.99	5.73
7	Porosity	Apparent Polarity	4.92	5.70

Table 4.5. Multi-attribute list with corresponding error for PP data (% porosity).

Application of multi-attribute regression to the real logs (Figure 4.15) gives us a total correlation of 62%, which is very close to the correlation coefficient for the density logs (61%).

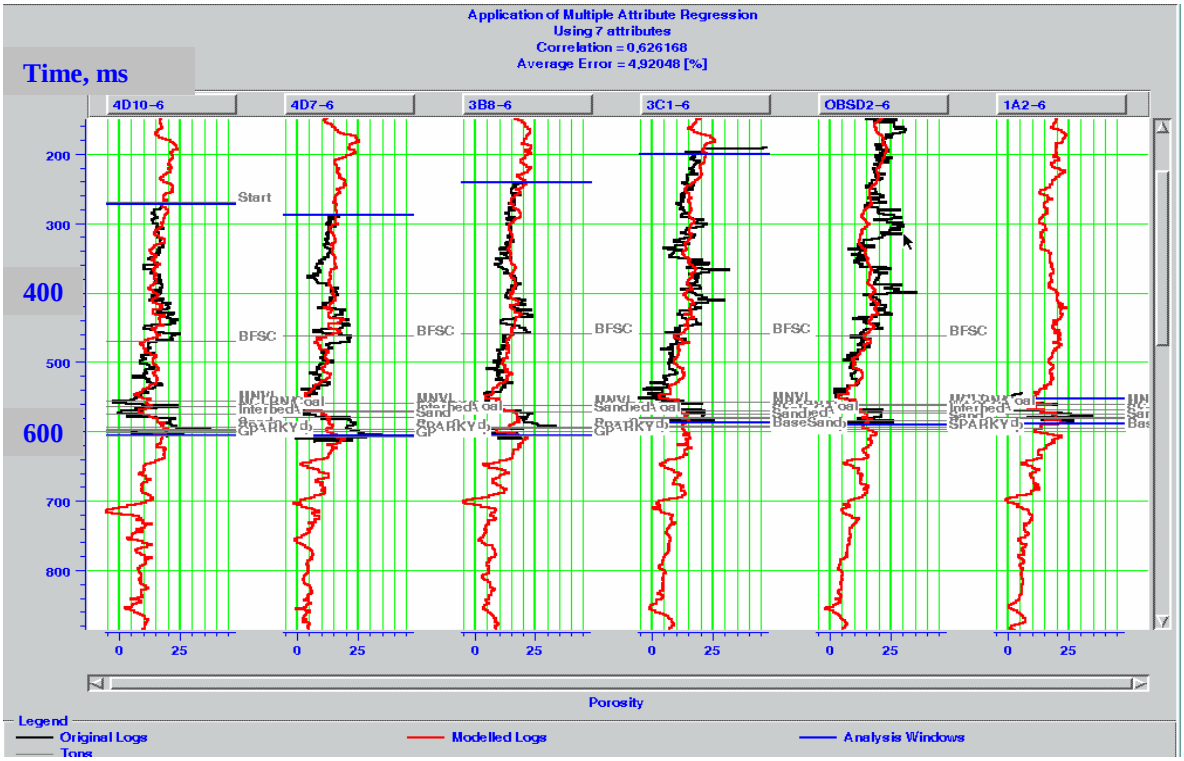

Figure 4.15. Application of multi-attribute regression using 7 attributes, where the predicted porosity log (red) is plotted versus the original log (black). The correlation is 0.63.

Applying this result to the seismic section, we can estimate the porosity between the control points (Figures 4.16, 4.17). As might be expected, the well locations coincide with the high porosity zones (blue and purple colour). Again, the anomalous zone is observed between CDP 680-700 on the southern part of the seismic line (Figure 4.18).

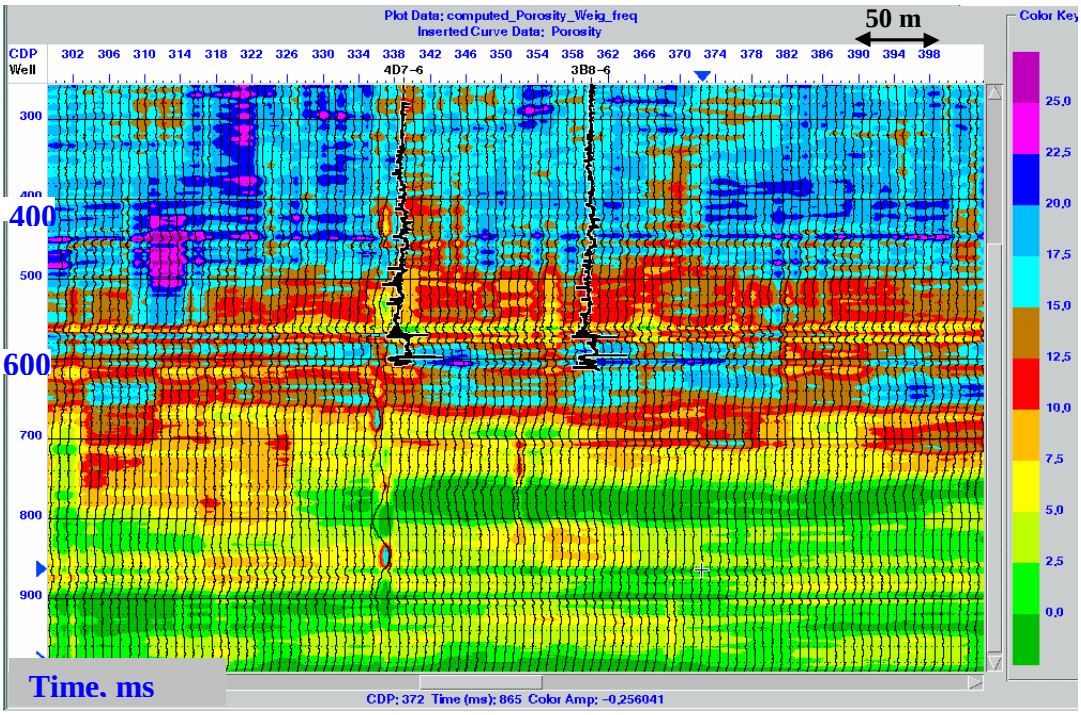

Figure 4.16. Predicted porosity section along the seismic line with inserted porosity logs. CDP 300-400.

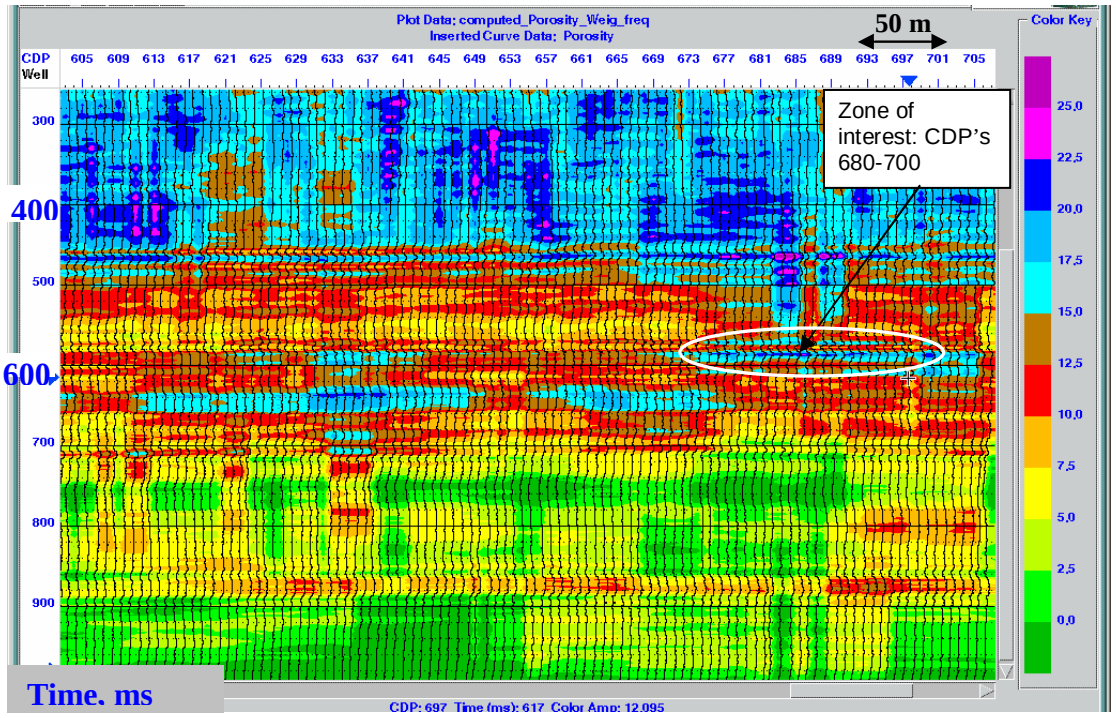

Figure 4.17. Predicted porosity section along the seismic line with the circled zone of interest. CDP 605-705.

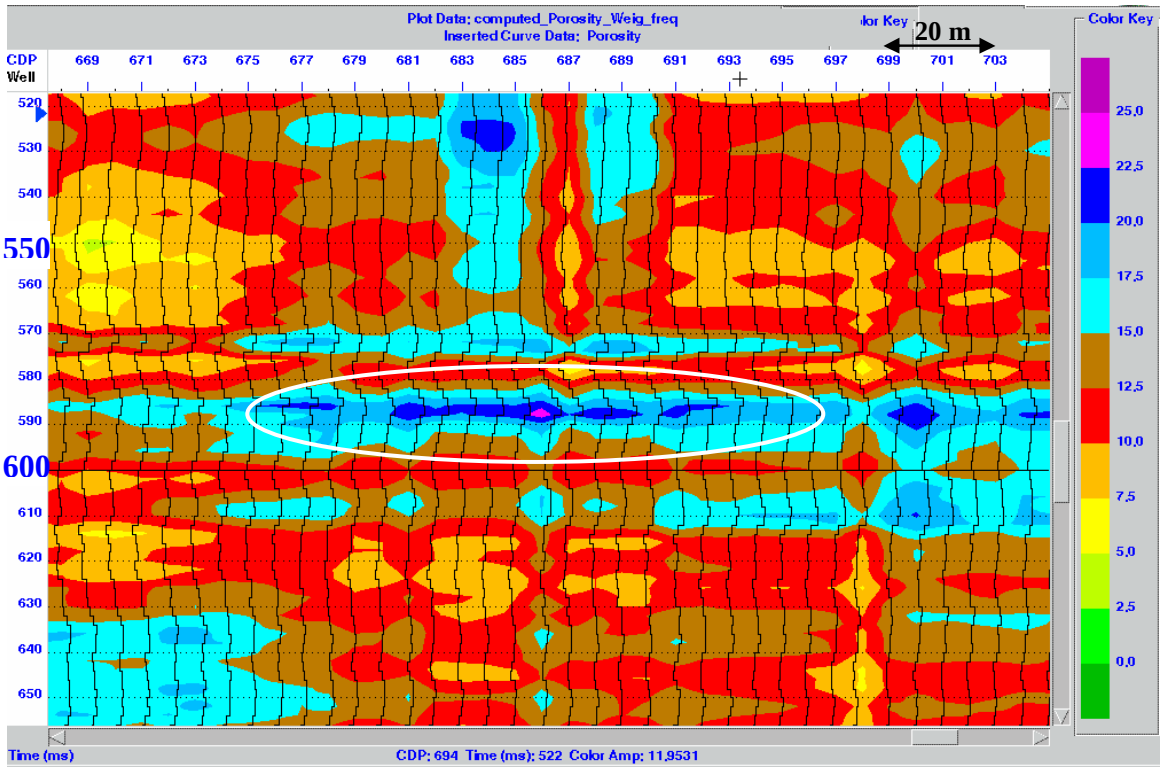

Figure 4.18. Predicted porosity within the zone of interest (CDP's 680-700). Note the porosity increase at around 590 ms.

4.2.2. Application to the PS data

Based on the density and porosity prediction along the PP seismic line, an anomalous zone was found between CDPs 680 and 700 on the seismic line. To confirm the anomaly, I also incorporated the PS data and PS inversion result into the multi-attribute analysis. S-waves, being generally less sensitive to rock saturants, can be used to penetrate gas and oil-saturated sediments (Stewart, 2002). They demonstrate high sensitivity to the lithological changes, so can be used to discriminate highly porous sands from non-porous sands and shales. The whole process of porosity prediction is analogous to one for the PP data except that it used the PS data in PP time as a primary seismic data and the PS inversion result as an external attribute (Figure 4.19).

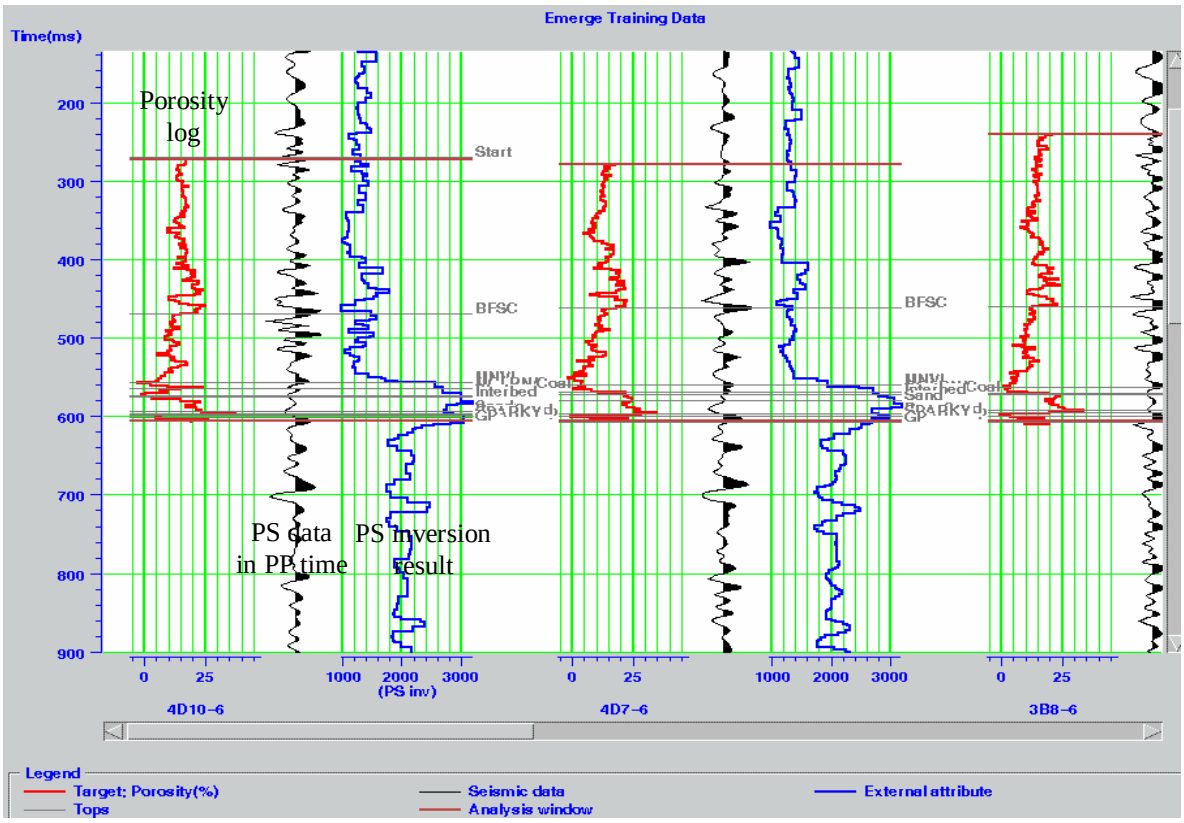

Figure 4.19. Training data window with loaded porosity logs (red), seismic trace extracted from the PS data at the well location (black) and the PS inverted trace (blue).

After multi-attribute analysis, the program selected the amplitude envelope from the PS data as a best single attribute, the amplitude envelope and integrated absolute amplitude as a best couple of attributes, and the amplitude envelope, integrated absolute amplitude and squared PS inverted trace as a best triplet. The application of the step-wise regression to the PS seismic data gave us the desired rock property between the drilled wells (Figure 4.20). In general, the producing wells are concentrated in the high porosity zones (marked with ovals). Note that the porosity anomaly is observed between CDPs 685 and 710 on the PS seismic line (Figure 4.21). Comparing the predicted porosity using the PP (Figure 4.16) and PS datasets (Figure 4.21), I can confirm the existence of the anomaly between CDPs 680 and 700, with the best porosity characteristics corresponding to CDP 687 on the seismic line.

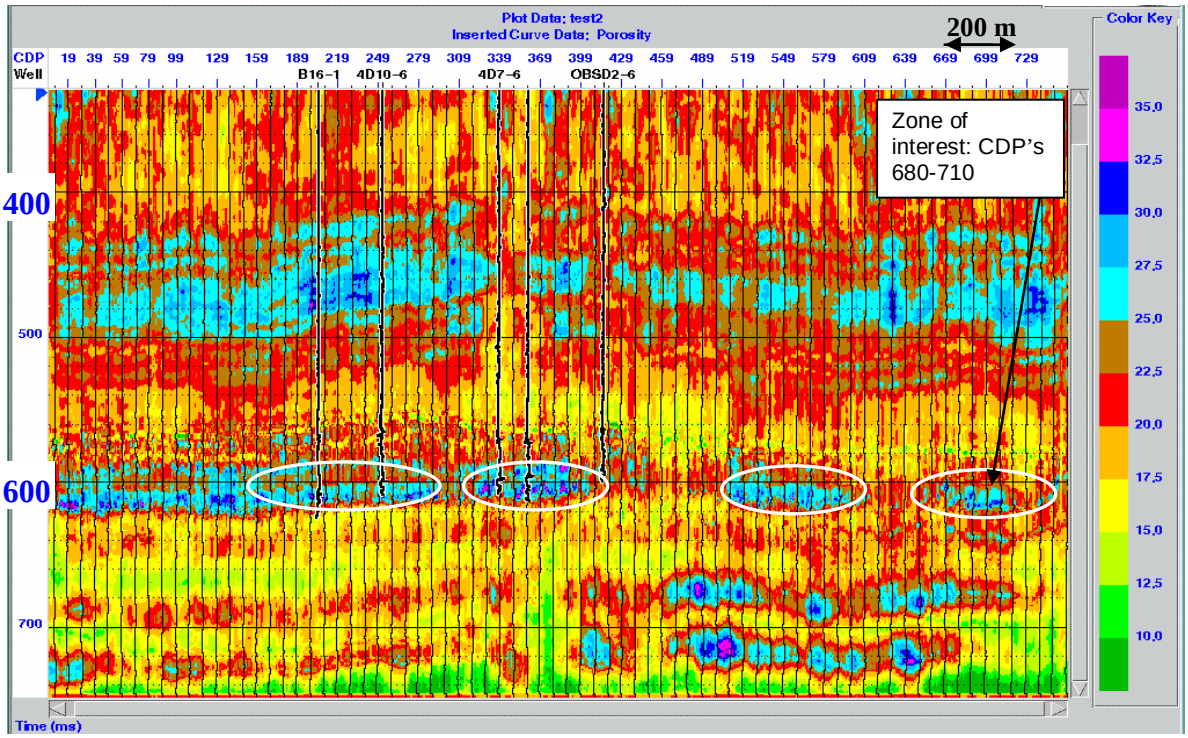

Figure 4.20. Predicted porosity section along the PS seismic line with the circled high porosity zones. Trace increment is 10.

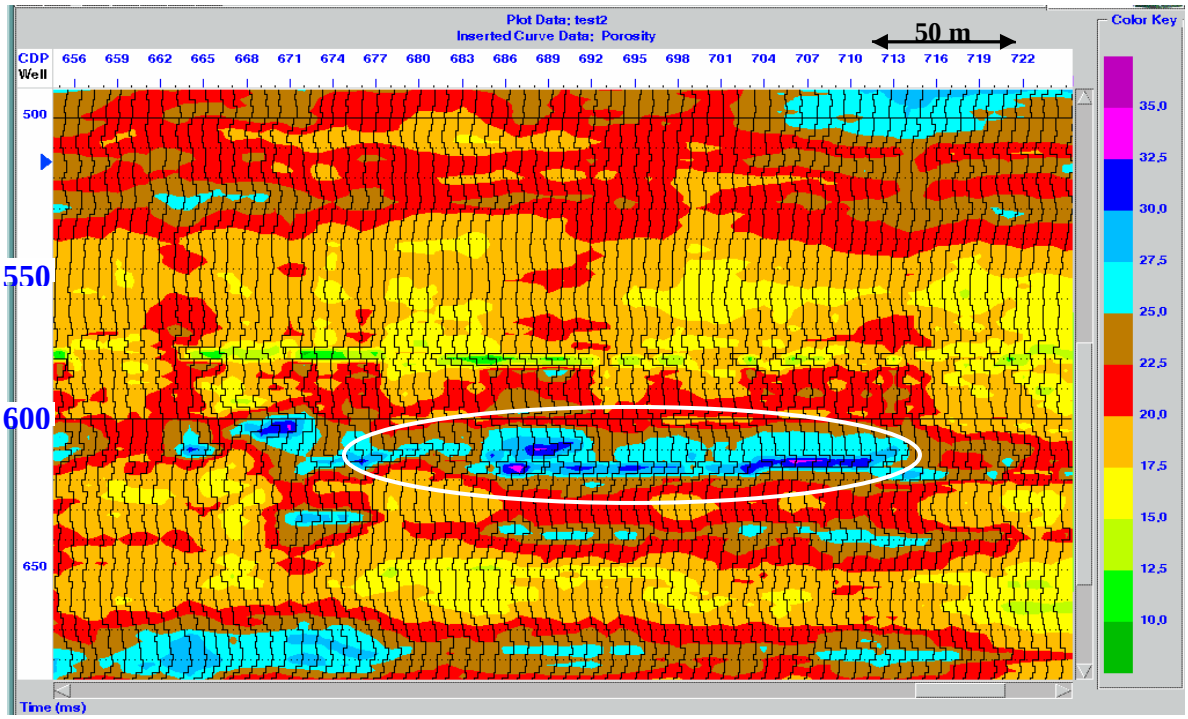

Figure 4.21. Enlarged zone of interest in the predicted porosity section

4.3. Hydrocarbon reserves estimation

Besides the oil output at the Pikes Peak field, a certain amount of gas and water is also produced. Figure 4.22 shows the comprehensive production for well 3C1-6, which corresponds to CDP 409 on the seismic line. This type of information is stored in the AccuMap system and updated every month. So, for the last three months (year 2005) 62370 m^3 of oil, 516 m^3 of gas, and 1907*10^3 m^3 of water (Figure 4.22b) was produced from well 3C1-6. Figure 4.22a represents the same diagram but for the whole well life cycle.

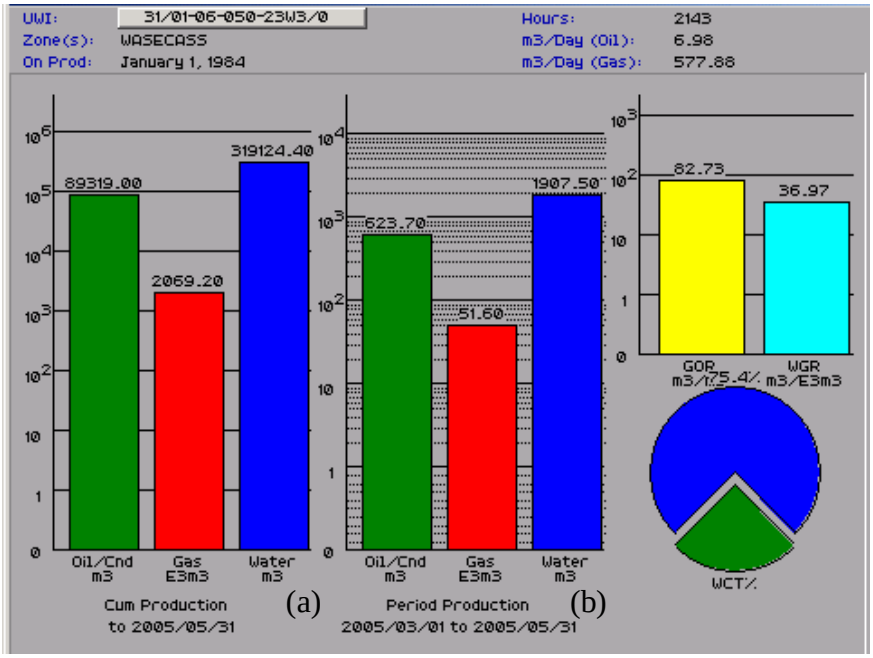

Figure 4.22. Comprehensive production summary for well 3C1-6, showing the cumulative production (a) and last three months production (b) of oil, gas and water (from AccuMap).

Oil reservoirs are shut in when the production rate drops below the economic limit, i.e. when the profit generated from oil sales is less than the cost of continued operation. To find out the approximate volume of hydrocarbon to be produced, the Original Oil in Place (OOIP) index is typically calculated:

$$OOIP = A * Z * S * \phi * S_0 / B \quad (7)$$

Where A is the area size, Z is the average pay thickness, S is the sand percentage, ϕ is the porosity, S_0 is the oil saturation and B is the formation factor. For the Pikes Peak field these parameters have been evaluated and summarized in the Table 4.6.

Average pay thickness (Z)	22 m
Oil saturation (S_0)	85 %
Porosity (ϕ)	$(25 \pm 5)\%$
Sand percentage (S)	80%
Area size (A)	5760000 m^2
Formation factor (B)	1.1

Table 4.6. Reservoir parameters for the Pikes Peak field (Husky Energy report, 2004).

By substituting everything into the Equation (7), the OOIP index was found to be equal $19{,}584{,}000 \pm 3{,}916{,}800 m^3$ or $123{,}185{,}306 \pm 24{,}637{,}061$ barrels of oil. The same parameter estimated by Husky looks more optimistic (150 million barrels) since they approximated the average porosity as 34%. However, it was suggested by Hulten (1984) and indicated from the porosity logs (Figure 4.13), that 25% of porosity is perhaps a more geologically realistic number. Thus, the oil reserves may be approximately 99-148 million barrels of heavy oil.

Chapter 5

Conclusions

5.1 Conclusions

The integration of well logs and multicomponent seismic data has been described in this thesis. In the Pikes Peak case, the productive zone has been delineated using three different methods: inversion, geostatistics and texture map analysis.

I have shown that the main changes in the well logs roughly correspond to the facies changes. Calculated Vp/Vs values were helpful for sand and shale discrimination. The considerable Vp/Vs drop from 4.4 to 1.7 indicates the beginning of the Colony formation.

In the Chapter 3, the PP and PS impedance sections were created and analysed. The top of the productive interval has been interpreted as a PP impedance drop and PS increase. Inversion and other attributes have been used to predict the reservoir properties along the seismic line**.** Examples of predicted porosity and density sections have been shown and interpreted. The productive zone has been characterised as a density decrease (2170 kg/m^3) and porosity increase (22%).

Dip and spectral maps were also used to determine the subsurface architecture and frequency content of the seismic data. An anomalous low-frequency zone was observed just below the reservoir.

Combining different types of information can lead to greater understanding of the data and successful development of existing fields.

5.2 Future work

1. Estimate and compare Vp/Vs from amplitude inversions versus Vp/Vs from time-thicknesses in more detail.
2. Account for reflectivity changes with offset for the PS inversion.
3. Investigate any association of attenuation of seismic waves and reservoir location.

5.3 References

Allen, J.L., 1993, Amplitude Variation with Offset: Gulf Coast case studies: Society of Exploration Geophysicists.

Doventon, J.H., 1994, Geologic Log Interpretation, SEPM Short Course #29: Society for Sedimentary Geology.

Downton, J.E., Russell, B.H. and Lines, L.R., 2000, AVO for managers: pitfalls and solutions: CREWES Research Report, 12.

Downton, J. E. and Lines, L. R., 2001, Preliminary results of the AVO analysis at Pikes Peak: CREWES Research Report, 12.

Hampson, D., 1988, Using multi-attribute transforms to predict log properties from Seismic data: On-line guide for Emerge Software.

Hilterman, F.J., 1990, Is AVO the seismic signature of lithology? A case history of Ship Shoal – South Addition: The Leading Edge, 9, no.6, 15-22.

Hilterman, F.J., 2001, Seismic Amplitude Interpretation: Society of Exploration Geophysicists, 2001 Distinguished Instructor Short Course, No 4.

Hoffe, B. and Bertram, M., 2000, Acquisition and processing of the Pikes Peak 3C-2D seismic survey: CREWES Research Report, 12.

Hulten, V., 1984, Petroleum geology of Pikes Peak heavy oil field, Waseca formation, Saskatchevan: Canadian Society of Petroleum Geologist, 9, 441-454.

Lines, L.R. and Treitel, S., 1985, Wavelets, well logs and Wiener filters: The First Break, 3, 9-14.

Lines, L.R. and Newrick, R., 2004 Fundamentals of Geophysical Interpretation: Society of Exploration Geophysicist.

Luthi, S.M., 2001, Geological well logs: Springer-Verlag Berlin Heidelberg New York.

Newrick, R.T., Lawton, D.C. and Spratt, D.A., 2001, Seismic velocity anisotropy analysis at Pikes Peak, Saskatchewan, Canada: SEG San Antonio, 2001 Expanded Abstracts.

Osborne, C. and Stewart, R.R., 2001, Analysing the Pikes Peak multi-offset VSP dataset: CREWES Research Report, 13.

Pinnegar, C.R. and Eaton, D.W., 2003, Application of the S-transform to pre-stack noise attenuation filtering: Jornal of Geophysical Research, 108, B9, 2422.

Pinnegar, C.R. and Mansina, L., 2003, The local spectral analysis for non-stationary time series: the S-transform for noisy signals: World Scientific Publishing Company, 3, 3,357-364.

Pinnegar, C.R. and Mansina, L., 2003, The S-transform with windows of arbitrary and varying shape: Geophysics, 68, 1, 381-385.

Prohorov, I.V., 1990, Physical encyclopaedia, Russia.

Russell, B., 1988, Introduction to Seismic Inversion Methods: Society of Exploration Geophysicist, Course Notes Series, 2.

Rutherford, S.R. and Williams, R.H., 1989, Amplitude-versus-offset in gas sands: Geophysics, 54, 680-688.

Stewart, R.R., Lawton, D. and Gaiser, J., 2002, Converted-wave seismic exploration: Methods: Geophysics, 67, 5, 1348-1363.

Stewart, R.R., 2001, VSP: an in-depth seismic understanding: CSEG Recorder, 80-83.

Strata, 2006, on-line software guide.

Shuey, R.T., 1985, A simplification of the Zoeppritz equations: Geophysics, 50, 609-614.

Todorov, I.T., 2000, Integration of 3C-3D seismic data and well logs for rock property estimation.: M.Sc. Thesis, University of Calgary, Department of Geology and Geophysics.

Treitel, S. and Lines, L.R., 1994, Geophysical inversion and application: Memorial University of Newfoundland.

Watson, I., 2004, Integrated geological and geophysical reservoir analysis: M.Sc. Thesis, University of Calgary, Department of Geology and Geophysics.

Xu, C., Stewart, R.R. and Osborne, C.A., 2001, Walkaway VSP Processing and Q estimation: Pikes Peak, Saskatchewan: CSEG, 2001 Expanded Abstracts.

Yarus, J.M. and Chambers, R., 1994, Stochastic modelling and Geostatistics: American Association of Petroleum Geologists.

Zou, Y., Bentley, L.R. and Lines, L.R, 2002, Time-lapse seismic modelling of the Pikes Peak field: CREWES Research Report, 14.

Appendix 1

Processing flow for PP data

Filtered migration (whiten + f-x) Matrix Geoservices Ltd., May 2000
Area Pikes Peak, Sask. Line HOO-131 (Vertical) UTM coordinates CM=111W
Shot March 2000 for Husky Oil Ltd. by Veritas DGC (Land) Party 5
Instrument: ARAM 24 Serial NO
Data traces/record 381 auxiliary traces/record CDP Fold 6600%
Sample interval 2 ms samples/trace 8001 this tape 751
Recording format SEGY Format this reel SEGY Measurement system Metric, Sample code: IBM floating PT field gain type: FP, Filters: 3-164 Hz slope: - Db/oct Notch out
Source: Type Vibroseis Number/point 1 Point interval 20 meters, 2 Vibrators, 4 SweepSNP, 16 Sec sweep, 8-150 Hz non-linear, Spread:1310-10-VP-10-1310meter, Group interval 10meters, Geophones: single 3-component, Processing: for Husky Oil Ltd.
Reformat: Record length 16000 ms, Sample rate 2 ms
Sum and Correlate Field Records; Extract Vertical Component, Geometry Assignment; Trace Kills and Edits
Amplitude Recovery: Spherical divergence correction + 4 dB/second, Surface-Consistent Deconvolution: Spiking
Resolved: Source, Receiver, CDP, Offset Applied: Source, Receiver, CDP, Operator length 60 ms, Prewhitening 0.1 %
Design window 196-1348 ms at 0 m offsel 880-1422 ms at 1319 m offset, Phase Compensation: Correction for vibroseis deconvolution, Time-Variant Spectral Whitening: 2/8-150/170 Hz
Refraction Statics: Datum elevation 630 m Replacement velocity 2000 m/s, Velocity Analysis
Surface-Consistent Statics: Max shift 20 ms 4 event-tracking windows, Normal Moveout Correction
Front-End Muting: Offset(m) 180 220 600 1320 T(ms) 0 177 658 891, Time-Variant Scaling: Center-to-center 0-300,200.900,700-1300
CD P Trim Statics: Max shift 8 ms Correlation window: 1 00-1200 ms
CD P Stack: Alpha-trimmed, reject 15%, 1 00 ms bulk shift
Time-Variant Spectral Whitening: 2/8-150/170 Hz
Trace Equalization: mean window 100-1200 ms
fox Prediction Filtering: 40 traces by 1 00 ms, 50% overlap, 7 point filter
Wave Equation Datuming: Final Datum: -10 ms Replacement velocity 2000 m/s
Migration: Phase-shifl Aperture 0-90 degrees, 100% smoothed stacking velocities
Bandpass Filter: Orrnsby 10/14-150/170 Hz
Trace Equalization: 100-1200 ms

Processing flow for PS data

Filtered migration (whiten + f-x) Matrix Geoservices Ltd., May 2000
Area Pikes Peak, Sask. Line HOO-131(Slow shear) UTM coordinates CM=lllW
Shot March 2000 for Husky Oil Ltd. by Veritas DGC (Land) Party 5
Instrument: ARAM 24 Serial NO
Data traces/record 381 auxiliary traces/record CDP fold 6600%
Sample interval 2 ms samples/trace 8001 this tape 1751
Recording format SEGY Format this reel SEGY Measurement system Metric
Sample code: IBM floating PT field gain type: FP
Filters: 3-164 Hz slope: - Db/oct notch out
Source: type Vibroseis, number/point 1 Point interval 20 Meters
2 Vibrators, 4 Seeps/VP, 16 sec Sweep, 8-150 Hz non-linear
Spread: 1310 - 10 - VP - 10 - 1310 meter Group interval10 meters
Geophones: single 3-component
Processing: for Husky Oil Ltd.
Reformat: Record length 16000 ms, Sample rate 2 ms
Sum & Correlate Field Data; Extract Horizontal Components; Rotate Into Slow
Assign Geometry; Asymtotic Binning, Vp/Vs = 3.16
Reverse Polarity of Negative Offsets; Trace Kills & Edits
Amplitude Recovery: Spherical divergence correction + 4 dB/second
Shot f-k Filter; Arbitrary polygons to remove source noise
Surface-Consistent Deconvolution: Spiking
Resolved: Source, Receiver, CDP, Offset Applied: Source, Receiver, CDP
Operator length 90 ms, Prewhitening 0.1%
Design window 252-2453 ms at 10 m offset, 1156-2529 ms at 1319 m offset
Phase Compensation: Correction for vibroseis deconvolution
Time-Variant Spectral Whitening: 2/8-60/80 Hz
Structure Statics: source from vertical data, receiver from shear refraction
Velocity Analysis; Residual Receiver Statics
Surface-Consistent Statics: Max shift 20 ms 3 event-tracking windows
Converted-Wave NMO Correction
Front-End Muting: Offset(m) 210 250 640 960 1310 T(ms) 0 410 810 1256 1500
Time-Variant Scaling: Center-to-center 0-600,400-1700,1400-2400,2100-3400
ACP Trim Statics: Max shift 12 ms Correlation window: 350-2350 ms
Converted Wave Stack: Vp/Vs from vertical correlations, +300 ms bulk shift
Time-Variant Spectral Whitening: 2/8-60/80 Hz
Trace Equalization: mean window 200-1900 ms
f-x Prediction Filtering: 40 traces by 150 ms, 50% overlap, 7 point filter
Migration: Kirchhoff, Aperture 0-40 degrees, 100% P-S migration velocities
Bandpass Filter: Ormsby 2/8-40/50 Hz; Trace Equalization: 200-1900 ms

Processing flow for array gathers

Filtered migration gathers (NMO applied) Matrix Geoservices Ltd., May 2000
Area Pikes Peak, Sask. Line HOO-131(Array) UTM coordinates CM=lllW
Shot March 2000 for Husky Oil Ltd. by Veritas DGC (Land) Party 5
Instrument: ARAM 24 Serial NO
Data traces/record 381 auxiliary traces/record CDP fold 6600%
Sample interval 2 ms samples/trace 8001 this tape 751
Recording format SEGY Format this reel SEGY Measurement system Metric
Sample code: IBM floating PT field gain type: FP
Filters: 3-164 Hz slope: - Db/oct notch out
Source: type Vibroseis, number/point 1 Point interval 20 Meters
2 Vibrators, 4 Seeps/VP, 16 sec Sweep, 8-150 Hz non-linear
Spread: 1310 - 10 - VP - 10 - 1300 meter Group interval 20 meters
Geophones: 6 geophones over 10 m
Processing: for Husky Oil Ltd.
Reformat: Record length 16000 ms, Sample rate 2 ms
Sum & Correlate Field Data; Extract array data
Assign Geometry; Trace kills and edits
Amplitude Recovery: Spherical divergence correction + 4 dB/second
Surface-Consistent Deconvolution: Spiking
Resolved: Source, Receiver, CDP, Offset Applied: Source, Receiver, CDP
Operator length 60 ms, Prewhitening 0.1%
Design window 196-1348 ms at 0 m offset, 880-1422 ms at 1319 m offset
Phase Compensation: Correction for vibroseis deconvolution
Time-Variant Spectral Whitening: 2/8-150/170 Hz
Refraction statics: datum elevation 630 m, Replacement velocity 2000 m/s
Surface-Consistent Statics: Max shift 20 ms 4 event-tracking windows
Velocity analysis, NMO correction
Trace equalization: 100-1200 ms
CDP trim statics: Max shift 8 ms, Correlation window: 100-1200 ms
Form common offset planes, 25-1305 m, 40 mincrement between planes
f-x Filtering: 40 traces by 80 ms window, 50% overlap, 7 point filter
Migration: Prestack Kirchhoff, 100% of smoothed stacking velocities
Restore normal moveout
Long offset normal moveout correction
Shift to final processing datum time of 100 ms.

Appendix 2

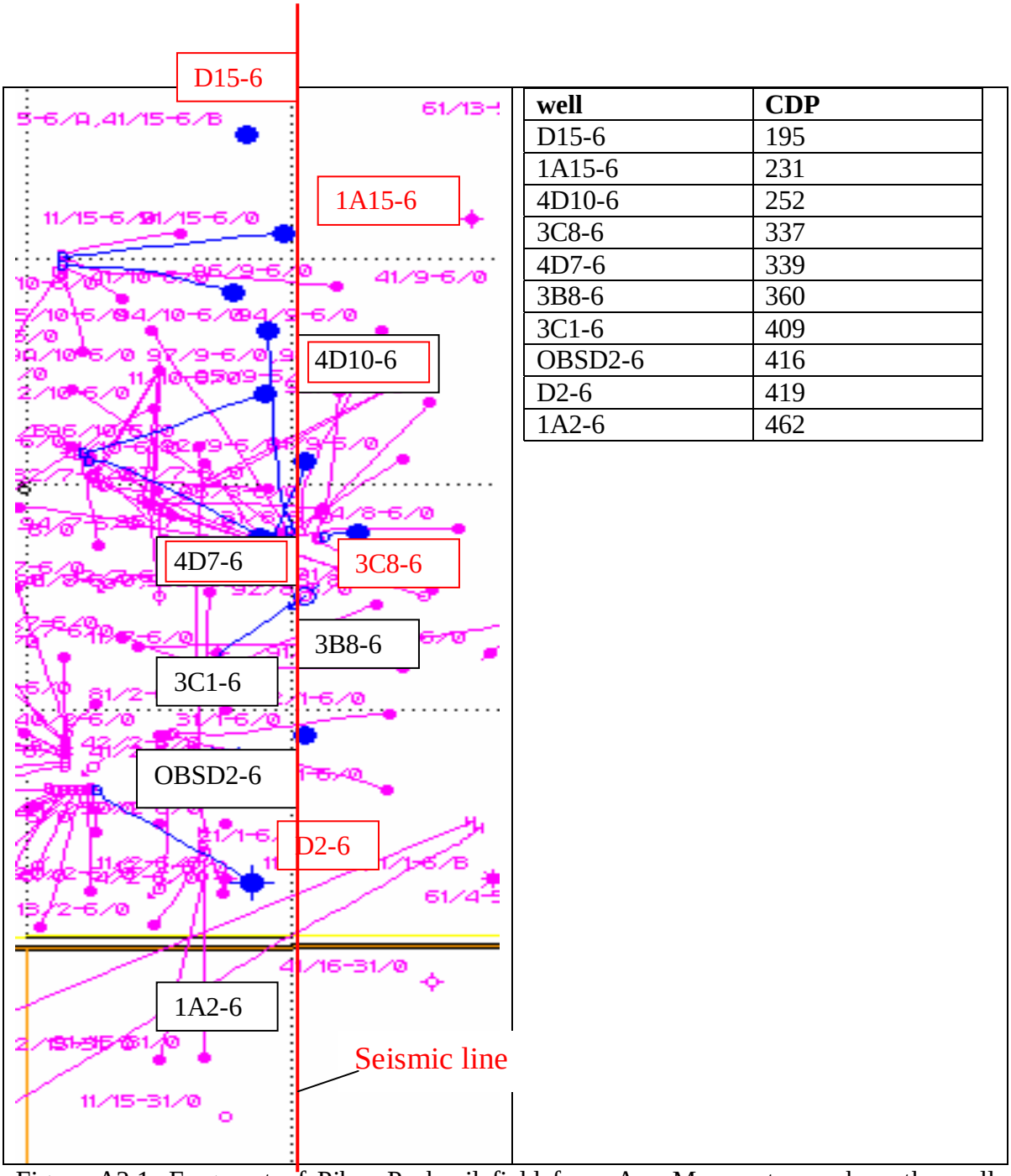

well	CDP
D15-6	195
1A15-6	231
4D10-6	252
3C8-6	337
4D7-6	339
3B8-6	360
3C1-6	409
OBSD2-6	416
D2-6	419
1A2-6	462

Figure A2.1. Fragment of Pikes Peak oil field from AccuMap system, where the wells indicated in red were used for the density prediction, wells indicated in black were used for the porosity prediction.

Appendix 3

Application of the Stockwell transform

A3.1 Theory

The P-wave seismic data from Pikes Peak heavy oil field were also analyzed using various signal processing transforms in the Resolution software package from Calgary Scientific Inc (Figure A3.2). This software allows display of both standard Fourier transform and Stockwell (S) -transforms for creating seismic image, angle and frequency maps. The software can also be used to filter the area of interest on the seismic image. The basic theory for the Stockwell transform was developed by Pinnegar (2003).

The S-transform is a time-frequency spectral localization method, similar to the short-time Fourier transform, but with a Gaussian window whose width scales inversely, and whose height scales linearly with the frequency. The time-domain expression of the S-transform of a continuous function *h* is given by the formula:

$$S(\tau, f, p) = \int_{-\infty}^{\infty} h(t) w(\tau - t, f, p) \exp(-2\pi i f t) dt , \qquad \text{(A1)}$$

where *t* is time, f is frequency, *w* is the modulating window which translates along the time axis, τ is the position of the modulating window, and *p* is any parameters that define *w*. The S-transform has an advantage over the wavelet transform because it retains the absolute phase of each localized frequency component. This led to its application for detection and interpretation of events in time series in a variety of disciplines including seismology.

Any seismic image analysed in the Resolution package can be treated as a number of white and black stripes (peaks and troughs) at different directions. For cases with simple geology,

these stripes are close to parallel; for complex subsurface structures, like salt domes or thrust faults, the directions of seismic events vary considerably throughout the area. The idea of the Resolution software is to find the number of wave cycles, later referred as wave number *k*, in both horizontal k_x and vertical k_y directions for any image.

Based on the wave number, some approximations about the frequency at a particular point of the seismic image are made, and this, in turn, can help to localize any frequency anomalies on the seismic section.

Let us consider a signal with the wave vector (e.g. 6,4 in the k_x , k_y domain), as shown in Figure A3.1a. According to the Fermat's principle, the vector of the dominant frequency is perpendicular to the wave front (Pinnegar, 2003).

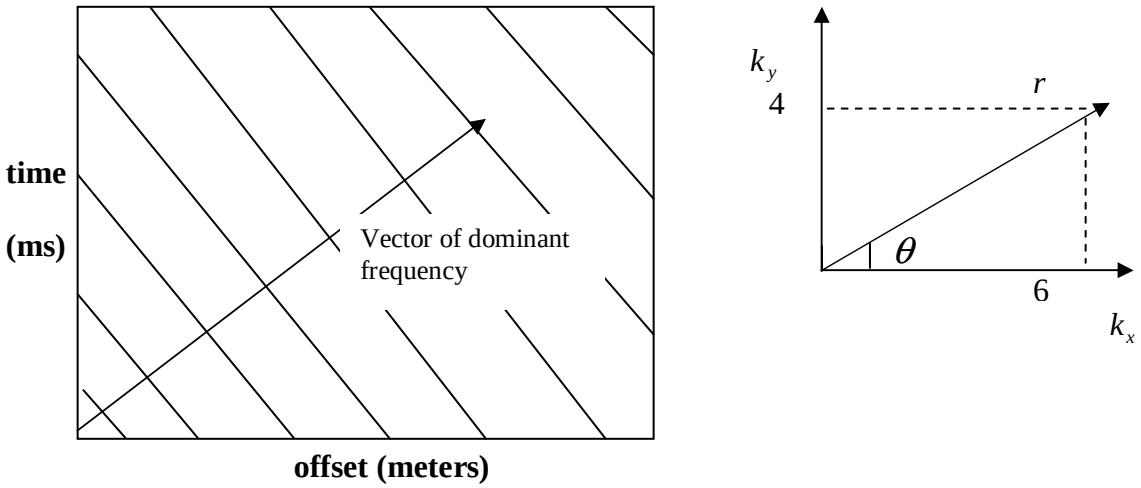

(a) (b)

Figure A3.1. (a) The schematic diagram of the signal with a wave vector (6,4), and (b) its decomposition in frequency domain.

The frequency vector can be characterized by its length *r* and the angle from the horizontal direction θ (Figure A3.1b). So, the wavelength and the angle of the dominant frequency can be defined as follows:

$$r = \sqrt{k_x{}^2 + k_y{}^2} \tag{A2}$$

$$\theta = \arctan\left(\frac{k_y}{k_x}\right) \tag{A3}$$

The above mentioned parameters (Equations (A2) and (A3)) play a key role in generating the spectral and dip maps.

A3.2 FFT and local spectrum for the Pikes Peak data

P-wave data from the Pikes Peak multicomponent seismic line are analysed using the above techniques (Figure A3.2). The software interface is divided into four panes: where two windows on the left have the units of space, and two on the right have units of spatial frequency. The standard Fourier transform is shown here for the whole seismic image. As seen from the FFT window (Figure A3.2b), all useful frequencies are concentrated in a narrow frequency range (the two symmetrical light blue zones), where k_x is close to zero and k_y varies from 0 to 0.15 scaled units of frequency. Since the Pikes Peak geology is quite flat, the main direction for a dominant frequency is almost vertical, no cycles can be detected in the horizontal direction. The fast Fourier transform representation is shown here with the direct current in the middle so the image looks symmetrical.

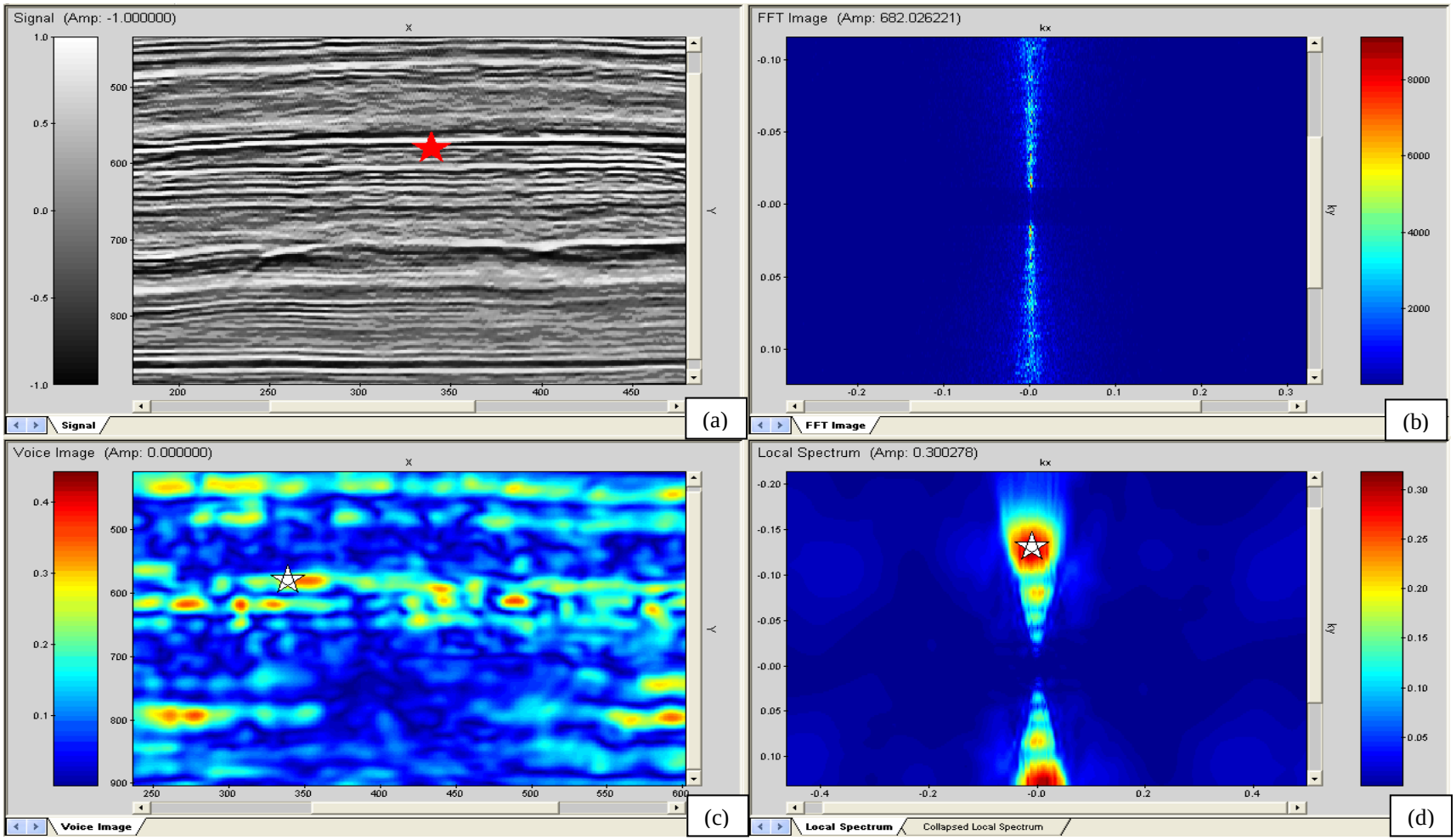

Figure A3.2. Pikes Peak seismic data, where (a) is the seismic image in time, (b) Fourier transform for the whole image, (c) voice image and (d) local spectrum for the particular point.

Both top images (Figure A3.2a and A3.2b) are standard ways to represent seismic signals and their spectra. The S-transform (Figure A3.2c and A3.2d) is a unique method which allows us to create another representation or decomposition of a seismic image.

Figure A3.2d is generated for a single point selected at the image pane (a, red star). Here I transformed the signal from the time to the frequency domain using Equation (A1). The result or local spectrum is used to identify all frequencies that are present at a selected point in the image. If we draw the line between two dominant frequencies (Figure A3.2d, dark red points) we can get an impression about the direction of the frequency vector. In our case, the dominant frequency comes from the vertical direction, which indicates almost horizontal layering in the area of survey. Figure A3.2c shows the corresponding "voice" image for a single frequency selected from the local spectrum. We define the voice image as a spatial distribution of one conjugate pair of frequencies. It is generated to show all points within the signal image where the chosen frequency occurs. Typically, the voice image can be useful in identifying unwanted signals.

The local spectrum (Figure A3.2d) is an input to create dip, spectral and peak amplitude maps in MatLab using the scripts developed by Calgary Scientific Inc. The dip map is intended to show the angle of layering for a geological structure and the spectral map – its frequency component. The peak amplitude map indicates the points where seismic amplitude is at its maximum.

A3.3 Dip, spectral and peak amplitude maps

A portion of the seismic data (400-900 ms) was loaded into Resolution (Figure A3.2) and the S-transform calculated for the seismic image. Then the maps of interest were generated.

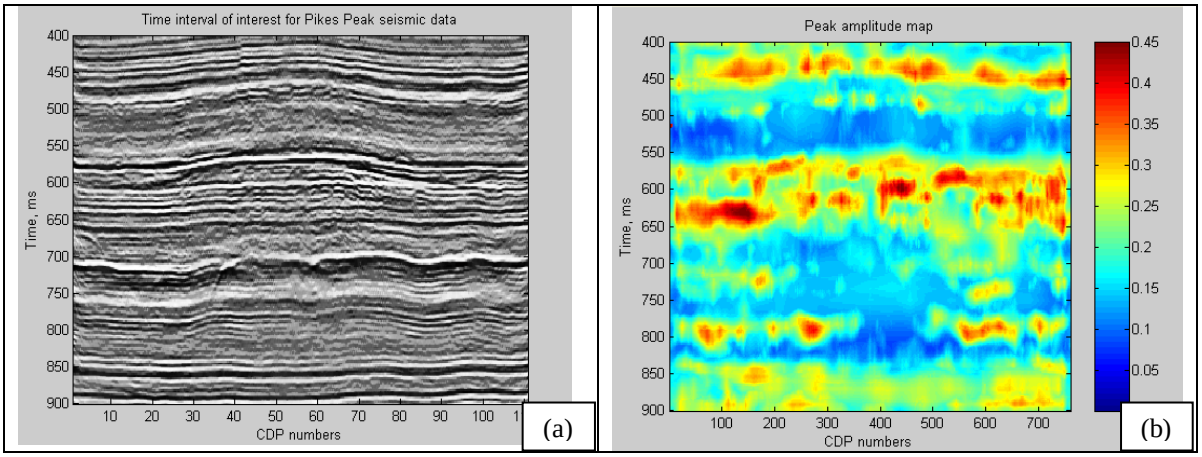

Figure A3.3. Seismic image (a) and peak amplitude map (b).

The PP seismic data and corresponding peak amplitude map are shown on Figure A3.3. Note that the visible amplitude peaks correspond to the brightest reflections on the seismic section. In other words, the maximum amplitudes occur when a considerable contrast in densities and seismic velocities between two neighbouring layers exists. For this case, the main reflections can be easily seen by the naked eye. However, for some cases, when the seismic image is not that clear, the peak amplitude map provides additional information about the main horizons and position of the anomaly on the section.

Originally, the dip map returned the angle of frequency vector for every pixel from the seismic image. Since we know that the vector of dominant frequency is perpendicular to the bedding, we rotate the dip values by 90 degrees to come up with the dipping angle for the structure.

Figure A3.4 demonstrates the dip and spectral maps for the same line. As we can see, the majority of points have zero degree dip (Figure A3.4a). According to the colour bar, we can assume that the left part of the image (yellow and light blue) is tilted to the left, the right part of the image (dark blue, blue) is tilted to the right, which confirms the presence of a mild anticline centred at around 400 CDP.

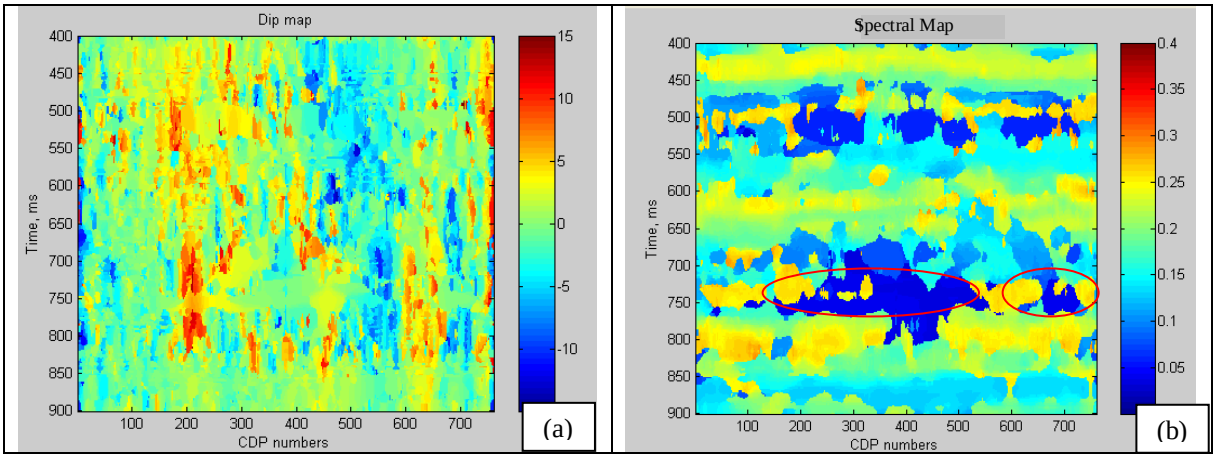

Figure A3.4. Dip (a) and spectral (b) maps.

The spectral map (Figure A3.4b) shows the wavelength of the frequency vector (Equation (A2)) at different spatial points. It is given in units of sampling frequency from 0 to 0.4. The interesting detail that we found is the low-frequency anomaly (dark blue) just below the productive zone. The first anomalous zone (dark blue, CDP 150-500) coincides with the well known productive zone (however it is shifted down at about 100 ms), and the second zone matches the area that I picked as a proposed channel location earlier in the thesis.

According to Hilterman (2001), there are some indicators of a hydrocarbon reservoir:

- Amplitude changes on stack section
- Velocity changes
- Wavelet changes
- *Frequency changes*

- Flat spots
- Changes in amplitude with offset.

In terms of frequency changes, there can be a decrease in frequency immediately beneath the reservoir because of deconvolution and attenuation (Hilterman, 2001). We were encouraged by this fact, since the same situation was observed with the other data. In particular, 10 datasets out of 15 processed in Resolution revealed the low-frequency anomaly below the productive interval (Figures A3.5, A3.6).

On the dip maps (Figures A3.5b and A3.6b) the transition from yellow to blue indicates the centre of the anticline structure. Both spectral maps (Figures A3.5c and A3.6c) reveal the low frequency anomaly (dark blue) below the proposed reservoir location.

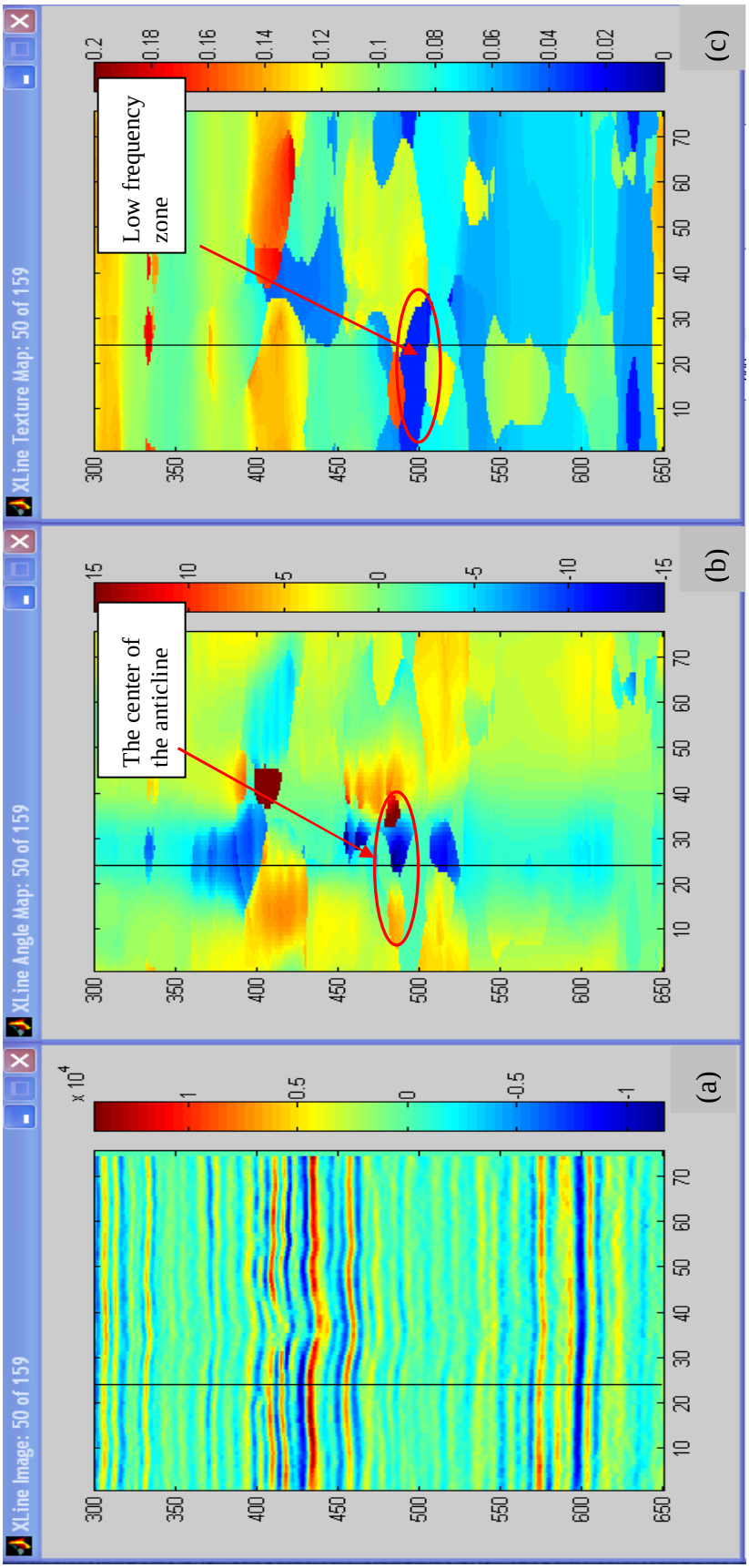

Figure A3.5. Seismic image (a), dip map (b) and spectral map (c) for XLine 50 from 3D survey in the Driver area, Saskatchewan; the black line indicates the well location

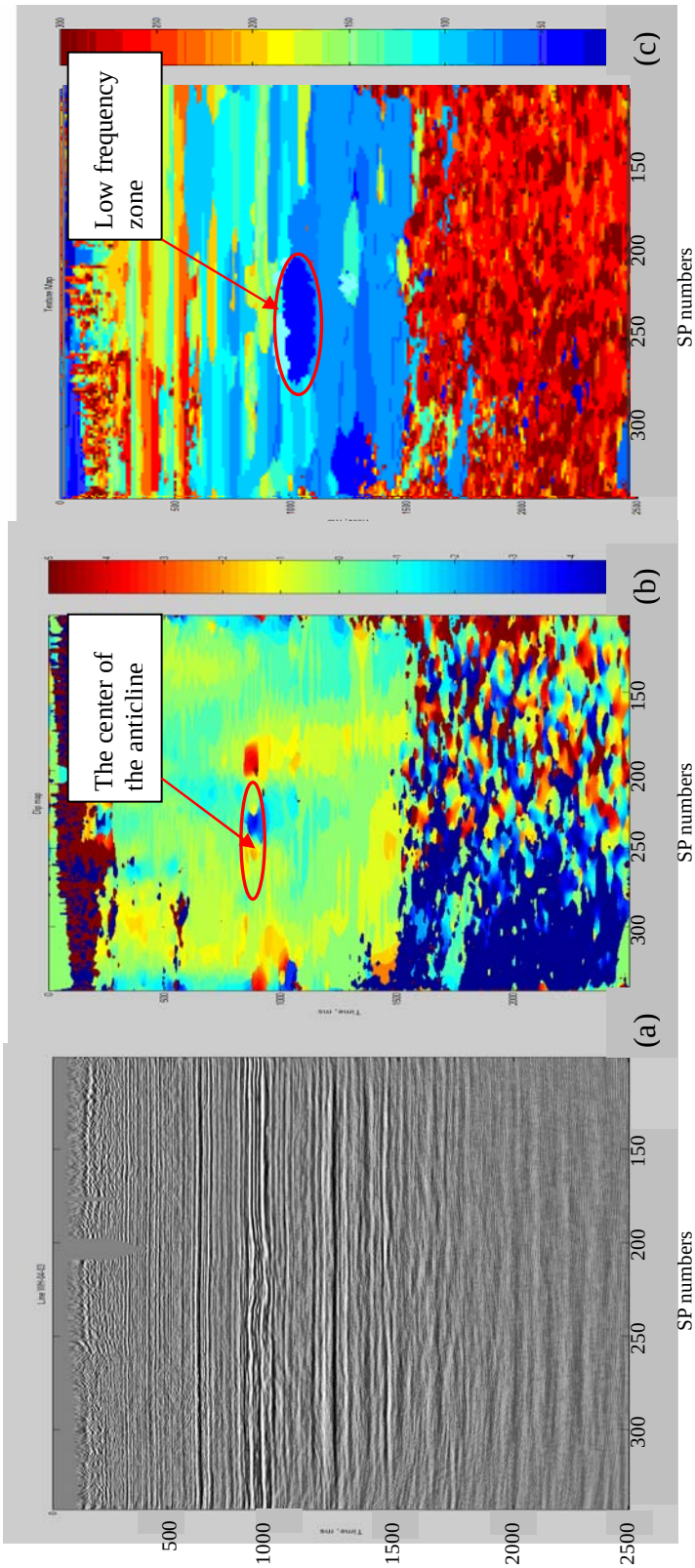

Figure A3.6. Seismic image (a), dip map (b) and spectral map (c) for line WH-04-03 from 2D survey in the Whiteside area, Saskatchewan.

A3.4 Consideration on the application of dip and spectral maps

1. Dip maps are a seismic transform that allow us to:
   - determine the dipping angle of the layers
   - determine the position of an anomaly (anticline or syncline) on a seismic section

   However, they give us no idea about the lithological content of an anomaly: whether it is gas sand, oil sand, a shale channel or sand saturated with water.

2. Spectral maps indicate the frequency content of the data. So they can provide some idea about the lithology. Harder rocks may have a higher quality factor, so waves within such rocks attenuate slowly. Similarly, in a softer rock, the attenuation might be high. Rocks have a range of quality factors. So, we can make some approximations about the nature of the rock, looking at spectral maps.
3. A low-frequency anomaly on the spectral map might be considered as an additional indicator of a hydrocarbon reservoir.
4. All maps should be used in conjunction with the seismic section. Combining all the types of available data (seismic section, CSI Maps, well log data) may well lead to a more accurate prediction of the productive zone.